ORBIT DETERMINATION STRATEGY AND VERIFICATION FOR GEOSYNCHRONOUS SATELLITES

A THESIS SUBMITTED TO
THE GRADUATE SCHOOL OF NATURAL AND APPLIED SCIENCES
OF
MIDDLE EAST TECHNICAL UNIVERSITY

BY

ABDULKADİR KÖKER

IN PARTIAL FULFILLMENT OF THE REQUIREMENTS
FOR
THE DEGREE OF MASTER OF SCIENCE
IN
AEROSPACE ENGINEERING

SEPTEMBER 2019

Approval of the thesis:

ORBIT DETERMINATION STRATEGY AND VERIFICATION FOR GEOSYNCHRONOUS SATELLITES

submitted by **ABDULKADİR KÖKER** in partial fulfillment of the requirements for the degree of **Master of Science in Aerospace Engineering Department, Middle East Technical University** by,

Prof. Dr. Halil Kalıpçılar
Dean, Graduate School of **Natural and Applied Sciences** _____

Prof. Dr. İsmail Hakkı Tuncer
Head of Department, **Aerospace Engineering** _____

Prof. Dr. Ozan Tekinalp
Supervisor, **Aerospace Engineering, METU** _____

Examining Committee Members:

Assoc. Prof. Dr. İlkay Yavrucuk
Aerospace Engineering, METU _____

Prof. Dr. Ozan Tekinalp
Aerospace Engineering, METU _____

Prof. Dr. Kemal Leblebicioğlu
Electrical and Electronics Engineering, METU _____

Dr. Yakup Sabri Özkazanç
Electrical and Electronics Engineering, Hacettepe _____

Assist. Prof. Dr. Ali Türker Kutay
Aerospace Engineering, METU _____

Date: 09.09.2019

I hereby declare that all information in this document has been obtained and presented in accordance with academic rules and ethical conduct. I also declare that, as required by these rules and conduct, I have fully cited and referenced all material and results that are not original to this work.

Name, Surname: ABDULKADİR KÖKER

Signature:

ABSTRACT

ORBIT DETERMINATION STRATEGY AND VERIFICATION FOR GEOSYNCHRONOUS SATELLITES

KÖKER, ABDULKADİR
Master of Science, Aerospace Engineering
Supervisor: Prof. Dr. Ozan Tekinalp

September 2019, 114 pages

In this thesis, the batch and sequential orbit determination procedures for the geostationary satellites are presented. The aim of the study is to investigate the effect of the angle only and standard angle-range measurements on orbit determination accuracy. The effect of various factors on estimation accuracy such as measurement frequency, observation duration, and number of observation sites are investigated using the simulated measurement data. Estimation methods namely, nonlinear least square, extended and unscented Kalman filters are employed and compared. In angle-only estimation, only sequential methods are applied to the simulated angular measurements in order to estimate the position and velocity vectors of a GEO satellite. In standard orbit determination, batch and sequential methods are investigated separately by using both angle and range measurements. The estimation results obtained from simulations for both methods are compared. Finally, the developed batch orbit determination algorithm is compared with the reference software used at TURKSAT ground stations. It is shown that the batch software developed performs as good as if not better than the reference software.

Keywords: Orbit Determination, Estimation, Turksat Satellite, Kalman Filter

ÖZ

YER EŞ ZAMANLI YÖRÜNGEKİ UYDULAR İÇİN YÖRÜNGE BELİRLEME STRATEJİSİ VE DOĞRULAMALARI

KÖKER, ABDULKADİR
Yüksek Lisans, Havacılık ve Uzay Mühendisliği
Tez Danışmanı: Prof. Dr. Ozan Tekinalp

Eylül 2019, 114 sayfa

Bu tezde, yer eş zamanlı uydular için tümel ve ardışık yörünge belirleme algoritmaları sunulmuştur. Bu çalışmanın amacı sadece açısal ve standart açı-mesafele ölçümlerinin yörünge belirleme hassasiyeti üzerindeki etkilerini incelemektir. Ölçüm sıklığı, ölçüm süresi ve toplam ölçüm istasyonu sayısı gibi faktörlerin etkileri simule edilmiş ölçümler kullanılarak incelenmiştir. Kestirim metodu olarak, linear olmayan en az kareler yöntemi, genişletilmiş ve kokusuz (unscented) Kalman filtresi yöntemleri uygulanmış ve bu yöntemler karşılaştırılmıştır. Sadece açısal yörünge belirleme yönteminde, yer eş zamanlı bir uydunun konum ve hız vektörlerini kestirmek için ardışık kestirim yöntemleri simule edilmiş açı ölçümü ile birlikte kullanılmıştır. Standart yörünge belirleme metodunda, hem tümel hem ardışık kestirim yöntemleri açı ve mesafe ölçümleri ile birlikte kullanılarak incelenmiştir. Her iki metodun kestirim sonuçları simulasyon yapılarak kıyaslanmıştır. Son olarak, geliştirilen tümel kestirim yöntemi sonuçları, TÜRKSAT yer istasyonunda kullanılan referans yazılım ile karşılaştırılmıştır. Geliştirilen tümel yazılımın, referans yazılımına benzer hatta daha iyi performans sergilediği gözlemlenmiştir.

Anahtar Kelimeler: Yörünge Belirleme, Kestirim, Türksat Uydusu, Kalman Filtresi

To my family

ACKNOWLEDGEMENTS

I would like to express my deepest gratitude to my advisor Prof. Dr. Ozan TEKİNALP for his help, guidance and continuous support throughout the course of this thesis.

I would like to thank TÜBİTAK UZAY which involved me as a researcher for the orbit control software development project for the geostationary satellites.

I would like to thank TURKSAT, Ümit Cezmi Yılmaz and Cemal ŞAKACI. Their guidance provided insight into this work and their encouragement strengthened my confidence. They provide me valuable the real measurement data which helps me for the verification of the orbit determination algorithm developed in this thesis.

I would like to thank my colleagues Enes DAĞ, Murat GÖKCE, Burak YAĞLIOĞLU, Egemen IMRE, Kezban ÜÇÜNCÜ, Biter Boğa İNALTEKİN, Mustafa Yavuz ÖZTÜRK for their help.

TABLE OF CONTENTS

ABSTRACT v

ÖZ vii

ACKNOWLEDGEMENTS x

TABLE OF CONTENTS xi

LIST OF TABLES xiv

LIST OF FIGURES xviii

LIST OF ABBREVIATIONS xx

LIST OF SYMBOLS xxi

CHAPTERS

1. INTRODUCTION 1

1.1. Background 1

1.2. Overview of Geosynchronous Orbit Determination 4

1.2.1. Observation Availability 5

1.2.2. Measurement Systematic Error 5

1.2.3. Dynamical model error 6

1.3. Mission Requirement 6

1.4. Contributions of Thesis 7

2. MODELLING OF ORBITAL DYNAMICS 9

2.1. Orbit Model 9

3. MEASUREMENT MODELLING AND GENERATION 17

3.1. Measurement Modelling 17

3.2. Measurement Generation 19

3.3. Measurement Configuration 20
4. ORBIT ESTIMATION METHODOLOGY 25
4.1. Introduction 25
4.2. Batch Estimation 25
4.2.1. Methodology 25
4.2.2. Implementation 27
4.3. Sequential Estimation 34
4.3.1. Extended Kalman Filter 34
4.3.2. Unscented Kalman Filter 36
4.3.3. Implementation 41
5. ANGLE ONLY ORBIT DETERMINATION RESULTS 43
5.1. Simulation Setup Parameters 43
5.2. Analysis Results 45
6. STANDARD ORBIT DETERMINATION RESULTS 51
6.1. Simulation Setup Parameters 51
6.2. Batch Orbit Estimation without Maneuver 55
6.3. Batch Orbit Estimation with Maneuver 63
6.4. Sequential orbit estimation without maneuver 67
6.5. Sequential orbit estimation with maneuver 74
7. VERIFICATION 79
7.1. Test Setup Parameters 79
7.2. Single Station Case Verification 86
7.3. Range and Turn-Around Case Verification 91
7.4. Range and Range Case Verification 94

7.5. Triple Station Case Verification 96
7.6. Summary of the Verification Results 97
8. Conclusıon 101
REFERENCES 105
APPENDICES 107

LIST OF TABLES

TABLES

Table 5.1. Analysis parameters for angle-only orbit determination 44
Table 6.1. Analysis Cases 51
Table 6.2. Measurement Bias Information 54
Table 6.3. Analysis parameters for standard orbit determination 55
Table 6.4. Measurement Noise Modes 55
Table 6.5. Case-1 3-D position estimation errors for various observation duration and noise modes 56
Table 6.6. Case-1 3-D velocity estimation errors for various observation duration and noise modes 56
Table 6.7. Case-2 3-D position estimation errors for various observation duration and noise modes 57
Table 6.8. Case-2 3-D velocity estimation errors for various observation duration and noise modes 57
Table 6.9. Case-3 3-D position estimation errors for various observation duration and noise modes 57
Table 6.10. Case-3 3-D velocity estimation errors for various observation duration and noise modes 58
Table 6.11. Case-1 position estimation errors in RSW frame for various observation duration 58
Table 6.12. Case-1 velocity estimation errors in RSW frame for various observation duration 59
Table 6.13. Case-1 orbital element estimation errors in RSW frame for various observation duration 59
Table 6.14. Case-1 parameter estimation errors for various observation duration 59

Table 6.15. Case-2 position estimation errors in RSW frame for various observation duration 60
Table 6.16. Case-2 velocity estimation errors in RSW frame for various observation duration 60
Table 6.17. Case-2 orbital element estimation errors in RSW frame for various observation duration..... 60
Table 6.18. Case-2 parameter estimation errors for various observation duration.... 61
Table 6.19. Case-3 position estimation errors in RSW frame for various observation duration 61
Table 6.20. Case-3 velocity estimation errors in RSW frame for various observation duration 61
Table 6.21. Case-3 orbital element estimation errors for various observation duration 62
Table 6.22. Case-3 parameter estimation errors for various observation duration.... 62
Table 6.23. 3D position estimation error for Case 1, 2 and 3 for various force model configuration..... 63
Table 6.24. North-South Maneuver Velocity Increments. 64
Table 6.25. Case-1 N-S maneuver orbital element estimation errors in RSW frame for various observation. 65
Table 6.26. Case-1 N-S maneuver velocity increments errors in RSW for various observation duration..... 65
Table 6.27. Case-2 N-S maneuver orbital element estimation errors in RSW frame for various observation. 65
Table 6.28. Case-2 N-S maneuver velocity increments errors in RSW for various observation duration..... 66
Table 6.29. Case-3 N-S maneuver orbital element estimation errors in RSW frame for various observation. 66
Table 6.30. Case-3 N-S maneuver velocity increments errors in RSW for various observation duration..... 66
Table 6.31 Sequential 3D position estimation errors for various noise modes. 67

Table 6.32. Sequential 3D velocity estimation errors for various noise modes. 67
Table 6.33 Estimation results for different force model configuration without Q tuning. 73
Table 6.34 Estimation results for different force model configuration with Q tuning. 73
Table 7.1. Case Summary for satellite T4B 80
Table 7.2. Estimated position (3D) and velocity (3D) difference between batch estimation and Reference Software for Single Station Case 86
Table 7.3. Total rms and solar radiation pressure coefficient (Cp) comparison between batch estimation and Reference Software for Single Station Case 87
Table 7.4. Estimated orbital element difference between batch estimation and Reference Software for Single Station Case 88
Table 7.5. Azimuth residual rms comparison and estimated azimuth bias difference between batch estimation and Reference Software for Single Station Case 88
Table 7.6. Elevation residual rms comparison and elevation estimated elevation bias difference between batch estimation and Reference Software for Single Station Case 89
Table 7.7. Range residual rms comparison between batch estimation and Reference Software for Single Station Case 90
Table 7.8. Maneuver velocity estimation difference in RSW frame between batch estimation and Reference Software for Single Station Case 90
Table 7.9. Estimated position and velocity difference between batch estimation and Reference Software for Range and Turn-Around Case 91
Table 7.10. Total rms and solar radiation pressure coefficient (Cp) between batch estimation and Reference Software for Range and Turn-Around Case 92
Table 7.11. Total rms and solar radiation pressure coefficient (Cp) between batch estimation and Reference Software for Range and Turn-Around Case 92
Table 7.12. TAR residual rms comparison and estimated Tar bias difference between batch estimation and Reference Software for Range and Turn-Around Case 93

Table 7.13. Range residual rms comparison between batch estimation and Reference Software for Range and Turn-Around Case 93
Table 7.14. Maneuver velocity estimation difference in RSW frame between batch estimation and Reference Software for Range and Turn-Around Case 94
Table 7.15. Estimated position and velocity difference between batch estimation and Reference Software for Range and Range Case 94
Table 7.16. Total rms and solar radiation pressure coefficient (Cp) between batch estimation and Reference Software for Range and Range Case 95
Table 7.17. Estimated orbital element difference between batch estimation and Reference Software for Range and Range Case 95
Table 7.18. Estimated position and velocity difference between batch estimation and Reference Software for Triple Station Case 96
Table 7.19. Azimuth residual rms comparison and estimated azimuth bias difference between batch estimation and Reference Software for Triple Station Case 96
Table 7.20. Elevation residual rms comparison and estimated elevation bias difference between batch estimation and Reference Software for Triple Station Case 97
Table 7.21. Average estimation difference for all cases 98
Table A.1. Case-1 semi-major axis estimation errors for various observation duration and noise modes 107
Table A.2. Case-1 inclination estimation errors for various observation duration and noise modes 107
Table A.3. Case-1 longitude estimation errors for various observation duration and noise modes 107

LIST OF FIGURES

FIGURES

Figure 3.1. Geometry of Earth observation of satellite motion [5] 17
Figure 3.2. Ranging procedure 21
Figure 3.3. Turn-around ranging procedure 22
Figure 3.4. Maneuver firing simulation flow chart 23
Figure 4.1. Finite differencing method for F and H matrix calculation 28
Figure 4.2. Nonlinear Least Square Implementation Flow Chart 31
Figure 4.3. Batch orbit estimation procedure for North-South maneuver 33
Figure 4.4. Monte-Carlo simulation flow chart 34
Figure 4.5. Example of the UT for mean and covariance propagation [12] a) actual, b) first-order linearization (EKF), c) UT. 38
Figure 4.6. Unscented Kalman Filter Algorithm [11] 40
Figure 5.1. Angle-only estimation procedure 44
Figure 5.2. Position error for GEO frequency case 47
Figure 5.3. Position error for frequency case 45
Figure 5.4. Position error for GEO frequency case 46
Figure 5.5. Position error for duration case 50
Figure 5.6. Position error for duration case 48
Figure 5.7. Position error for duration case 49
Figure 6.1. Batch estimation Flow Chart 52
Figure 6.2. Sequential Estimation Flow Chart 53
Figure 6.3. Batch orbit estimation procedure for North-South maneuver 64
Figure 6.4. Case-1 sequential position and velocity estimation errors 68
Figure 6.5. Case-2 sequential position and velocity estimation errors 69
Figure 6.6. Case-3 sequential position and velocity estimation errors 70
Figure 6.7. Orbital elements estimation errors for Case-1, Case-2 and Case-3 71

Figure 6.8. Parameter estimation results for Case-1, Case-2 and Case-3 72
Figure 6.9. Case-1 sequential position and velocity estimation errors for N-S maneuver 74
Figure 6.10. Orbital elements estimation errors for Case-1, Case-2 and Case-3 for N-S maneuver 75
Figure 6.11. Inclination estimation errors for Case-1, Case-2 and Case-3 for N-S maneuver 76
Figure 6.12. Cross-Track (north) maneuver velocity estimation error for Case-1, Case-2 and Case-3 for N-S maneuver 77
Figure 7.1 Orbit determination procedure during Station-Keeping operation 81
Figure 7.2 Orbit Determination Flow Chart for Verification 82
Figure 7.3 Azimuth (top), elevation (mid), range (bottom) measurements taken from TURKSAT ground station antenna during March for single station case 84
Figure 7.4 Range (top), turn-around range (bottom) measurements taken from TURKSAT ground station antenna during March for two station case 84
Figure 7.5 Batch Estimation Algorithm Flow Chart for Verification 85
Figure 7.6 Orbital elements and position difference after propagating estimated initial conditions during two week. 99
Figure 7.7 Longitude error after propagating estimated initial conditions during two week for range- TAR measurement configuration. 100
Figure B.1. Case-2 sequential position and velocity estimation errors for N-S maneuver 109
Figure B.2. Case-3 sequential position and velocity estimation errors for N-S maneuver 110
Figure B.3. Parameter estimation results for Case-1, Case-2 and Case-3 for N-S maneuver 111

LIST OF ABBREVIATIONS

TAR = Turn-Around Range

GEO = Geosynchronous

RSW = Radial (R), Along-Track (S), Cross-Track (W)

LSQ = Nonlinear Least Square

EKF = Extended Kalman Filter

UKF = Unscented Kalman Filter

UT = Unscented Transformation

ECI = Earth Centered Inertial

ECEF = Earth Centered Earth Fixed

LIST OF SYMBOLS

Cp = Solar Radiation Pressure Coefficient

ρ = Range

az = Azimuth

el = Elevation

a = Semi-major axis

i = Inclination

w = Argument of Perigee

Ω = Longitude of Ascending Node

ν = True Anomaly

e = Eccentricity

E/W = East-West Maneuver

N/S = North-South Maneuver

CHAPTER 1

INTRODUCTION

1.1. Background

A number of methods, that use different sensors, are proposed in the literature for the orbit determination of non-collaborating objects. Radar, telescope and laser systems are the most well-known. Although the laser systems are more accurate, its development cost is relatively high. Radar systems are good at determining Low Earth Orbit (LEO) object orbits. On the other hand, their accuracy dramatically decreases when orbital estimation of Medium Earth Orbit (MEO), and Geostationary Orbit (GEO) objects are needed. Telescope systems may be used for all altitudes and their development costs are lower compared to other systems. However, telescopes can only give two angles, namely, azimuth and elevation, which is normally insufficient to determine the object position accurately. Range measurements are not available for these systems. Objects at different altitudes have different observation duration from Earth due to their orbital period. LEO objects are seen for a limited time of the day. However, GEO objects may be continuously observed. Therefore, orbit determination accuracy may be different for objects at different altitudes. Different estimation algorithms are also used for orbit estimation.

In standard orbit determination system, ground station measurements (both angle and range) are used to determine the position of the collaborating satellites. This approach is similar to the radar system since it has the range information. However, the noise in angular measurements is much higher than telescope angle measurements. The advantage of this system over optical systems is continuous observation opportunity. In nominal orbit determination process, in addition to the orbit information, other parameters such as measurement bias, solar radiation pressure coefficient and velocity

change due to maneuver firing are also estimated in order to improve orbit determination accuracy and to calculate maneuver efficiency.

There are several researches related to orbit determination systems for GEO satellites. Tombasco, in his work, performs angle-only estimation method for GEO satellites. By using short sampling measurement intervals (10 to 30 seconds) and 3 or more hours long nightly track lengths, he claims that 10-meter accuracy is achievable [12]. He also shows the effect of the different measurement sampling interval on the orbit determination accuracy [12]. In this thesis, similar, but more limited, approaches and scenarios are investigated for angle-only estimation method. Park and Roh, in their work, perform batch estimation method for the satellite orbit determination [7]. They use traditional and unscented batch non-linear least square method in order to compare these two method. In their analysis, the orbit and air-drag coefficient of the satellite are estimated for different measurement configurations. In this thesis, traditional non-linear least square approach is selected for the orbit determination process. Lee and Alfriend, in their work, investigated the sigma point filter performance for the orbit determination of the LEO satellite and compared these filter with a traditional Extended Kalman Filter (EKF) [11]. They also implement Herrick-Gibbs method and Monte Carlo simulation to generate a good initial condition and uncertainty for LEO satellite [11]. In this thesis, initial orbit determination methods such as Herrick-Gibbs and Gibbs method, are not considered. Instead, initial conditions are corrupted with fixed error in order to initialize the estimation algorithm. Similar to Lee and Alfriend, EKF and Unscented Kalman Filter (UKF) methods are compared for the different measurement cases. UKF method is also investigated in more detail. Hwang and Lee, in their work, perform orbit determination analysis of The Communication, Ocean, and Meteorological Satellite (COMS) satellite by using single station antenna tracking data [16]. They also repeated their analysis by using an additional ground station in order to estimate the angular measurement bias. They conclude that if the angular measurement bias is estimated for only using single station data, orbit determination accuracy is around 1.5 km [5], [17]. When the range measurement from a second

ground station is available for the estimation, the error is reduced to around 1 km. Hwang and Lee use batch nonlinear least square algorithm in their work. In this thesis, similar analysis is performed as in Hwang and Lee's work in two parts. In the first part, batch estimation method performance is investigated by using simulated measurements. In the second part, batch method is applied to the measurements taken from TURKSAT ground station for T4B satellite. Hwang and Lee only use two measurement configuration as stated previously. The first one was angular and range measurements from single station and the second one was similar with first one with additional range measurements from second ground station. In this thesis, in simulated analysis, three different measurement configurations are used for estimation process. The first one is single station angular and range measurements similar to Hwang and Lee's approach. The second one includes range and turn-around range measurements from two ground stations. The third one is two separate range measurements from two ground stations. The details of the measurement configurations will be explained in Chapter 3.

Hwang and Lee, in their another work, performed more detailed orbit determination analysis for COMS satellite [17]. They tried to estimate angular bias by using two different approaches. The first one is the use of second ground station and the second method is the prediction of angular bias by only using single station. Their results showed that the range measurement from two ground stations gives better estimation accuracy compared to the single station case. However, they also claimed that the estimation error for single station is less than 1.5 km (3 sigma). In both work, they use the orbit determination results calculated by using range measurement from two ground stations along with 2-day observation as a reference value in order to check the accuracy of the single station's results. In their second work [17], they also compared final orbit determination results with the optical system in order to validate their results. In this thesis, the angular measurement biases are estimated for single station configuration similar to Hwang and Lee's work [17]. The reference software

results are used for the limited verification of the batch algorithm. The details of the verification will be given in Chapter 7.

In this thesis, the orbit estimation of GEO objects using telescope angle only measurement and ground station angle and range measurements is addressed. Various factors, such as measurement noise, the number of observation sites, and measurement duration, and the effect of estimation algorithm, namely nonlinear least square (LSQ), Extended Kalman Filter (EKF) and Unscented Kalman Filter (UKF) are investigated. The accuracy of the sequential estimation methods is calculated and only checked by using the simulated measurements. However, the batch estimation method's accuracy is investigated by using both simulated and real measurements. In verification process, batch algorithm is applied to the real measurements taken from the ground antennas located at TURKSAT facilities as stated before. Final estimated orbit information and parameters are also compared with the reference orbit determination software used at TURKSAT ground stations. TURKSAT is one of the world's leading companies providing all sorts of satellite communications through the satellites of TURKSAT as well as the other satellites. In TURKSAT ground station, the orbit control operations of the several satellite are performed for many years. These operations include orbit determination, orbit propagation, station-keeping maneuvers as well as other orbit control operations.

1.2. Overview of Geosynchronous Orbit Determination

A general orbit tracking and estimation technique is necessary to increase operational commonality and to achieve station keeping operation for GEO satellites. An efficient approach should be used to obtain more accurate orbit information. However, there are some challenges including the availability of observations, and systematic measurement error for angle-only orbit determination approach. The dynamic model challenges include realistically modeling orbit perturbations which should also be

addressed. In standard orbit determination approach, main challenges are not the geometry but reducing systematic measurement bias error.

1.2.1. Observation Availability

Optical observations can only be used when the satellite illuminated while telescope station is not. This causes interruption during night observations. The cloudy weather and lunar illumination also have significant effect on the availability of measurements. Additionally, the measurement quality may be degraded due to atmospheric refraction and city lights. Therefore, optical system should be located to limited number geographic locations such that above observation restriction can be minimized. Furthermore, optical sensors typically track lots of objects during the night and are not devoted to tracking a single object [12]. However, in standard orbit determination, angle and range measurements from ground station antenna can be taken at any time without considering weather and light conditions. Therefore, continuous observation is available for GEO objects. However, only single object can be tracked with the ground station antenna system.

1.2.2. Measurement Systematic Error

Optical systems contain systematic measurement errors and biases which reduce measurement quality. 1 arc second of angular error from the ground causes to approximately 200 meters of position error for GEO satellite [12]. As such, mitigating systematic measurement error is crucial to achieve accurate geosynchronous orbit estimation. Systematic measurement errors may be related to the type of the sensor, station location, and pointing direction. A possible way of mitigation is to estimate for the unmodelled measurement errors. In angle-only orbit determination, it is generally difficult to estimate measurement bias since range measurements are absent. When

the range measurements are available, the estimation of measurement bias, especially angular bias, is standard operation for the antenna system.

1.2.3. Dynamical model error

The accuracy of orbit estimation is further degraded by the dynamic model error due to mismodelling the forces acting on an object. The main disturbing forces on objects in geosynchronous orbits are perturbations due to the oblateness of the Earth, lunisolar gravitational attraction, and solar radiation pressure. Certain perturbations, such as gravitational forces, can be modeled generically for all spacecraft since the modelling parameters are well defined and accurate. However, solar radiation pressure perturbation is generally dependent on the mass, solar exposed area and the reflectivity of the spacecraft. In order to have accurate orbit model, the solar radiation disturbing forces should be modelled unique to individual objects.

1.3. Mission Requirement

The one of the main purpose of this thesis is the development of orbit determination algorithm used for orbit control of the GEO satellites during real operations. In the orbit control operations, the station-keeping maneuver is planned in order to maintain the location of the satellite at desired longitude. In order to achieve this, the position of the satellite should be determined within the accuracy defined in mission requirements. In nominal operations, 48-hour range measurements from two ground station are used to estimate the orbit of GEO satellite. Measurement frequency is once an hour during whole observation period. The following requirements are used to check the accuracy of the orbit determination:

- Semi-major axis error should be less than 30 meter (3 sigma)
- Inclination error should less than 1 mili degree (3 sigma)
- Longitude error should be less than 3 mili degree (3 sigma)

Although these requirements are valid for two station configuration, same requirements also are applied to single station case in order to investigate its estimation accuracy. When the second ground station is not available due to the unexpected problem, single station measurement should be used to continue station-keeping operation. If the estimation accuracy deviates from the requirements too much, it may affect negatively the performance of the station-keeping maneuvers by increasing the fuel consumption. In addition to this, error in orbit determination process also causes further error contribution when the orbit of the satellite is propagated to future time. Therefore, there should be another requirement such that two-week orbit propagation error including orbit determination error should be lower than 9 mili degree longitude error in order to maintain the longitude of the satellite within a ± 0.05 degree control box. This control box is around ± 36 km from the reference longitude.

1.4. Contributions of Thesis

In this work, the orbit estimation methods of GEO satellites using angles-only and the combination of the angular and range measurements for ground-based tracking systems are presented. Specifically,

- The estimation accuracy of the using angles-only observations for various observation duration and frequency is investigated and presented.
- An estimation strategy using angle and range observations for various observation duration and measurement configurations is developed and evaluated.
- Different estimation methods are compared.
- The batch estimation algorithm is compared with the reference software used for real operation and the quality of the current approach over reference software's outputs is demonstrated.

CHAPTER 2

MODELLING OF ORBITAL DYNAMICS

2.1. Orbit Model

The equations of motion of a satellite are usually described in an inertial reference frame as being composed of a sum of gravitational, non-gravitational and empirical or un-modeled forces. In the current research, the equations of motion for an Earth orbiting satellite are given by [10]

$$\dot{r} = v \tag{2.1}$$

$$\dot{v} = \frac{-\mu}{r^3} r + a_{geo} + a_{third-body} + a_{SRP} \tag{2.2}$$

where r and v are the position and velocity vectors in the inertial frame. The forces ($\dot{v}$) acting on the satellite consist of the two-body effect and the perturbing accelerations. a_{geo} is the geo-potential force due to the gravitational force of the Earth and can be expressed as a spherical harmonic expansion of the gradient of the Earth's solid body distribution as shown by [10]

$$\vec{a}_{geo} = \frac{\partial U}{\partial r}\left(\frac{\partial r}{\partial \vec{r}}\right)^T + \frac{\partial U}{\partial \emptyset_{gc_{sat}}}\left(\frac{\partial \emptyset_{gc_{sat}}}{\partial \vec{r}}\right)^T + \frac{\partial U}{\partial \lambda_{sat}}\left(\frac{\partial \lambda_{sat}}{\partial \vec{r}}\right)^T \tag{2.3}$$

where U is the gravitational potential, r is the satellite position vector, $\emptyset_{gc_{sat}}$ and λ_{sat} are the satellite's geocentric latitude and longitude. Partial derivatives of the gravitational potential with respect to satellite position vector, geocentric latitude and longitude are shown in Eq. (2.4) [10], [4].

$$
\begin{aligned}
\frac{\partial U}{\partial r} = & -\frac{\mu}{r^2}\sum_{l=2}^{\infty}\sum_{m=0}^{l}\left(\frac{R_{\oplus}}{r}\right)^{l}(l+1)P_{l,m}\left[sin\left(\emptyset_{gc_{sat}}\right)\right]x \\
& \left\{C_{l,m}\,cos(m\lambda_{sat}) + S_{l,m}\,sin(m\lambda_{sat})\right\} \\
\frac{\partial U}{\partial \emptyset_{gc_{sat}}} = & \frac{\mu}{r}\sum_{l=2}^{\infty}\sum_{m=0}^{l}\left(\frac{R_{\oplus}}{r}\right)^{l}\left\{P_{l,m+1}\left[sin\left(\emptyset_{gc_{sat}}\right)\right]\right. \\
& \left. - m\,tan\left(\emptyset_{gc_{sat}}\right)P_{l,m}\left[sin\left(\emptyset_{gc_{sat}}\right)\right]\right\} \\
& x\left\{C_{l,m}\,cos(m\lambda_{sat}) + S_{l,m}\,sin(m\lambda_{sat})\right\} \\
\frac{\partial U}{\partial \lambda_{sat}} = & -\frac{\mu}{r^2}\sum_{l=2}^{\infty}\sum_{m=0}^{l}\left(\frac{R_{\oplus}}{r}\right)^{l}(l+1)\;P_{l,m}\left[sin\left(\emptyset_{gc_{sat}}\right)\right]x \\
& \left\{S_{l,m}\,cos(m\lambda_{sat}) - C_{l,m}\,sin(m\lambda_{sat})\right\}
\end{aligned}
\tag{2.4}
$$

$C_{l,m}$ and $S_{l,m}$ are the empirical coefficients which represent sectoral and tesseral harmonics. P , which is Legendre polynomials expressions and other partial derivative terms are shown in Eq. (2.5) [10].

$$
\begin{aligned}
\frac{\partial r}{\partial \vec{r}} &= \frac{\vec{r}^{T}}{r} \\
\frac{\partial \emptyset_{gc_{sat}}}{\partial \vec{r}} &= \frac{1}{\sqrt{r_I^2 + r_J^2}}\left(-\frac{\vec{r}^{T} r_K}{r^2} + \frac{\partial r_K}{\partial \vec{r}}\right) \\
\frac{\partial \lambda_{sat}}{\partial \vec{r}} &= \frac{1}{r_I^2 + r_J^2}\left(r_I\frac{\partial r_J}{\partial \vec{r}} - r_J\frac{\partial r_I}{\partial \vec{r}}\right) \\
P_{l,m}[\,\gamma] &= \frac{1}{2^l l!}(1-\gamma^2)^{m/2}\frac{d^{l+m}}{d\gamma^{l+m}}(\gamma^2-1)^l
\end{aligned}
\tag{2.5}
$$

$a_{third-body}$ is the lunar and solar gravitational perturbation, which are usually modeled as point masses within the Newtonian framework. By assuming satellite mass is negligible, the acceleration affecting satellite can be formulated by [10], [13]

$$
a_{third-body} = -\frac{\mu_{\oplus}\vec{r}_{\oplus/sat}}{r^3_{\oplus/sat}} + \mu_{tb}\left(\frac{\vec{r}_{sat/tb}}{r^3_{sat/tb}} - \frac{\vec{r}_{\oplus/tb}}{r^3_{\oplus/tb}}\right) \tag{2.6}
$$

where subscription, $\oplus$,refers to the Earth. $\vec{r}_{\oplus/sat}$ means that the position of the Earth with respect to the satellite. $\vec{r}_{sat/tb}$ means that the position of the satellite with respect to the third-body. $\vec{r}_{\oplus/tb}$ means that the position of the Earth with respect to the third-body. If only the effect of the Sun and Moon is considered and other bodies are neglected, Eq. (2.6) can be used to calculate the acceleration on the satellite due to the Sun and Moon separately.

a_{SRP} is the force due to solar radiation pressure on the satellite given by [10], [13]

$$a_{SRP} = -\frac{P_{srp} C_p A}{m} \frac{\vec{r}_{sat}}{|\vec{r}_{sat}|} \tag{2.7}$$

where P_{srp} is the solar radiation pressure, C_p is the pressure coefficients, A is the exposed area to the Sun and $\vec{r}_{sat}$ is inertial position of the satellite.

All the equations of motion are numerically integrated by the 6th order symplectic propagator. Derivations and details of the propagation method can be found in reference [18].

2.2. Coordinate Systems and Transformations

In this thesis, several coordinate systems are used to calculate the forces acting on satellite and to represent the estimated position and velocity of the satellites. The equation of the motion as defined in Eq. (2.1) and (2.2) is valid for Earth Centered Inertial (ECI) Frame. Therefore, in order to predict the orbit of the satellite, all equation of motion equations should be propagated in ECI frame as shown in Figure 2.1. ECI frame uses the Earth' equator and the axis of rotation to define an orthogonal set of vectors [8] . The vernal equinox direction is fixed at a specific epoch for most applications [10]. Position and velocity estimation results are generally presented in ECI frame unless otherwise stated.

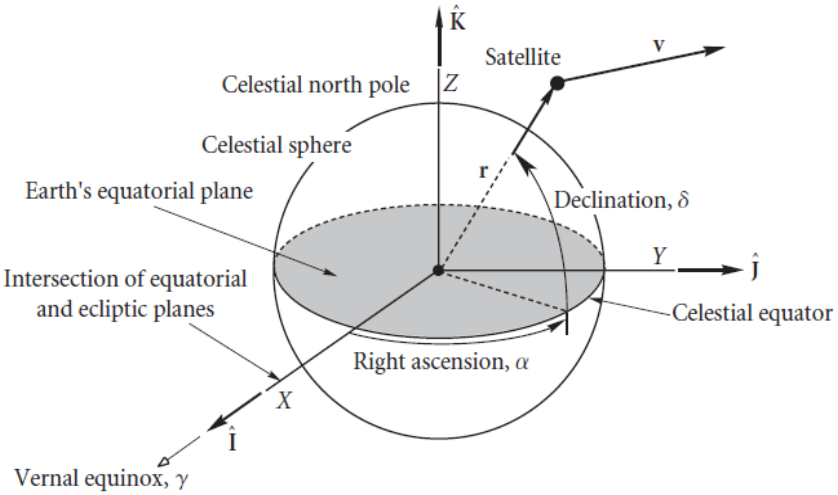

Figure 2.1. Earth Centered Inertial (ECI) Frame [19].

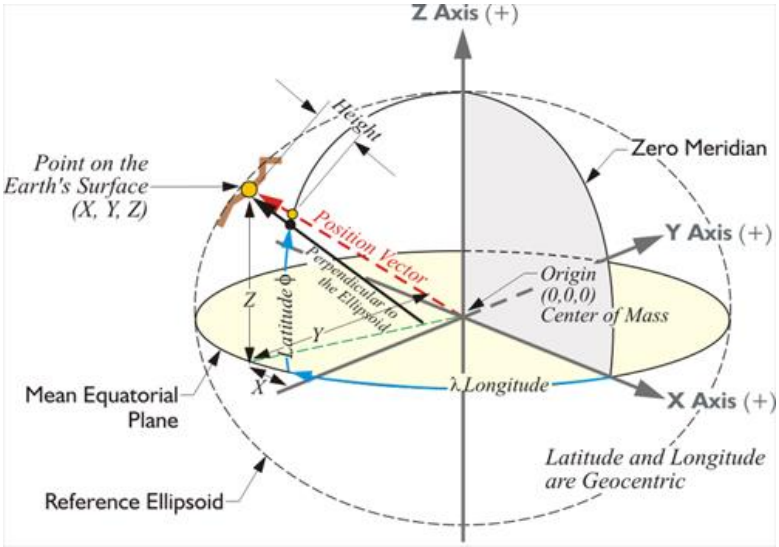

Figure 2.2. Earth Centered Earth Fixed (ECEF) Frame [20].

Other coordinate frame used in this work is Earth Centered Earth Fixed (ECEF) Frame as shown in Figure 2.2. The origin of ECEF frame is at the center of Earth and axes are realized by the adopted coordinates of defining stations on the Earth's surface [10]. The empirical coefficient used for the calculation of the geo-potential perturbations,

as shown in Eq. (2.4), are defined in ECEF frame. Therefore, in order to perform numerical propagation by using Eq. (2.3) and (2.4), partial derivatives of the gravitational potential should be calculated in ECEF frame by using empirical coefficients. After that, the coordinate transformation between ECI and ECEF frame is necessary [13], [10]. The coordinate transformation matrices are shown in Eq. (2.8) [10] .

$$r_{ECI} = [P(t)][N(t)][R(t)][W(t)]r_{ECEF} \tag{2.8}$$

where r_{ECI} and r_{ECEF} are the position of the satellite in ECI and ECEF frame respectively. P and N are the precession-nutation matrices of date t, R is the sidereal-rotation matrix of date t, W is the polar-motion matrix of date t. The rotations in Eq. (2.8) are collectively known as an Earth orientation model [10], [13]. The details of this coordinate transformation can be found in references [10] and [13].

There are also satellite based coordinates systems. RSW coordinate system is shown in Figure 2.3. These coordinate systems move with the satellite. The R (radial) axis points out from the satellite along the geocentric radius vector, the W (cross-track) axis is normal to the orbital plane, and the S (along-track) axis is normal to the position vector and positive in the direction of the velocity vector. This coordinate frame can be useful for presenting the estimated position and velocity errors of the satellite since the error direction can be defined more easily.

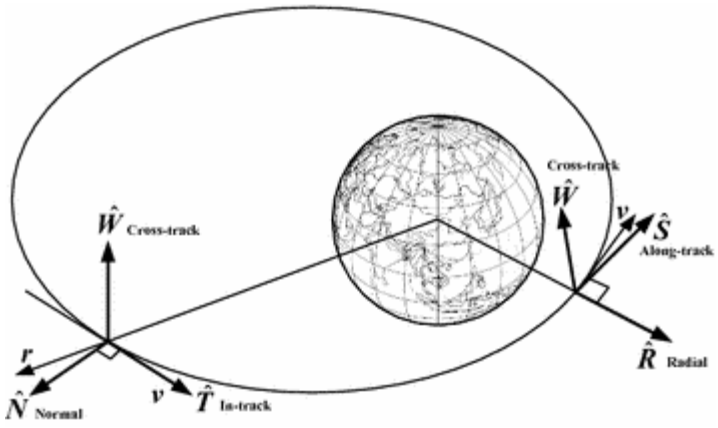

Figure 2.3. Satellite Coordinate Systems, RSW [10].

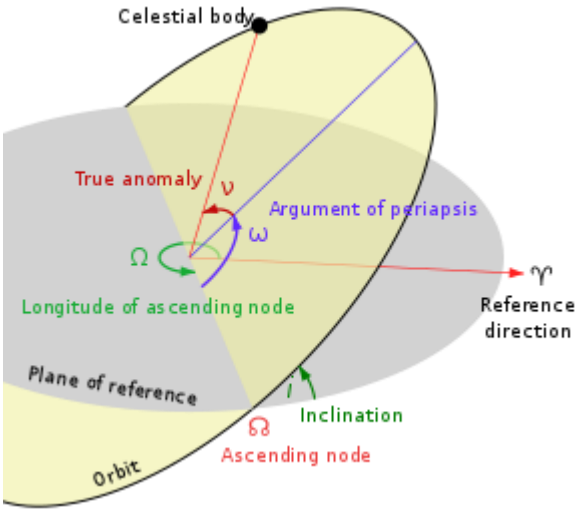

Figure 2.4. The classical orbital elements [21].

In normally, we need six quantities to define the state of a satellite in space. Three dimensional position and velocity vectors are sufficient for this representation. However, as shown in Chapter 1.3, the mission requirements are defined in orbital elements. Therefore, in order to calculate estimation accuracy of the orbital elements, the position and velocity vectors should be converted to classical orbital elements as shown in (2.4). These elements include followings [21]: Semi-major axis (a) , is the

sum of the periapsis and apoapsis distances divided by two. Eccentricity (e) is the shape of the ellipse, describing how much it is elongated compared to a circle. Inclination (*i*) is the vertical angle of the ellipse with respect to the reference plane, measured at the ascending node. Longitude of the ascending node (Ω) is the horizontally orients the ascending node of the ellipse with respect to the reference frame's vernal point. Argument of periapsis (ω) defines the orientation of the ellipse in the orbital plane, as an angle measured from the ascending node to the periapsis. True anomaly defines the position of the orbiting body along the ellipse at a specific time. The conversion formula between the position and velocity vector to the classical orbital elements can be found in references [10], [13].

CHAPTER 3

MEASUREMENT MODELLING AND GENERATION

3.1. Measurement Modelling

We consider a tracking station on the ground that measures a range, azimuth and elevation of a satellite in orbit. Actually, telescope system is also a ground tracking station without the range information. The geometry associated with this observation is shown in Figure 3.1.

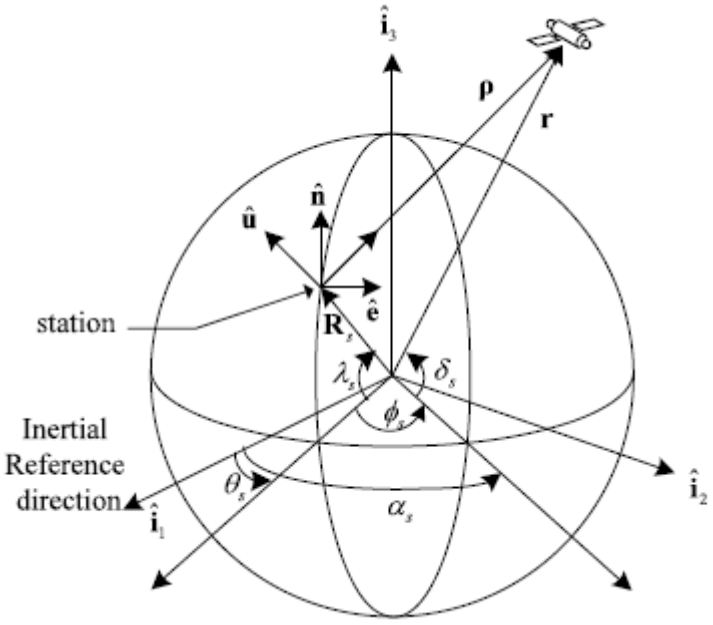

Figure 3.1. Geometry of Earth observation of satellite motion [7]

ρ is the slant range vector, r is the radius vector locating the satellite in inertial frame (ECI), R_s is the radius vector locating the ground tracking station in ECI frame, α_s and δ_s are the right ascension and declination of the satellite, respectively, θ_s is the

sidereal time of the ground station, λ_s is the latitude of the ground tracking station, and φ_s is the east longitude from the ground tracking station to the satellite. The fundamental observation is given by [7]

$$\rho = r - R_s \tag{3.1}$$

In non-rotating equatorial components the vector ρ is given by [7]

$$\rho = \begin{bmatrix} x - |R_s| \cos\lambda_s \cos\theta_s \\ y - |R_s| \cos\lambda_s \sin\theta_s \\ z - |R_s| \sin\lambda_s \end{bmatrix} \tag{3.2}$$

where x, y, and z are the components of the vector r in ECI frame. The ground tracking station coordinate system (up, east and north) is described in Figure 3.1. The conversion from the earth-fixed frame to ground tracking station coordinate is given by [7], [4]

$$\begin{bmatrix} \rho_u \\ \rho_e \\ \rho_n \end{bmatrix} = \begin{bmatrix} \cos\lambda_s & 0 & \sin\lambda_s \\ 0 & 1 & 0 \\ \sin\lambda_s & 0 & -\cos\lambda_s \end{bmatrix} \begin{bmatrix} \cos\theta_s & \sin\theta_s & 0 \\ -\sin\theta_s & \cos\theta_s & 0 \\ 0 & 0 & 1 \end{bmatrix} \rho \tag{3.3}$$

A ground tracking station measures the azimuth (az), elevation (el), and range (ρ). The measurement equations are given by following Eqs. (3.4) through (3.6) [7], [4] :

$$\rho = \sqrt{{\rho_u}^2 + {\rho_e}^2 + {\rho_n}^2} \tag{3.4}$$

$$az = \tan^{-1}\left(\frac{\rho_e}{\rho_n}\right) \tag{3.5}$$

$$el = \tan^{-1}\left(\frac{\rho_u}{\sqrt{{\rho_n}^2 + {\rho_e}^2}}\right) \tag{3.6}$$

When only one ground station is operated, the azimuth (az), elevation (el), and range (ρ) are the standard measurements. There is also the forth measurement type, turn-around range, generated by mixing two ground station's range measurements.

$$\rho_{tar} = \rho_1 + \rho_2 \tag{3.7}$$

where ρ_1 and ρ_2 is geometrical range calculated from ground station 1 and 2, respectively by using Eq. (3.4).

Since telescope system only gives angle measurements, range information is unavailable. Range is ignored in order to simulate telescope systems. For standard orbit determination procedure, both angle and range information is used to generate necessary simulated measurements.

3.2. Measurement Generation

In order to generate noisy measurements, bias and noise is added to geometrical angular and range measurements as shown in Eqs. (3.8) through (3.10).

$$\rho' = \rho + b_r + v_r \tag{3.8}$$

$$az' = az + b_{az} + v_{az} \tag{3.9}$$

$$el' = el + b_{el} + v_{el} \tag{3.10}$$

$$\rho_{tar} = \rho_1 + \rho_2 \,, \qquad b_{tar} = b_{r1} + b_{r2}, \quad v_{tar} = v_{r1} + v_{r2}$$
$$\rho'_{tar} = \rho_{tar} + b_{tar} + v_{tar} \tag{3.11}$$

where b is constant measurement bias and v is white noise.

For tar, b_{tar} and v_{tar} includes range measurement biases and noises from two ground station.

3.3. Measurement Configuration

In this section, various measurement configuration is defined to be used for the orbit determination process.

Following configurations are explained:

- Azimuth, elevation and range measurements from single ground station.
- Range and turn around range measurements (TAR) from two ground station.
- Range measurements from two ground station.

In single station configuration, the bias is only added to angular measurements. Bias-free range measurements are used to estimate angular bias. Nominal observation duration for GEO satellites operations is 48 hours. Various observation durations are also investigated in order to show their effect on orbit determination accuracy. Both range and angular measurements are generated once an hour during observation duration. Range and angular measurements are modeled without time synchronization since in real operations angular and range measurements are generated via different mechanism from each other.

In two station range and TAR configuration, TAR and range measurements are coupled with each other. TAR includes range measurements from first station. Therefore, bias is added to range from second ground stations and range from first station is bias-free. Bias of the second range measurements can be thought as a bias for TAR measurements. For bias estimation, bias-free first range measurements are used. Nominal observation duration and frequency is same with single station case. Range and TAR measurements are also not generated in the same time. In normal ranging procedure shown in Figure 3.2, the signal from ground station antenna is sent

to the satellite and signal comes back. In this way, delay in signal transfer is measured to determine range information between satellite and ground station.

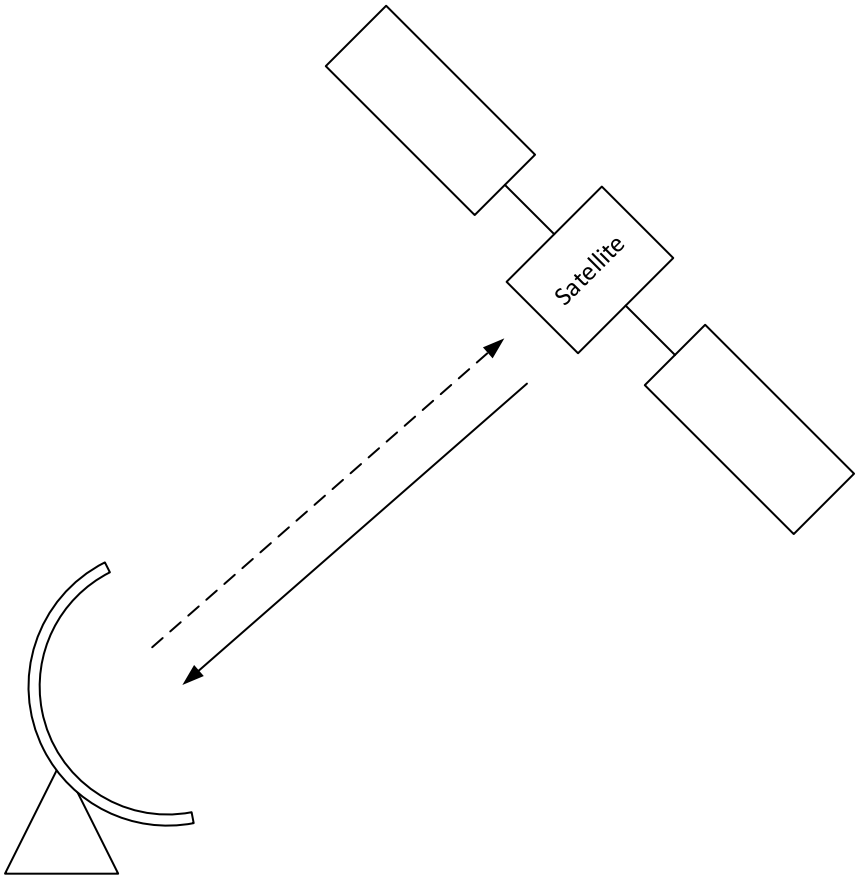

Figure 3.2. Ranging procedure

In TAR case as shown in Figure 3.3, first station sends signal to the satellite and the satellite sends this signal to the second station. Second station send back the signal to the first station by transferring signal along the satellite. Delay in this procedure gives us TAR measurements. Since signal travels more path, TAR noise is higher than range noise.

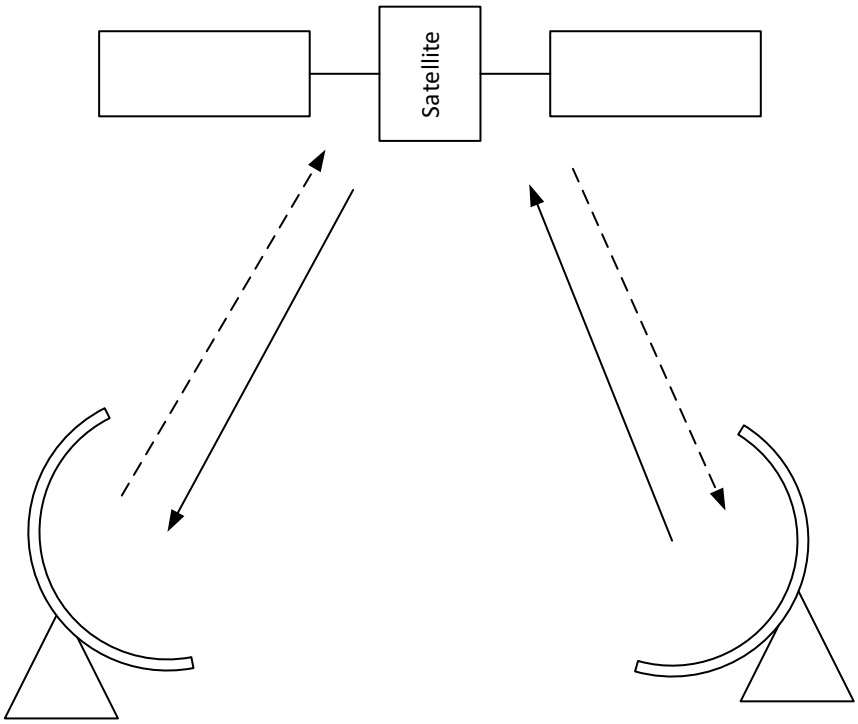

Figure 3.3. Turn-around ranging procedure

In two station range configuration, bias is added to the one of range measurements. Other observation parameters are same with range and TAR configuration. Only difference is that generation of range measurements are independent from each other. Therefore, these range measurements do not also have same time tag. Noise values are similar for both measurements.

If the maneuver is included during observation, 48 hours observation is done before and after maneuver firing time. Total 96 hour measurements with the frequency of one hour are used for the estimation process. Details of the maneuver firing simulation is shown at Figure 3.4. Initial conditions (R(0), V(0)) are propagated to time where the impulsive maneuver firing is performed (R(tf') ,V(tf')).

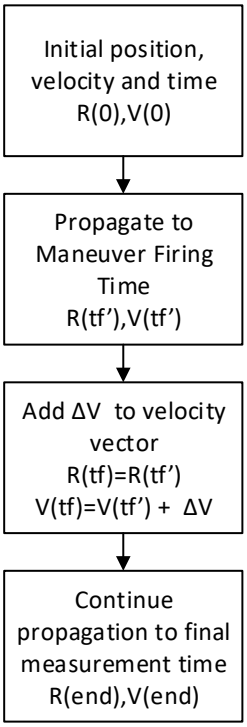

Figure 3.4. Maneuver firing simulation flow chart

At the maneuver firing time, position vector is kept as a constant and velocity change due to the maneuver is added to velocity vector in order to simulate impulsive firing. After that, new position and velocity vector including maneuver velocity is propagated to the final time of the measurements.

In angle-only orbit determination, there is only one configuration which includes azimuth and elevation measurements from one station. This configuration is similar with standard orbit determination configurations. Main difference is that angular noise level is lower than standard one. Measurement bias and other orbit parameter estimation is also not considered during angle-only estimation.

CHAPTER 4

ORBIT ESTIMATION METHODOLOGY

4.1. Introduction

Orbit estimation is the process of determining the statistically most probable spacecraft state based on erroneous observations of the spacecraft and mismodelled spacecraft motion. There are two main categories for orbit estimation: batch processing and sequential filtering. Batch estimation algorithms process all available observation set at once in order to determine the spacecraft initial state and covariance information at an epoch time. In contrast, sequential filtering processes each observation individually in order to determine the spacecraft state and covariance at the time of each observation. This chapter provides an overview for batch and sequential estimation algorithms.

4.2. Batch Estimation

4.2.1. Methodology

The batch least squares filter selects the estimate of state at a chosen epoch as the value that minimizes the sum of the squares of measurement residuals, and it is processed using an entire set of measurements simultaneously. So, the measurement function is represented as [7]

$$y_k = \begin{bmatrix} y_1 \\ y_2 \\ y_3 \\ \cdot \\ \cdot \\ \cdot \\ y_N \end{bmatrix} = \begin{bmatrix} H(x_1) \\ H(x_2) \\ H(x_3) \\ . \\ . \\ . \\ H(x_N) \end{bmatrix} + \begin{bmatrix} v_1 \\ v_2 \\ v_3 \\ \cdot \\ \cdot \\ \cdot \\ v_N \end{bmatrix} = h(x_k) + v_k \quad k = 1, \dots, N \tag{4.1}$$

where N is the number of measurement epochs, v is the measurement noise, h is measurement functions related to conversion between states and measurements as defined by using Eqs. (3.1) through (3.6). In batch least square approach, the dynamics of the unknown true orbit is linearized about the assumed reference orbit and given by

$$\Delta\dot{x}_k = F_k \Delta x_0 \tag{4.2}$$

where F represents partial derivate of the system functions related to equation of motion for satellite. h nonlinear measurement functions can be linearized as follows,

$$\Delta y_k = H_k \Delta x_k + v_k \tag{4.3}$$

where H matrix is the partial derivative of h matrix with respect to state vector.

Then, the nonlinear orbit determination problem can be transformed to the linear problem about the state deviation (Δx). When we wish to estimate the state deviation vector Δx_0 at reference time, t_0, the best estimate value ($\Delta\hat{x}_0$) of state is expressed by the normal equation as follows [7]

$$\begin{gathered} \Delta\hat{x}_0 = (AWA^T)^{-1}(AW\Delta z) \\ \hat{P}_0 = (AWA^T)^{-1} \end{gathered} \tag{4.4}$$

$$AWA^T = \sum_{k=1}^{N} (H_k F_k)^T W_k \, (H_k F_k) \tag{4.5}$$

$$AW\Delta z = \sum_{k=1}^{N} (H_k F_k)^T W_k \, \Delta z_k \tag{4.6}$$

$\Delta\hat{x}_0$ and $\hat{P}_0$ are the estimated differential correction of the state and covariance at the epoch time. The measurement residual, Δz_k, is the difference between the actual measurement and predicted measurement. . W_k is the measurement weight matrix.

4.2.2. Implementation

In current problem, measurement function partial derivative matrix , H, are composed of Eqs. (3.1) through (3.6). System function partial derivative matrix, F, is calculated by using Jacobian approximation finite difference method as shown in Eqs. (4.7) through (4.8) . Subscript k refers to the number measurements. Subscript K refers to z component of the position or velocity vector. Finite differencing method is also shown step by step in Figure 4.1.

FOR i = 1 to the number of states

Initiate with nominal initial condition

$x_{nom} = (r_{nom}, v_{nom})$

Propagate nominal state to next measurement time

$f(r_{nom}, v_{nom}, \Delta t \rightarrow r_k, v_k)$

Convert propagated nominal state to predicted measurements (obs)

h($r_k, v_k \rightarrow az_{nom}, el_{nom}, \rho_{nom}$)

Modify each component of the the nominal state vector

$\varepsilon_i = x_{nom_i}(0.01)$ modify by %1 of the original vector

$x_{mod_i} = x_{nom_i} + \varepsilon_i$

Propagate modified state to next measurement time

$f(r_{mod}, v_{mod}, \Delta t \rightarrow r_{k,} v_k)$

Convert propagated modified state to predicted measurements (obs)

h($r_k, v_k \rightarrow az_{mod}, el_{mod}, \rho_{mod}$)

Find F matrix elements by differencing modified and nominal state

$$\frac{\partial x_i}{\varepsilon_i} = \frac{x_{mod} - x_{nom}}{\varepsilon_i}$$

Find H matrix elements by differencing modified and nominal measurements

$$\frac{\partial obs_i}{\varepsilon_i} = \frac{obs_{mod} - obs_{nom}}{\varepsilon_i}$$

Reset the modified component x_{mod_i} to the its original value x_{nom_i}

Continue with next component of the state vector

Figure 4.1. Finite differencing method for F and H matrix calculation

As seen on Figure 4.1, the nominal initial state vector is propagated to the measurement time by using Eqs. (2.1) to (2.7) and converted to the predicted measurement by using Eqs. (3.1) through (3.6). In next steps, each element of the nominal initial state vector is modified to form the modified state vector. After that, modified state vector undergoes same procedure with nominal state in order to calculate modified propagated state and modified predicted measurements. By applying Eqs. (4.7) through (4.8), each element of the partial derivative matrixes is calculated.

$$F_{k,pv} = \frac{f(x_k + \varepsilon) - f(x_k)}{\varepsilon} = \frac{\partial x_k}{\partial x_0} \tag{4.7}$$

$$\frac{\partial x_k}{\partial x_0} = \begin{bmatrix} \frac{\partial r_{I_k}}{\partial r_{I_0}} & \frac{\partial r_{I_k}}{\partial r_{J_0}} & \frac{\partial r_{I_k}}{\partial r_{K_0}} & \frac{\partial r_{I_k}}{\partial v_{I_0}} & \frac{\partial r_{I_k}}{\partial v_{J_0}} & \frac{\partial r_{I_k}}{\partial v_{K_0}} \\ \frac{\partial r_{J_k}}{\partial r_{I_0}} & \frac{\partial r_{J_k}}{\partial r_{J_0}} & \frac{\partial r_{J_k}}{\partial r_{K_0}} & \frac{\partial r_{J_k}}{\partial v_{I_0}} & \frac{\partial r_{J_k}}{\partial v_{J_0}} & \frac{\partial r_{J_k}}{\partial v_{K_0}} \\ \frac{\partial r_{K_k}}{\partial r_{I_0}} & \frac{\partial r_{K_k}}{\partial r_{J_0}} & \frac{\partial r_{K_k}}{\partial r_{K_0}} & \frac{\partial r_{K_k}}{\partial v_{I_0}} & \frac{\partial r_{K_k}}{\partial v_{J_0}} & \frac{\partial r_{K_k}}{\partial v_{K_0}} \\ \frac{\partial v_{I_k}}{\partial r_{I_0}} & \frac{\partial v_{I_k}}{\partial r_{J_0}} & \frac{\partial v_{I_k}}{\partial r_{K_0}} & \frac{\partial v_{I_k}}{\partial v_{I_0}} & \frac{\partial v_{I_k}}{\partial v_{J_0}} & \frac{\partial v_{I_k}}{\partial v_{K_0}} \\ \frac{\partial v_{J_k}}{\partial r_{I_0}} & \frac{\partial v_{J_k}}{\partial r_{J_0}} & \frac{\partial v_{J_k}}{\partial r_{K_0}} & \frac{\partial v_{J_k}}{\partial v_{I_0}} & \frac{\partial v_{J_k}}{\partial v_{J_0}} & \frac{\partial v_{J_k}}{\partial v_{K_0}} \\ \frac{\partial v_{K_k}}{\partial r_{I_0}} & \frac{\partial v_{K_k}}{\partial r_{J_0}} & \frac{\partial v_{K_k}}{\partial r_{K_0}} & \frac{\partial v_{K_k}}{\partial v_{I_0}} & \frac{\partial v_{K_k}}{\partial v_{J_0}} & \frac{\partial v_{K_k}}{\partial v_{K_0}} \end{bmatrix} \tag{4.8}$$

$$F_k = \begin{bmatrix} F_{k,pv} & 0 & 0 \\ 0 & F_{bias} & 0 \\ 0 & 0 & F_{param} \end{bmatrix} \tag{4.9}$$

F matrix represents partial derivative of state vector with respect to initial conditions. F matrix includes position and velocity partial derivatives as well as bias and dynamic parameters. H matrix represents partial derivative of measurement with respect to current state vector. H matrix includes observational partial derivatives and bias parameters. By using product of H and F matrix, A partial derivative matrix of measurements with respect initial conditions can be calculated as seen on Eq. (4.12).

$$H_{k,obs} = \frac{\partial obs_k}{\partial X_k} = \begin{bmatrix} \frac{\partial \rho_k}{\partial r_{I_k}} & \frac{\partial \rho_k}{\partial r_{J_k}} & \frac{\partial \rho_k}{\partial r_{K_k}} & \frac{\partial \rho_k}{\partial v_{I_k}} & \frac{\partial \rho_k}{\partial v_{J_k}} & \frac{\partial \rho_k}{\partial v_{K_k}} \\ \frac{\partial az_k}{\partial r_{I_k}} & \frac{\partial az_k}{\partial r_{J_k}} & \frac{\partial az_k}{\partial r_{K_k}} & \frac{\partial az_k}{\partial v_{I_k}} & \frac{\partial az_k}{\partial v_{J_k}} & \frac{\partial az_i}{\partial v_{K_k}} \\ \frac{\partial el_k}{\partial r_{I_k}} & \frac{\partial el_k}{\partial r_{J_k}} & \frac{\partial el_k}{\partial r_{K_k}} & \frac{\partial el_k}{\partial v_{I_k}} & \frac{\partial el_k}{\partial v_{J_k}} & \frac{\partial el_k}{\partial v_{K_k}} \end{bmatrix} \tag{4.10}$$

$$H_k = \begin{bmatrix} H_{k,obs} & 0 \\ 0 & H_{bias} \end{bmatrix} \tag{4.11}$$

$$A_k = H_k F_k \tag{4.12}$$

W_k is the weight matrix to be used for scaling measurement's noise. Diagonal elements of the weight matrix is formed by using standard deviation of azimuth, elevation and range measurements as shown in Eq. (4.13).

$$W_k = \begin{bmatrix} {}^{1}/_{\sigma_{az}} & 0 & 0 \\ 0 & {}^{1}/_{\sigma_{el}} & 0 \\ 0 & 0 & {}^{1}/_{\sigma_{\rho}} \end{bmatrix} \tag{4.13}$$

Nonlinear LSQ implementation is shown more detailed in Figure 4.2. Initial conditions are propagated to measurement time. Then residual is calculated by subtracting estimated measurements from actual measurements. Partial derivative matrixes for dynamic model (F) and measurement model (H) is calculated by using finite differencing. $A^T W A$ and $A^T W \Delta z$ matrix is calculated for each measurement set. These matrices are accumulated until the final measurements are reached. After all, the differential correction of the state is calculated and RMS of the current estimation is compared with previous RMS values. If differences are higher than the threshold, iteration procedures start again with the corrected initial conditions. When RMS differences are within tolerances value, estimation procedures stops.

$$RMS = \sqrt{\frac{\Delta z^T W \Delta z}{n_{meas}(N)}} = \sqrt{\frac{1}{N} \frac{\frac{\sum_{k=1}^{N} (\Delta \rho_i)^2}{\sigma_{\rho}^2} + \frac{\sum_{k=1}^{N} (\Delta az_i)^2}{\sigma_{az}^2} + \frac{\sum_{k=1}^{N} (\Delta el_i)^2}{\sigma_{el}^2}}{3}} \tag{4.14}$$

RMS formulation is shown in Eq. (4.14) where $\Delta\rho$ refers to range difference between predicted and actual range measurements. Δaz and Δel refers to angular (azimuth and elevation) residuals. σ_{ρ}, σ_{az} and σ_{el} refers to standard deviation of the associated

measurements. N is the number of total measurements. n_{meas} is the number of measurement type. RMS calculation includes the sum of each measurement residual normalized by its associated standard deviation.

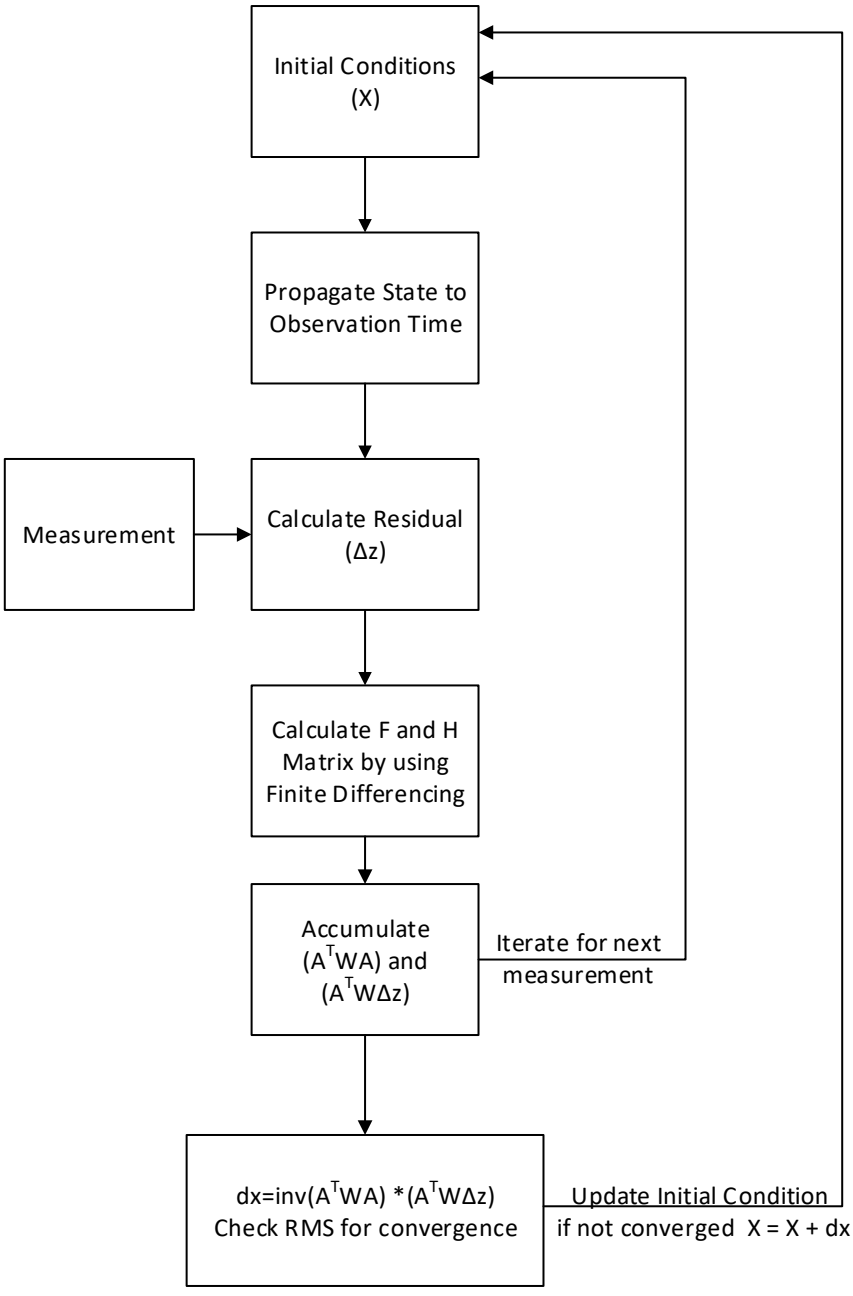

Figure 4.2. Nonlinear Least Square Implementation Flow Chart

In Eq. (4.14), the generic calculation is shown for RMS formulation. Exact calculation depends on measurement configuration. If there is only range measurement, only terms related to $\Delta\rho$ are used for RMS calculation.

Initial position and velocity information are estimated in all cases. Measurement bias estimation depends on measurement configurations. Bias parameters are considered as constant in the estimation process. Solar radiation pressure coefficient (C_p) is also estimated in all cases while keeping it as a constant. If the measurements span includes a maneuver, then maneuver velocity increments are also estimated.

For single station case, when the angular bias and maneuver velocity increments are included state matrix is shown as following way in Eq. (4.15):

$$x = \begin{bmatrix} X \\ Y \\ Z \\ V_x \\ V_y \\ V_z \\ C_p \\ b_{az} \\ b_{el} \\ \Delta V_x \\ \Delta V_y \\ \Delta V_z \end{bmatrix} \tag{4.15}$$

Symbols such as r_I, r_J, r_K and X, Y, Z can be interchangeably used. Both these terms refers to the position components as defined in x, y and z direction. Same approach is used for velocity terms between $v_I,\ v_J,\ v_K$ and V_x, V_y, V_z. Maneuver velocity increments are shown with the terms $\Delta V_x, \Delta V_y,\ \Delta V_z$.

Position and velocity parameters are estimated at initial condition's time tag. Maneuver velocity increments are estimated at time tag where maneuver is actually

fired. Typical batch estimation procedure including maneuver can be seen in Figure 4.3.

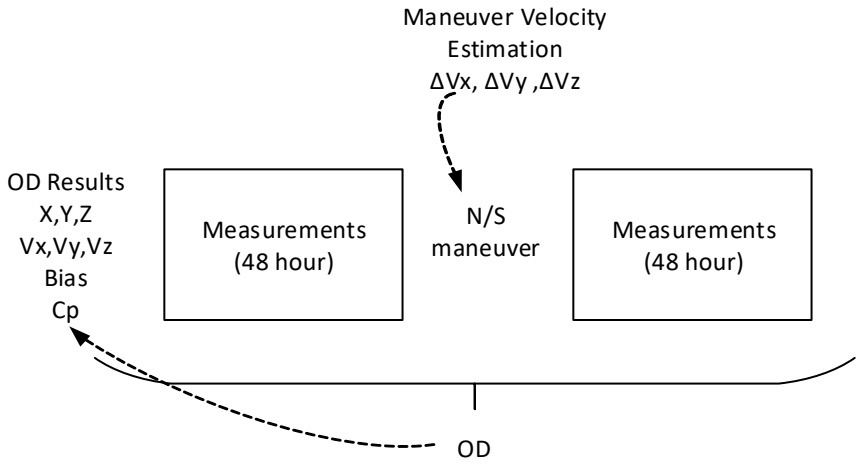

Figure 4.3. Batch orbit estimation procedure for North-South maneuver

For range-range and range-TAR configuration, state matrix is similar to Eq. (4.15). Only differences are related to bias parameter. If range-range configuration is used, only one range bias is estimated. For range-TAR configuration, only TAR bias is estimated. When there is no maneuver firing, all maneuver increment terms in state matrix are removed.

In order to model the effect of the random noise, Monte Carlo simulation is performed for all estimation procedure. Same analysis is repeated for 30 times with the different noisy measurements. Estimation results are the average of the Monte Carlo run's results as shown in Figure 4.4 and Eq. (4.16). The root mean square of the estimated state error , δx_i, is defined by

$$\delta x_i = \sqrt{\frac{1}{M}\sum_{j=1}^{M}[x_{i,j} - x_{i,ref}\,]^2} \tag{4.16}$$

where M is the number of Monte Carlo runs, subscript j denotes the jth simulation run, and subscript i represents the ith component of the state vector x and its reference value x_{ref}.

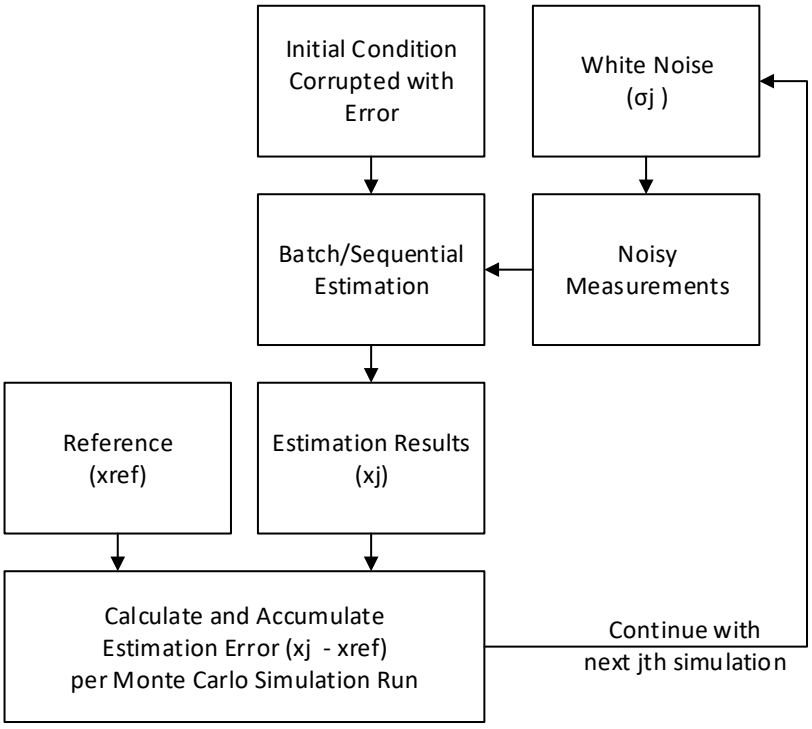

Figure 4.4. Monte-Carlo simulation flow chart

4.3. Sequential Estimation

4.3.1. Extended Kalman Filter

The extended Kalman filter provides the minimum variance estimate of the state based on statistical information about the dynamical and observation models. The continuous-time models can be converted into a discrete form through an approximate method [3]. In this section the EKF algorithm is reviewed for discrete-time nonlinear equations of the form [11], [3].

$$x_{k+1} = f(x_k, u_k, t_k) + w_k \tag{4.17}$$

$$y_k = h(x_k, t_k) + v_k \tag{4.18}$$

where x_k is the $Lx1$ state vector, y is the $nx1$ observation vector, w_k is state noise vector, and v_k measurement noise vector. It is assumed that the noise vectors are zero-mean Gaussian processes satisfying

$$E\{w_k w_j^T\} = \begin{cases} Q_k, & k = j, \\ 0, & k \neq j, \end{cases} \tag{4.19}$$

$$E\{v_k v_j^T\} = \begin{cases} R_k, & k = j, \\ 0, & k \neq j, \end{cases} \tag{4.20}$$

$$E\{v_k w_j^T\} = 0, \qquad \forall\, k, j \tag{4.21}$$

where the measurement and process noise covariance Q_k , R_k are assumed to be positive definite. Given a system model with initial state and covariance values, the EKF propagates the state vector and the error covariance matrix recursively. Then, the EKF updates the state and covariance matrix by using erroneous measurements. The update is accomplished through the Kalman gain matrix K, which is obtained by minimizing the weighted sum of the diagonal elements of the error covariance matrix. The EKF is based on the linearization by using the Taylor-series expansion of the nonlinear dynamical and measurement equations about the current estimate. For the nonlinear models as stated in Eqs. (2.1) through (2.7) ,the predictions of the state estimates and covariance are accomplished by [11]

$$\hat{x}_{k+1}^{-} = f(\hat{x}_k, t_k) \tag{4.22}$$

$$P_{k+1}^{-} = F_k P_k F_k^T + Q_k \tag{4.23}$$

where F_k is the Jacobian matrix of the nonlinear function. Measurement update equations are expressed by [11]

$$\hat{x}_{k+1}^{+} = \hat{x}_{k+1}^{-} + K_{k+1}(\tilde{y}_{k+1} - y_{k+1}^{-}) \tag{4.24}$$

$$\hat{P}_{k+1} = P_{k+1} - K_{k+1}P^{xy}{}_{k+1}K^{T}{}_{k+1} \tag{4.25}$$

$$K_{k+1} = P^{xy}{}_{k+1}(P^{y}{}_{k+1})^{-1} \tag{4.26}$$

where $\tilde{y}_{k+1}$ is the measurement vector $(n \times 1)$,y_{k+1}^{-} is the predicted measurement vector $(n \times 1)$, K_{k+1} is gain matrix $(L \times n)$. Cross covariance is expressed by [11]

$$P^{xy}{}_{k+1} = P_{k+1}^{-}H_{k+1}^{T} \tag{4.27}$$

$$P^{y}{}_{k+1} = H_{k+1}P_{k+1}^{-}H_{k+1}^{T} + R_{k+1} \tag{4.28}$$

Where $\bar{P}^{y}{}_{k}$ is measurement covariance matrix $(n \times n)$, $\bar{P}^{xy}{}_{k}$ is cross covariance matrix $(L \times n)$. In EKF algorithm the state distribution is approximated by a Gaussian random variable, which is then propagated through the first-order linearization of the nonlinear functions. These approximations, however, can introduce large errors in the true posterior mean and covariance. The UKF uses different approach to overcome this problem that is discussed in the next section.

4.3.2. Unscented Kalman Filter

UKF represents a derivative-free alternative to the extended Kalman filter (EKF), provides better performance for highly nonlinear systems. In orbit determination problem, orbit mechanics include very nonlinear force models. Therefore, UKF addresses nonlinearity problem by using unscented transformation (UT). UT is a method for calculating the statistics of a random variable which undergoes a nonlinear transformation [15] . Consider propagating a random variable x (dimension L) through a nonlinear function, $y = h(x)$. Assume x has mean $\bar{x}$ and covariance P_x . To

calculate the statistics of, we form a matrix X of $2L+1$ sigma vectors (with corresponding weights W_i), according to the following [15], [9]:

$$\begin{aligned} X_0 &= \bar{x} \\ X_i &= \bar{x} + \left(\sqrt{(L+\lambda) * P_x}\right)_i \quad i = 1, \dots, L \\ X_i &= \bar{x} - \left(\sqrt{(L+\lambda) * P_x}\right)_{i-L} \quad i = L+1, \dots, 2L \end{aligned} \tag{4.29}$$

$$\begin{aligned} W_0^{(m)} &= \lambda/(L+\lambda) \\ W_0^{(c)} &= \lambda/(L+\lambda) + (1 - \alpha^2 + \beta) \\ W_i^{(m)} &= W_i^{(c)} = 1/(2(L+\lambda)) \quad i = 1, \dots, 2L \end{aligned} \tag{4.30}$$

where $\lambda = \alpha^2(L+\kappa) - L$ is a scaling parameter. α determines the spread of the sigma points around $\bar{x}$. κ is a secondary scaling parameter which is usually set to 0, and β is used to incorporate prior knowledge of the distribution of (for Gaussian distributions $\beta = 2$, is optimal). $\left(\sqrt{(L+\lambda) * P_x}\right)_i$ is the ith row of the matrix square root. These sigma vectors are propagated through the nonlinear function,

$$y_i = h(x_i) \;\; i = 0, \dots, 2L,$$

and the mean and covariance for y are approximated using a weighted sample mean and covariance of the posterior sigma points [9],

$$\bar{y} = \sum_{i=0}^{2L} W_i^{(m)} y_i \tag{4.31}$$

$$P_y = \sum_{i=0}^{2L} W_i^{(c)} (y_i - \bar{y})(y_i - \bar{y})^T \tag{4.32}$$

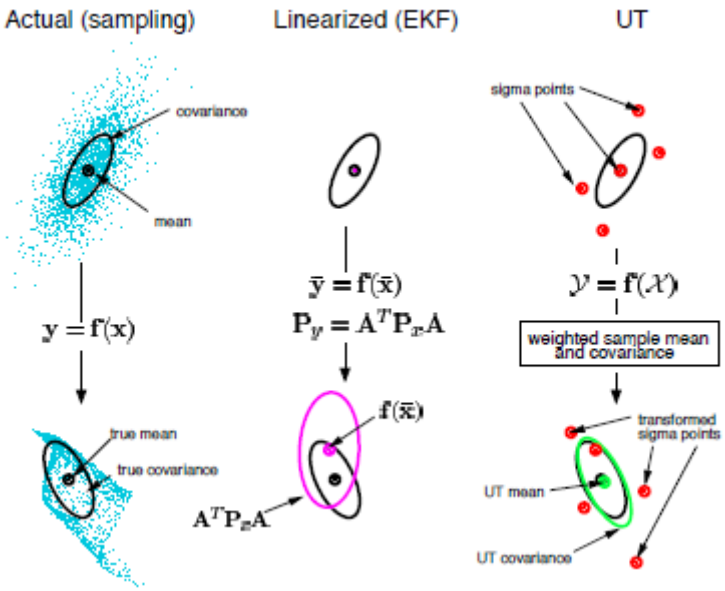

Figure 4.5. Example of the UT for mean and covariance propagation [15] a) actual, b) first-order linearization (EKF), c) UT.

In state estimation process, UKF has two main part; first one is state prediction, which is orbit propagation, and second one is updating state with measurements, which are azimuth, elevation angles and range.

Basic framework of nonlinear dynamic systems for kalman filter can be represented as

$$x_{k+1} = f(x_k, u_k, t_k) + w_k \tag{4.33}$$

$$y_k = h(x_k, t_k) + v_k \tag{4.34}$$

where x_k is state of nonlinear system, y_k is measurement, u_k is input, w_k and v_k are process and measurement noises respectively. f represents system functions related to equation of motion for satellite. h is measurement functions related to conversion between states (positions) to azimuth and elevation angles.

UKF equations are given with assuming addictive noise in Figure 4.6.

Initialize with:

$$\hat{x}_0 = E[x_0]$$

$$P_0 = E[(x_0 - \hat{x}_0)]$$

for $k \in \{1, \dots, \infty\}$,

Calculate sigma points:

$\hat{x}_{i|k} = [x_k \; x_k \pm \left(\sqrt{(L+\lambda) * P_k}\right)_i] \quad i = 1, \dots, 2L$

where L is the state dimension

Time (state) Update:

$\bar{x}_{i|k+1} = f(\hat{x}_{i|k}, t_k)$

$$\bar{x}_{k+1} = \sum_{i=0}^{2L} W_i^{(m)} \bar{x}_{i|k+1} \; i = 1, \dots, L$$

$$\bar{P}_{k+1} = \sum_{i=0}^{2L} W_i^{(c)} \left(\bar{x}_{i|k+1} - \bar{x}_{k+1}\right)\left(\bar{x}_{i|k+1} - \bar{x}_{k+1}\right)^T + Q_{k+1}$$

Measurement Update:

$\gamma_{i|k+1} = h(\bar{x}_{i|k+1}, t_{k+1})$

$$\bar{y}_{k+1} = \sum_{i=0}^{2L} W_i^{(m)} \gamma_{i|k+1} \; i = 1, \dots, L$$

$$\bar{P}^{y}{}_{k+1} = \sum_{i=0}^{2L} W_i^{(c)} \left(\gamma_{i|k+1} - \bar{y}_{k+1}\right)\left(\gamma_{i|k+1} - \bar{y}_{k+1}\right)^T + R_{k+1}$$

Cross covariance:

$$\bar{P}^{xy}{}_{k+1} = \sum_{i=0}^{2L} W_i^{(c)} \left(\bar{x}_{i|k+1} - \bar{x}_{k+1}\right)\left(\gamma_{i|k+1} - \bar{y}_{k+1}\right)^T$$

$$K_{k+1} = \bar{P}^{xy}{}_{k+1}(\bar{P}^{y}{}_{k+1})^{-1}$$

$$\hat{x}_{k+1} = \bar{x}_{k+1} + K_{k+1}(\tilde{y}_{k+1} - \bar{y}_{k+1})$$

$$\hat{P}_{k+1} = \bar{P}_{k+1} - K_{k+1}\bar{P}^{xy}{}_{k+1}K^{T}{}_{k+1}$$

where $\tilde{y}_{k+1}$ is observed measurement vector and its dimension $(n \times 1)$ (n is measurement number , K_{k+1} is is gain matrix $(L \times n)$, $\bar{y}_k$ is predicted measurement $(n \times 1)$, $\bar{P}^{y}{}_{k}$ is measurement covariance matrix $(n \times n)$, $\bar{P}^{xy}{}_{k}$ is cross covariance matrix $(L \times n)$.

Figure 4.6. Unscented Kalman Filter Algorithm [14]

4.3.3. Implementation

In single station case, state matrix is same with batch method as shown in Eq. (4.35).

$$x_k = \begin{bmatrix} X \\ \mathrm{Y} \\ \mathrm{Z} \\ V_x \\ V_y \\ V_z \\ C_p \\ b_{az} \\ b_{el} \\ \Delta V_x \\ \Delta V_y \\ \Delta V_z \end{bmatrix} \tag{4.35}$$

The measurements configurations are also same with batch method. Typical measurements are shown in Eq. (4.36).

$$y_k = \begin{bmatrix} az \\ el \\ \rho \end{bmatrix} \tag{4.36}$$

In range and TAR cases, bias parameter is switched with necessary parameters. However, state matrix is similar with batch method's state matrix. In sequential estimation process, all the parameter in state matrix are estimated continuously whenever an observation is available. F matrix includes nonlinear propagation of the equation of motion. H matrix include nonlinear transformation between state vector and observation vector. H and F the partial derivative matrixes can be calculated by using similar finite differencing method as shown in Eqs. (4.7) through (4.11) for Extended Kalman Filter algorithm. Q process noise matrix are shown in Eqs. (4.37) and (4.38).

$$Q_{k,pv} = \begin{bmatrix} Q_X & 0 & 0 & 0 & 0 & 0 \\ 0 & Q_Y & 0 & 0 & 0 & 0 \\ 0 & 0 & Q_Z & 0 & 0 & 0 \\ 0 & 0 & 0 & Q_{V_X} & 0 & 0 \\ 0 & 0 & 0 & 0 & Q_{V_Y} & 0 \\ 0 & 0 & 0 & 0 & 0 & Q_{V_Z} \end{bmatrix} \tag{4.37}$$

$$Q_k = \begin{bmatrix} Q_{k,pv} & 0 & 0 \\ 0 & Q_{bias} & 0 \\ 0 & 0 & Q_{param} \end{bmatrix} \tag{4.38}$$

$$R_k = \begin{bmatrix} \sigma_{az} & 0 & 0 \\ 0 & \sigma_{el} & 0 \\ 0 & 0 & \sigma_{range} \end{bmatrix} \tag{4.39}$$

R measurement noise matrix is shown in Eq. (4.39). Initial covariance matrix is shown in Eq. (4.40) and (4.41).

$$P_{k,pv} = \begin{bmatrix} P_X & 0 & 0 & 0 & 0 & 0 \\ 0 & P_Y & 0 & 0 & 0 & 0 \\ 0 & 0 & P_Z & 0 & 0 & 0 \\ 0 & 0 & 0 & P_{V_X} & 0 & 0 \\ 0 & 0 & 0 & 0 & P_{V_Y} & 0 \\ 0 & 0 & 0 & 0 & 0 & P_{V_Z} \end{bmatrix} \tag{4.40}$$

$$P_k = \begin{bmatrix} P_{k,pv} & 0 & 0 \\ 0 & P_{bias} & 0 \\ 0 & 0 & P_{param} \end{bmatrix} \tag{4.41}$$

CHAPTER 5

ANGLE ONLY ORBIT DETERMINATION RESULTS

5.1. Simulation Setup Parameters

In angle only orbit determination procedure, as stated before, only azimuth and elevation measurement from an optical ground station is used for position estimation. Simulation parameters [1] and the details of the angle-only orbit determination process is shown in Figure 5.1.

This analysis includes the following assumptions:

- None of the angular measurement biases are considered.
- No maneuver firing is included.
- Orbit propagation model is same for both reference orbit and estimation method.
- The weather conditions are always available for continuous observation.

The details of this analysis is presented in previous work [1]. In this section, the summary of the angle-only orbit estimation results is presented. In the following, the orbit determination procedure for GEO satellite tracked with telescope is addressed. Analysis parameters were shown at Table 5.1. In the analysis, only one observation site (Ankara) was used to estimate orbit for GEO satellites.

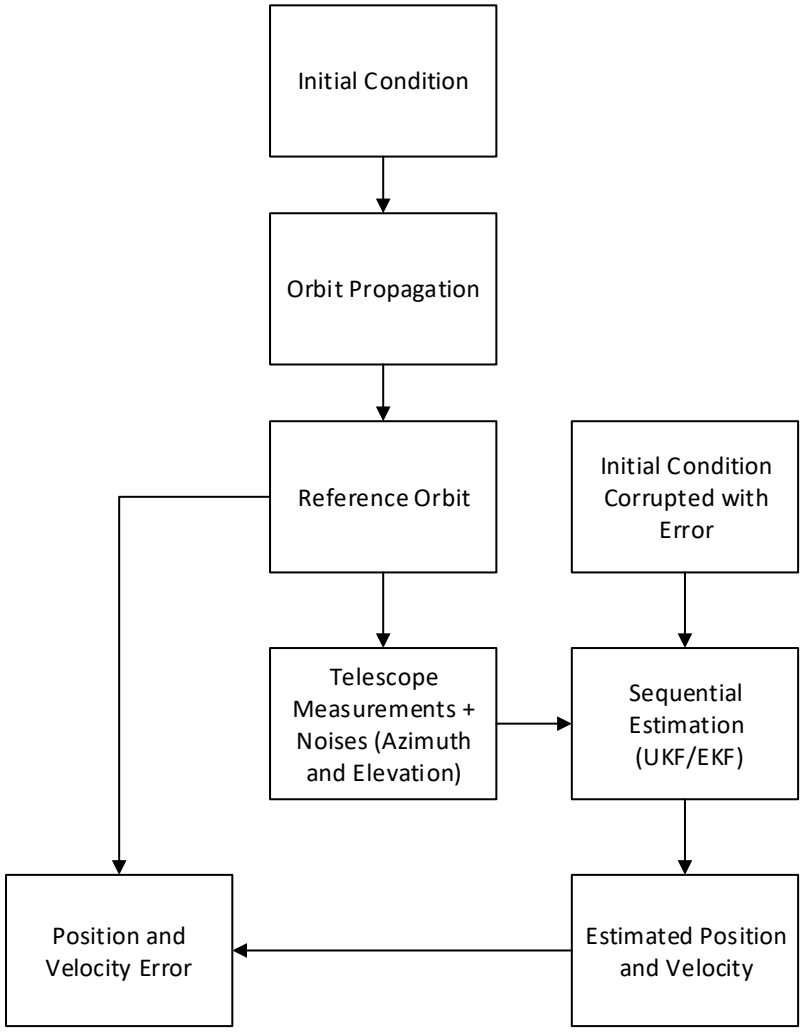

Figure 5.1. Angle-only estimation procedure

Table 5.1. Analysis parameters for angle-only orbit determination

Observation Sites	Ankara
Angle measurement noise (1 sigma)	0.00138 degree
Noise characteristics	Gauss
Initial average position error	17.32 km
Initial average velocity error	17.32 m/s
Orbit propagation model	Two-body, J8x8 potential, luni-solar attraction and solar radiation pressure

5.2. Analysis Results

GEO satellite can be observed continuously whole night with a telescope system at Ankara assuming weather conditions are available. The orbit estimation process was conducted with different observations, ranging from 600 to 10 samples. To test the effect of observation frequency same 600-minute observation period is sampled at different frequencies. These frequencies include 60, 72, 80, 120, 300, 600, 1800, 3600 second measurement periods. These periods represent 600, 500, 450, 300, 120, 60, 20, 10 observation data points.

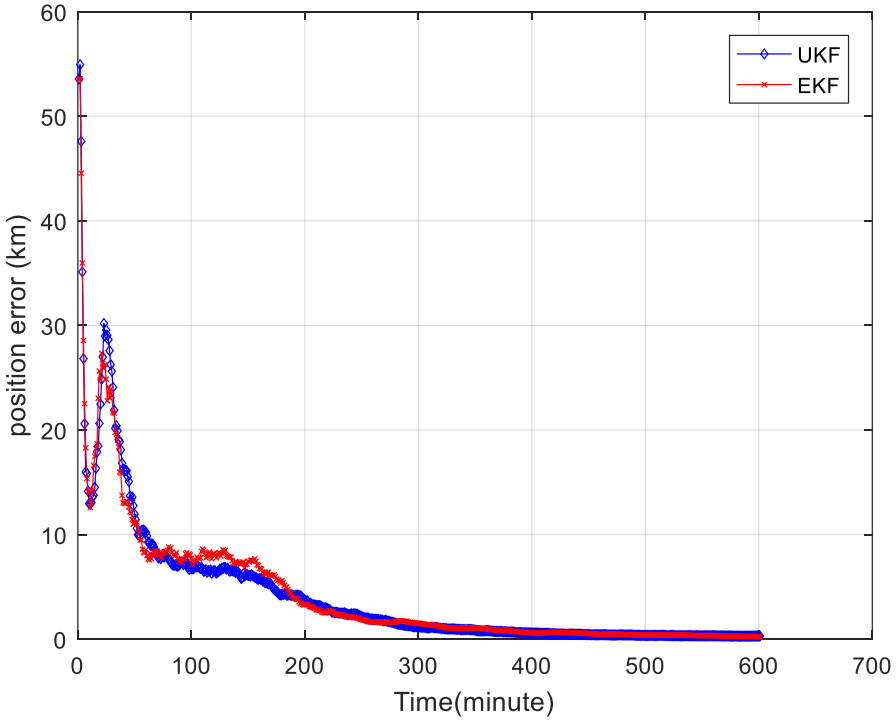

Figure 5.2. Position error for 1-minute measurement frequency with fixed 600-minute observation duration

In Figure 5.2, the sequential estimated position errors for both UKF and EKF are shown for 1-minute measurement frequency. It is clearly seen than both UKF and EKF results converges to almost same value which is around 0.2 km.

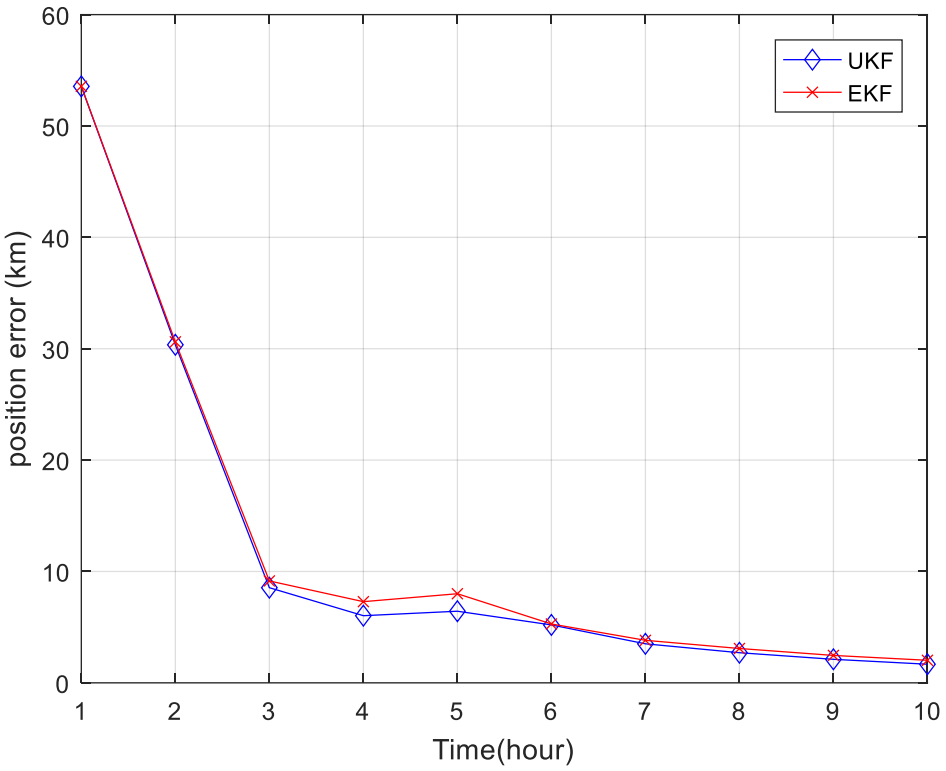

Figure 5.3. Position error for 1-hour measurement frequency with fixed 600-minute observation duration

In Figure 5.3, the sequential estimated position errors for both UKF and EKF are shown for 1-hour measurement frequency with fixed 600-minute observation duration. As seen on 1-minute measurement frequency condition, both UKF and EKF converges to the same value. Final EKF and UKF estimation results for frequency case are shown in Figure 5.4. In Figure 5.4, only final value of the sequential

estimation results is given in graph in order to compare the estimation accuracy of the different measurement frequencies.

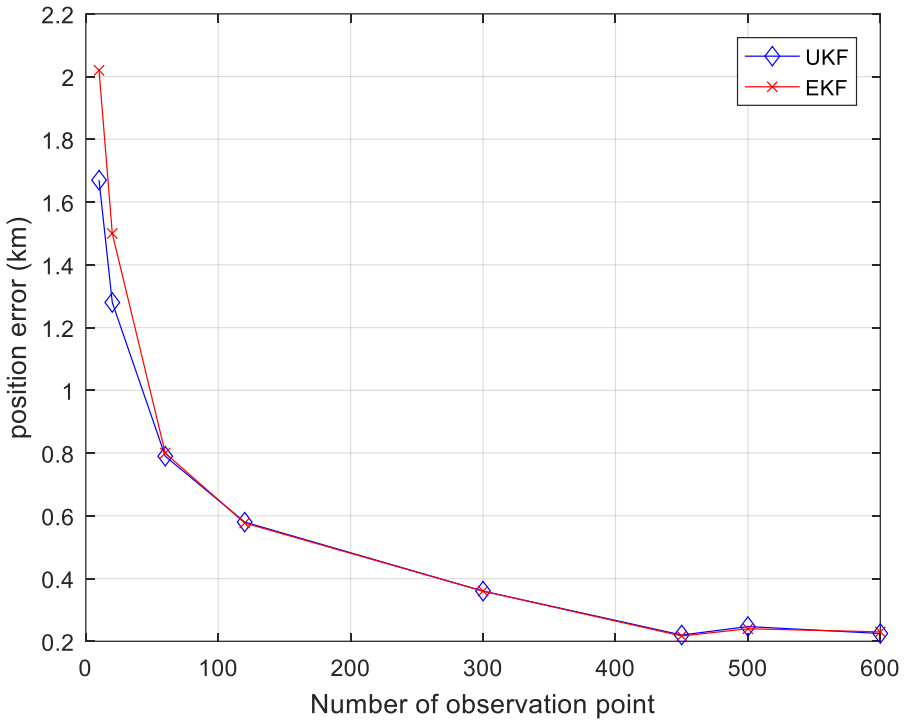

Figure 5.4. Position error for frequency case

For frequency case, as seen from Figure 5.4, when observation frequency lower than 2 minute with 60 measurement points, EKF results are deviated UKF results. This shows that nonlinear terms start to become important and ignoring these terms introduce high errors. However, when the number of measurement is higher than 60 measurement point, both UKF and EKF give similar results. Figure 5.4 also shows that increase in observation frequency can have clearly important effect on orbit estimation accuracy for GEO satellites. After some point, the increasing observation frequency doesn't improve the estimation accuracy significantly for fixed observation duration.

For duration case, to test the effect of observation duration, the data is sampled at 1 min intervals. Thus, when 60 samples are used in estimation, the observation period is 60 minutes. Different observation duration includes 60, 120, 300, 450, 500 and 600 observation points. Estimation results are shown in Figure 5.5 through Figure 5.7.

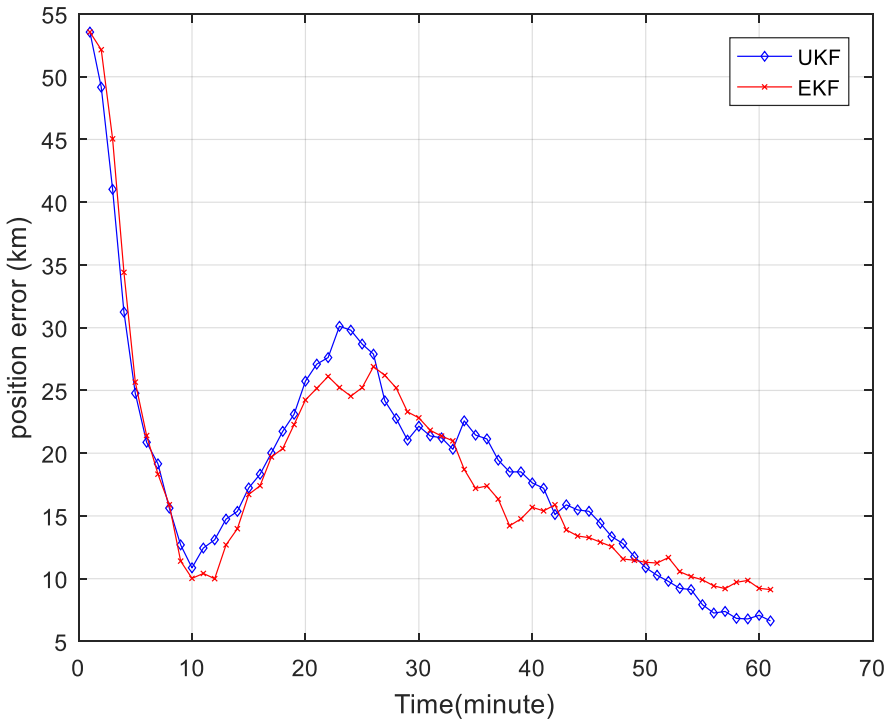

Figure 5.5. Position error for 60-minute observation with fixed 1-minute measurement frequency

In Figure 5.5, the sequential estimated position errors for both UKF and EKF are shown for 60-minute observation duration with fixed 1 minute measurement frequency. It is clearly seen than both UKF and EKF results doesn't converges to a final value since the oscillations in position error still exist. This show that 60-minute observation duration is not sufficient for the filter convergence.

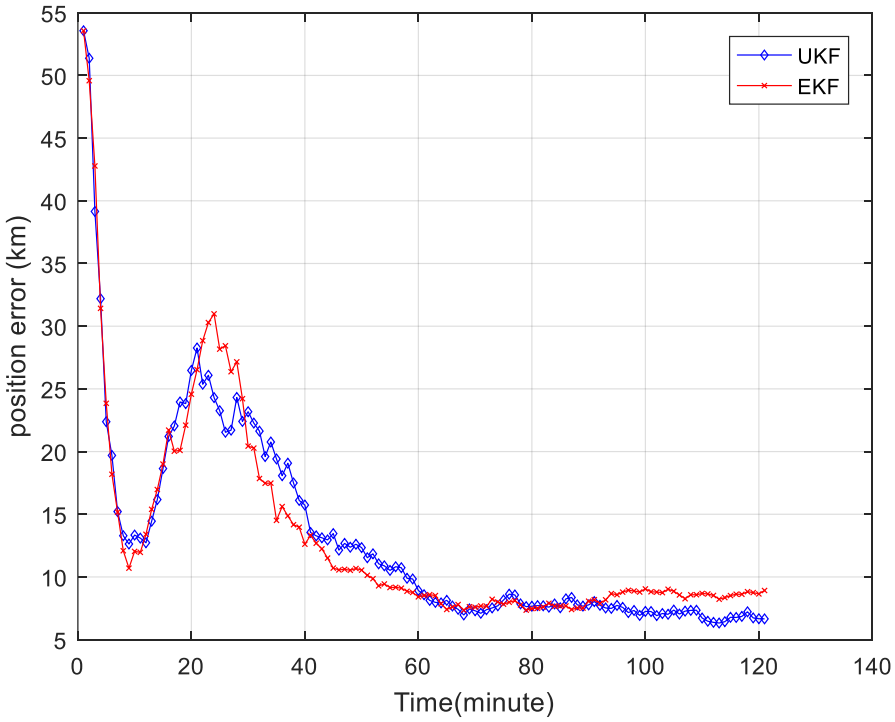

Figure 5.6. Position error for 120-minute observation with fixed 1-minute measurement frequency

In Figure 5.6, the sequential estimated position errors for 120-minute observation duration. It is clearly seen than both UKF and EKF results can converge to a final value although small oscillations exist. When observation duration exceeds approximately 90 minutes, UKF gives better results compared to EKF.

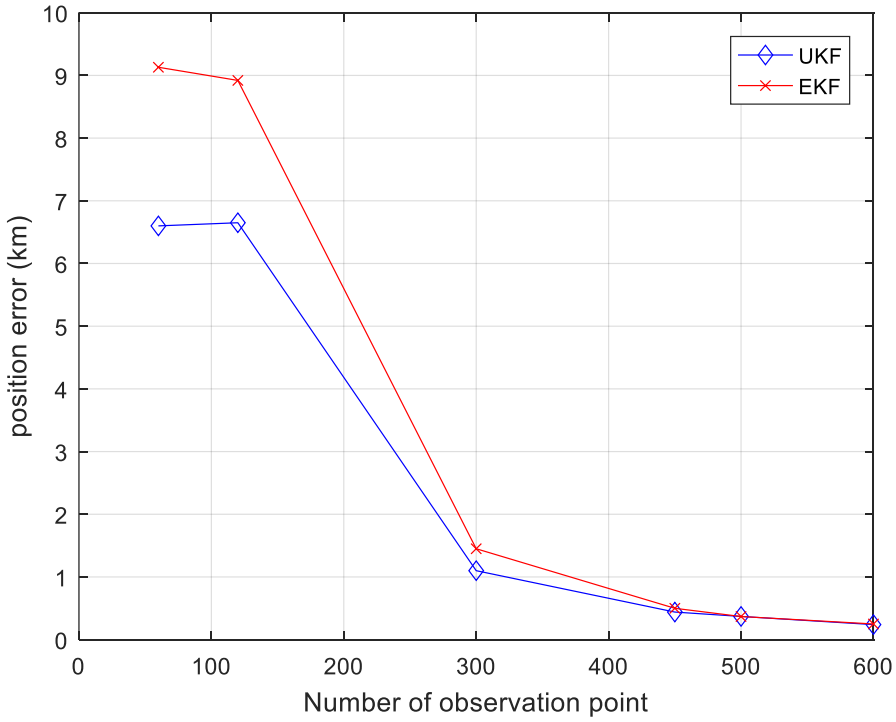

Figure 5.7. Position error for duration case

In Figure 5.7, final EKF and UKF estimation results for frequency case are shown for different observation duration. When number of observation point are higher than 450 points, both EKF and UKF give similar results. However, for 300 observation points and lower condition, UKF gives better results than EKF since the nonlinear terms start to become important and ignoring these terms introduce high errors.

As a result, it is clearly seen that UKF is generally better EKF when the number of observation points drop certain number. In this analysis, for frequency case 60 measurement points can be considered as a break point. For duration case, the break point can be accepted as 300 points.

CHAPTER 6

STANDARD ORBIT DETERMINATION RESULTS

6.1. Simulation Setup Parameters

In this analysis, both angle and range measurements generated by ground station are used to estimate the orbit information of satellite. The accuracy of the batch LSQ method is investigated through simulated measurements. Estimation results are also checked for the requirements as stated in CHAPTER 1. Similar batch analysis was also performed in previous works [2],[6] for analysis cases shown at Table 6.1. In first work [2], batch method is combined with sequential method in order to investigate this combined estimation algorithm effects on orbit determination accuracy. In this thesis, combined estimation strategy is not considered. The effect of the batch and sequential estimation methods on orbit determination process is addressed separately.

Table 6.1. Analysis Cases

Cases	Description	Ground stations
Case -1	Azimuth, elevation bias and Cp estimated	Ankara (angle and range measurements: 1 h interval)
Case -2	Turn-Around range bias and Cp estimated	Ankara (range measurements: 1 h interval) Balıkesir (Turn-Around range measurements: 1 h interval)
Case -3	Range bias and Cp estimated	Ankara (range measurements: 1 h interval) Balıkesir (range measurements : 1 h interval)

In second work [6], batch algorithm is investigated alone with same cases shown at Table 6.1. However, investigated configurations and parameter are much limited than the works performed during this chapter. Not all results of the batch were presented in

previous works. In this thesis, batch and sequential estimation method is analyzed for the different measurement configurations, duration and noise values, and different maneuver configurations.

There are two main estimation method used for orbit determination analysis as stated before. Required measurements are generated using simulations shown at Figure 6.2 and Figure 6.1.

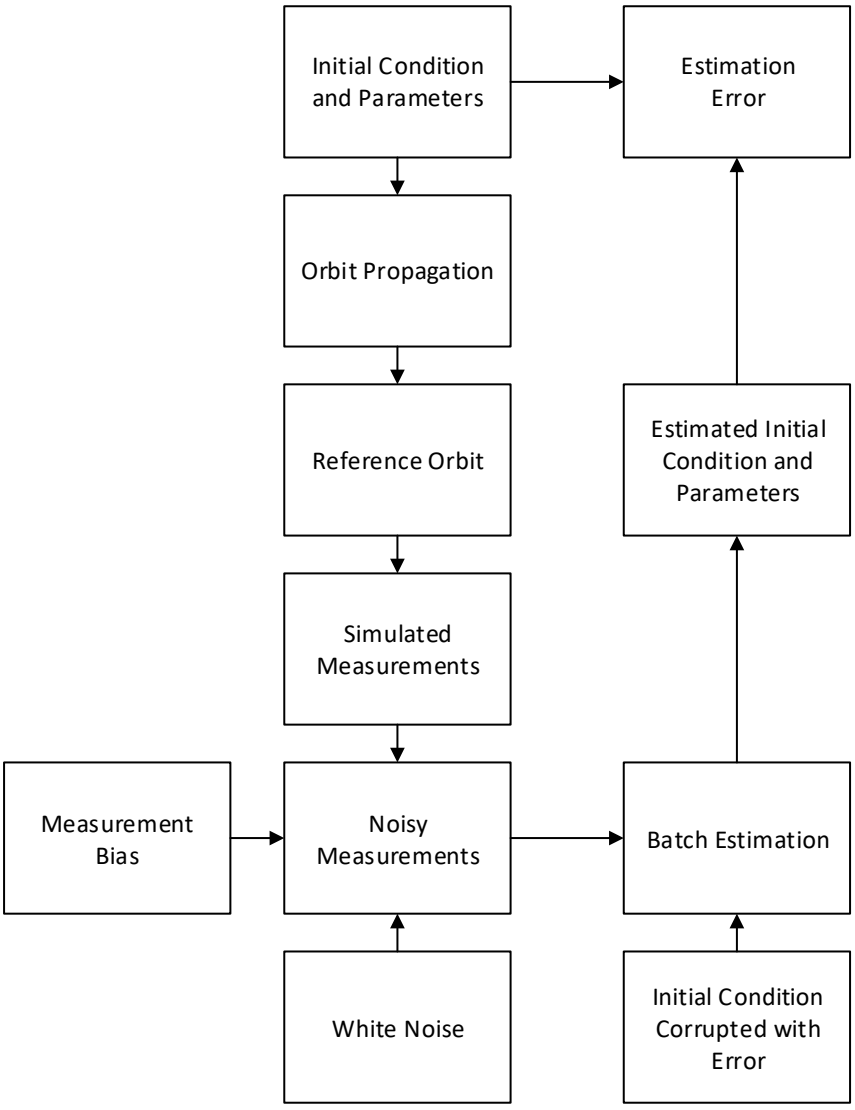

Figure 6.1. Batch estimation Flow Chart

Reference orbit is generated by propagating true initial condition to desired time. True measurements are then generated by using reference position vectors. Bias and noise values, shown at Table 6.2, are added to measurements. These noisy measurements become input for estimation algorithms. In batch estimation, whole measurements are used at once in order to estimate initial conditions and orbit parameters.

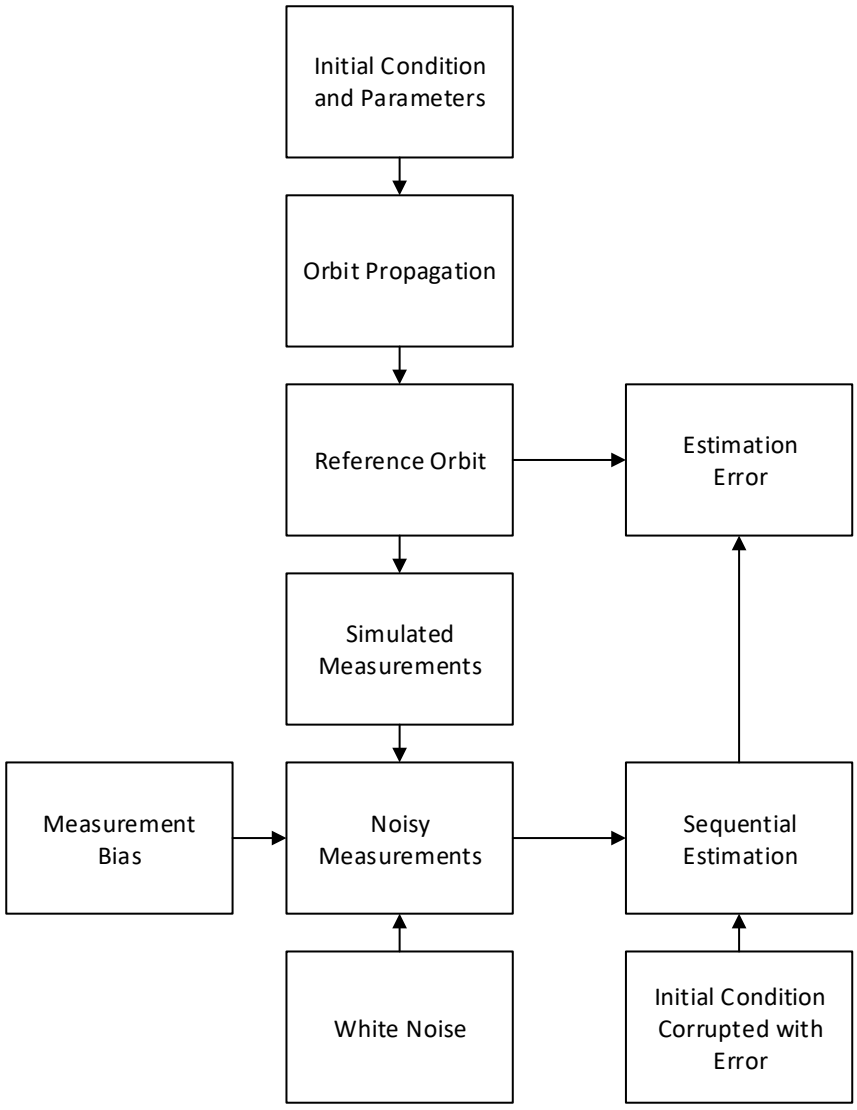

Figure 6.2. Sequential Estimation Flow Chart

Orbit parameters include measurements bias, solar radiation coefficient and, if available, maneuver velocity increments. After estimation process, estimated initial conditions and parameters are compared to true values and estimation error is calculated.

Table 6.2. Measurement Bias Information

Measurement info	Values
Angle Bias	0.01 deg
Range Bias	25 meter
TAR Range Bias	50 meter

In sequential estimation, orbit information and parameters are estimated whenever measurements are available. Estimated orbit is compared to reference orbit to calculate estimation error. Angle measurement noise and bias are same for both azimuth and elevation angles. In Case-1, only angle bias and Cp is estimated along with orbit information. In Case-2 and Case-3, turn-around bias and range bias are estimated respectively.

Analysis parameters are shown at Table 6.3. The ground stations located Ankara and Balıkesir are used for measurement generation. Constant values are added to initial position and velocity in order to represent the erroneous initial conditions. Force model for orbit propagation is intentionally configured with different parameter for estimation procedure and simulated measurement data. Force model for simulation is more accurate as shown in Table 6.3. This approach may be more realistic for testing. The orbit calculated from the more precise force model is considered as a reference orbit, and is also used for verifying the accuracy of the orbit determination. In order to test the parameter estimation ability of the batch and sequential algorithm, solar radiation pressure coefficient parameter (Cp) is set to 1.5 for estimation process and is set to 1.7 for reference orbit simulation. Then, it can be observed whether estimated parameter is close to true value. Same strategy is also applied to measurement bias.

Table 6.3. Analysis parameters for standard orbit determination

Observation Sites	Ankara-Balıkesir
Initial position error	10 km
Initial velocity error	10 m/s
Propagation force model for estimation	Two-body, J8x8 potential, luni-solar attraction and solar radiation pressure
Propagation force model for reference (simulated) orbit	Two-body, J40x40 potential, luni-solar attraction and solar radiation pressure

6.2. Batch Orbit Estimation without Maneuver

In this section, the bath estimation analysis is done for pre-defined cases. In first analysis, only position and velocity estimation errors are calculated and summarized for different observation durations and noise values shown at Table 6.4. Selected observation durations are 12, 24 and 48 hours. All noise value is assumed as a Gaussian (white) noise. Standard deviation of the noises is given in 3 sigma values.

Table 6.4. Measurement Noise Modes

Measurement info	Mode 1	Mode 2	Mode 3	Mode 4	Unit
Angle Noise (3 sigma)	7.5	15	30	45	mdeg
Range Noise (3 sigma)	4.5	7.5	15	30	m
TAR Range Noise (3 sigma)	9	15	30	60	m

All position and velocity estimation errors are given in three dimensional at 3 sigma values. Orbital element error for different noise modes are given in annex A.

Table 6.5. Case-1 3-D position estimation errors for various observation duration and noise modes

Duration (hour)	Mode 1	Mode 2	Mode 3	Mode 4	Unit
12	24.43	47.42	74.83	147.2	km
24	1.56	3.12	5.50	10.4	km
48	1.04	1.92	4.06	4.45	km

Table 6.6. Case-1 3-D velocity estimation errors for various observation duration and noise modes

Duration (hour)	Mode 1	Mode 2	Mode 3	Mode 4	Unit
12	179.2	345.9	549.5	1076.7	cm/s
24	12.0	22.7	41.1	79.3	cm/s
48	7.36	10.7	30.3	40.5	cm/s

From Table 6.5 and Table 6.6, error differences for different duration and modes are shown for Case-1. When the noise values are increased, estimation errors also increase as expected. For 24 and 48-hour duration, errors are relatively low compared to 12-hour duration case. 12 hour measurements are not enough for convergence since its error deviates from true value too much. Hwang and Lee, in their work, can achieve less than 1.5 km (3 sigma) position accuracy by using angular noise 11 mili degree and 10 meter range noise [16]. Their assumption was that azimuth bias is corrected with bias-free measurements additional ground station. In Table 6.5 , bias-free range measurements from single station instead of the additional ground station are applied to estimate angular bias. Therefore, the estimation error is around 1.9 km (3 sigma) for Mode-2 which has closest noise values to Hwang and Lee's parameter. If the noise values are adjusted according to Mode-1, the position accuracy less than 1.5 km (3 sigma) can be achievable as seen on Table 6.5.

Table 6.7. Case-2 3-D position estimation errors for various observation duration and noise modes

Duration (hour)	Mode 1	Mode 2	Mode 3	Mode 4	Unit
12	36.0	56.17	111.2	217.6	km
24	1.6	2.38	5.09	11.1	km
48	0.86	1.24	2.99	5.46	km

Table 6.8. Case-2 3-D velocity estimation errors for various observation duration and noise modes

Duration (hour)	Mode 1	Mode 2	Mode 3	Mode 4	Unit
12	260.6	409.4	802.3	1567.0	cm/s
24	10.5	19.0	33.1	67.2	cm/s
48	5.55	11.1	25.9	38.7	cm/s

From Table 6.7 and Table 6.8, case-2 estimation errors are lower than case-1. The change in error according to different durations and modes is similar to case-1. As stated before, Hwang and Lee achieved orbit determination accuracy less than 1 km (3 sigma) by using angular and range measurement two ground station [16]. In Table 6.7, the estimation error is around 1.2 km (Mode-2) which is higher than Hwang and Lee's results since TAR measurement higher noise may increase error. When the noise values for Mode-1 are used, similar accuracy can be achieved with Hwang and Lee.

Table 6.9. Case-3 3-D position estimation errors for various observation duration and noise modes

Duration (hour)	Mode 1	Mode 2	Mode 3	Mode 4	Unit
12	22.9	38.1	75.8	153.7	km
24	1.1	1.93	3.2	7.4	km
48	0.4	0.79	1.3	3.5	km

Table 6.10. Case-3 3-D velocity estimation errors for various observation duration and noise modes

Duration (hour)	Mode 1	Mode 2	Mode 3	Mode 4	Unit
12	165.9	275.8	548.3	1114.0	cm/s
24	7.8	13.1	23.0	49.5	cm/s
48	3.36	6.39	12.02	23.3	cm/s

From Table 6.9 and Table 6.10, it is clearly seen that lowest estimation error values are achieved since case-3 includes two separate range measurements from two ground station. Orbit determination accuracy less than 1 km can easily be achieved for Mode-1 and Mode-2. Although some parameters and configuration differences exist between this and Hwang and Lee' works, similar estimation accuracy is achieved for two ground station cases.

In this section, bath estimation analysis is performed more detailed for Mode-1. In addition to this, the results of this analysis are checked for whether orbit determination requirements are satisfied or not. Errors are given at 3 sigma values for below tables and are expressed at RSW coordinate frame. (R = Radial, S= Along-Track, W= Cross-Track).

Table 6.11. Case-1 position estimation errors in RSW frame for various observation duration

Duration (hour)	Along-Track (km)	Cross-Track (km)	Radial (km)	Three-dimensional (km)
12	24.3	1.87	0.77	24.4
24	1.04	1.16	0.12	1.56
48	0.24	1.01	0.10	1.04

As seen from Table 6.11 through Table 6.13, it is clearly seen that analysis with 24 and 48 hour measurements gives reduced error compared to initial condition errors.

However, 12 hour measurements are not sufficient to reduce error and so, results are not converged.

Table 6.12. Case-1 velocity estimation errors in RSW frame for various observation duration

Duration (hour)	Along-Track (cm/s)	Cross-Track (cm/s)	Radial (cm/s)	Three-dimensional (cm/s)
12	2.94	33.5	175.9	179.20
24	0.88	9.52	7.28	12.01
48	0.78	7.25	1.03	7.36

Table 6.13. Case-1 orbital element estimation errors in RSW frame for various observation duration

Duration (hour)	Semi-Major Axis (m)	Inclination (mdeg)	Longitude (mdeg)
12	789.5	6.7	33.0
24	41.7	2.37	1.4
48	3.85	1.92	0.32
Reference	30	1	3

Table 6.14. Case-1 parameter estimation errors for various observation duration

Duration (hour)	AzBias (mdeg)	ElBias (mdeg)	RangeBias (m)	Cp
12	20.45	10.88	0.000	1.66
24	10.14	10.03	0.000	1.71
48	9.98	10.07	0.000	1.70
True Value	**10**	**10**	**0**	**1.7**

From Table 6.14, angle bias value, especially azimuth bias, is not converged for 12 hour duration. Therefore, LSQ method couldn't find effectively initial condition. 48-hour duration results are better than 24 hour results as expected since increase in measurement number decreases estimation errors. It is also clearly seen that main error contribution occurs in cross-track direction for position and velocity values. Longitude requirement can be satisfied with 24 and 48 hour measurement duration as seen at

Table 6.13. However, semi-major axis requirement can only be satisfied with 48-hour duration. Inclination requirement can't be satisfied with any configuration for Case-1. This can be considered acceptable since the requirements are determined for two ground station cases. Therefore, single station case can be used as a redundant method when the measurement from second ground station is no available.

Table 6.15. Case-2 position estimation errors in RSW frame for various observation duration

Duration (hour)	Along-Track (km)	Cross-Track (km)	Radial (km)	Three-dimensional (km)
12	35.61	5.34	0.74	36.02
24	0.93	1.30	0.15	1.60
48	0.17	0.83	0.08	0.85

Table 6.16. Case-2 velocity estimation errors in RSW frame for various observation duration

Duration (hour)	Along-Track (cm/s)	Cross-Track (cm/s)	Radial (cm/s)	Three-dimensional (cm/s)
12	2.36	59.96	253.66	260.66
24	1.06	8.35	6.33	10.54
48	0.64	5.45	0.76	5.54

Table 6.17. Case-2 orbital element estimation errors in RSW frame for various observation duration

Duration (hour)	Semi-Major Axis (m)	Inclination (mdeg)	Longitude (mdeg)
12	1129.9	13.33	48.4
24	34.9	2.35	1.26
48	3.08	1.52	0.23
Reference	30	1	3

From Table 6.15 through Table 6.17, it may be observed that Case-2 overall estimation error is lower than Case-1 since range measurements are more accurate than the angular measurements. In this analysis, range and turn-around range measurements are used to estimate initial conditions and parameters similar to Case-1. 12-hour

duration results are worse than other duration sets as expected. As seen on Table 6.17, only semi-major and inclination requirements are satisfied while inclination error is higher than desired values. This shows that in order to achieve requirements for Case-2, the noise values for TAR and range measurements should be decreased.

Table 6.18. Case-2 parameter estimation errors for various observation duration

Duration (hour)	AzBias (mdeg)	ElBias (mdeg)	RangeBias (m)	Cp
12	0.000	0.000	151.7	1.72
24	0.000	0.000	51.2	1.71
48	0.000	0.000	49.9	1.70
True Value	**0**	**0**	**50**	**1.7**

Cp and bias parameters are estimated very close to real values according to Table 6.18 for Case-2 except for 12 hour duration set. Bias estimation error for 24-hour duration set is around 1.2 meter while 48-hour duration set can reduce error less than 0.1 meter.

Table 6.19. Case-3 position estimation errors in RSW frame for various observation duration

Duration (hour)	Along-Track (km)	Cross-Track (km)	Radial (km)	Three-dimensional (km)
12	22.6	3.53	0.46	22.96
24	0.89	0.71	0.09	1.14
48	0.10	0.39	0.04	0.41

Table 6.20. Case-3 velocity estimation errors in RSW frame for various observation duration

Duration (hour)	Along-Track (cm/s)	Cross-Track (cm/s)	Radial (cm/s)	Three-dimensional (cm/s)
12	1.42	38.5	161.4	165.9
24	0.62	4.67	6.22	7.80
48	0.31	3.30	0.57	3.36

Table 6.21. Case-3 orbital element estimation errors for various observation duration

Duration (hour)	Semi-Major Axis (m)	Inclination (mdeg)	Longitude (mdeg)
12	725.6	8.63	30.8
24	34.7	1.3	1.2
48	3.7	0.81	0.14
Requirement	30	1	3

Table 6.22. Case-3 parameter estimation errors for various observation duration

Duration (hour)	AzBias (mdeg)	ElBias (mdeg)	RangeBias (m)	Cp
12	0.000	0.000	99.7	1.64
24	0.000	0.000	25.6	1.70
48	0.000	0.000	24.9	1.70
True Value	0	0	25	1.7

From Table 6.19 through Table 6.21, it is clearly seen that Case-3 results are best among other cases. Also when compared to Case-2, two separate range measurements improve orbit estimation accuracy better than range and turn-around measurements. In Table 6.22, orbit parameters are converged to real values for 48 hour duration while 24 hour duration deviates from real value around 0.6 meter. In 12-hour duration condition range bias doesn't converge to desired value. From Table 6.21, it is clearly seen that all orbital element requirements are satisfied since range measurement noise is lower than TAR noise. In terms of the accuracy, using two separate range measurements from two station is better strategy than range-TAR configuration.

In following analysis, the effect of the various force model configurations on orbit determination accuracy is investigated with batch estimation method. Four different configuration is generated as shown at Table 6.23. In first three configurations, the degree of the geo-potential perturbations is decreased gradually from 8 to 2. It is clearly seen that degree change from 8 to 4 doesn't affect significantly orbit estimation

error for all cases. However, when the degree is lowered to 2, estimation error is increased by a factor of three times. In fourth configuration, third body perturbations (sun and moon) are removed from equation of motions. Estimation errors are too high compared to other configurations. Therefore, the mis-modelled dynamic model significantly affects estimation accuracy when the mis-model level increases. Since it is not possible compensate dynamic effects in batch estimation algorithm, the choice of the dynamic model level is crucial for effective orbit determination strategy.

Table 6.23. 3D position estimation error for Case 1, 2 and 3 for various force model configuration.

Force Model Configuration	Case 1	Case 2	Case 3	Units
Two Body + J8x8 + Third Body + SRP	1.04	0.85	0.41	km
Two Body + J4x4 + Third Body + SRP	0.85	0.94	0.49	km
Two Body + J2x2 + Third Body + SRP	2.85	3.38	3.68	km
Two Body + J8x8+ SRP	225.4	419.719	38.3	km

6.3. Batch Orbit Estimation with Maneuver

In this section, orbit estimation procedure is repeated with addition of N-S (North-South) maneuver. Cases, shown at Table 6.1, are used to analyze the results. All analysis is done for various time duration including 12, 24 and 48-hour observation duration before and after maneuver firing. This approach doubles total observation duration. In order to represent this approach, the notation such as 48x2 is used to show that observation is performed before and after maneuver. The reason for this strategy is to effectively estimate maneuver velocity increments. In simulation, the maneuver velocity increments are applied to the orbit of the satellite when initial conditions are propagated to the maneuver firing time as discussed in Figure 3.4. N/S maneuver value can be around 1 to 2 m/s [16],[17]. The exact value of the maneuver velocity depends on the satellite control requirements and the exact position of the satellite. Therefore, for the simulation analysis, 1.6 m/s value is used as shown at Table 6.24.

In order to test maneuver velocity estimation accuracy, the maneuver firing time is given to batch algorithm correctly, but, the maneuver velocity value is given wrong intentionally. Therefore, it can be observed whether batch algorithm can correctly find true value of the maneuver velocity or not.

Table 6.24. North-South Maneuver Velocity Increments.

	NS maneuver Velocity Increments	Unit
Along-Track	0.0	m/s
Cross-Track	-1.6	m/s
Radial	0.0	m/s

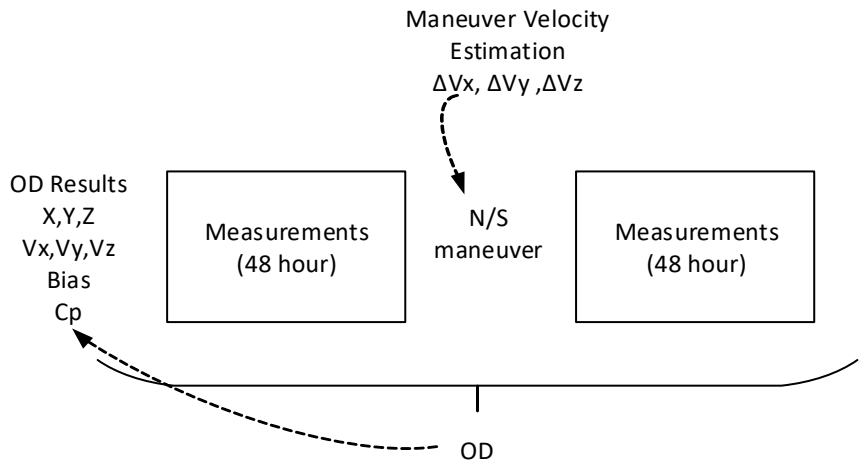

Figure 6.3. Batch orbit estimation procedure for North-South maneuver

In Figure 6.3, N-S maneuver batch orbit estimation procedure is shown for 48 hour measurements sets. In analysis, the different duration sets are investigated to see their effects on the orbit estimation accuracy. Only orbital element and maneuver velocity error values are shown in next tables.

Table 6.25. Case-1 N-S maneuver orbital element estimation errors in RSW frame for various observation.

Duration (hour)	Semi-Major Axis (m)	Inclination (mdeg)	Longitude (mdeg)
12x2	79.03	3.18	3.16
24x2	20.85	2.0	0.69
48x2	3.35	1.35	0.19
Reference	30	1	3

Table 6.26. Case-1 N-S maneuver velocity increments errors in RSW for various observation duration.

Duration (hour)	East (cm/s)	North (cm/s)	Radial (cm/s)	Three-dimensional (cm/s)
12x2	0.10	24.69	2.65	24.84
24x2	0.05	10.65	1.14	10.71
48x2	0.02	5.42	0.58	5.46

From Table 6.25 and Table 6.26 , 48 hour observation duration sets give best results as expected. Overall orbital element errors are lower than case without maneuver since the number of measurements is doubled. For Case-1, the accuracy of the maneuver velocity is around 5.4 cm/s for 48-hour duration set. This error corresponds to %3 of the true maneuver velocity.

Table 6.27. Case-2 N-S maneuver orbital element estimation errors in RSW frame for various observation.

Duration (hour)	Semi-major axis (m)	Inclination (mdeg)	Longitude (mdeg)
12x2	69.36	3.34	2.97
24x2	20.84	1.80	0.67
48x2	2.71	1.25	0.19

Table 6.28. Case-2 N-S maneuver velocity increments errors in RSW for various observation duration.

Duration (hour)	Along-Track (cm/s)	Cross-Track (cm/s)	Radial (cm/s)	3D (cm/s)
12x2	0.07	19.76	2.13	19.87
24x2	0.02	7.72	0.85	7.77
48x2	0.01	3.98	0.42	4.01

From Table 6.27 and Table 6.28, 48 hour observation duration sets give best results as expected. Orbital element requirements are satisfied except inclination. However, errors are lower than Case-2 including no maneuver. The velocity increments correspond to %2.5 of the true values which is similar to the result of the Case-1.

Table 6.29. Case-3 N-S maneuver orbital element estimation errors in RSW frame for various observation.

Duration (hour)	Semi-major axis (m)	Inclination (mdeg)	Longitude (mdeg)
12x2	80.81	1.89	3.32
24x2	18.59	0.99	0.53
48x2	2.37	0.64	0.01
Reference	30	1	3

Table 6.30. Case-3 N-S maneuver velocity increments errors in RSW for various observation duration.

Duration (hour)	Along-Track (cm/s)	Cross-Track (cm/s)	Radial (cm/s)	3D (cm/s)
12x2	0.05	13.32	1.44	13.39
24x2	0.01	5.57	0.62	5.60
48x2	0.01	2.53	0.27	2.55

From Table 6.29 and Table 6.30, 48 hour observation duration sets give best results as expected. Velocity increments errors are better than other cases. All orbital element

requirements are satisfied with Case-3 for 24 and 48-hour duration set. However, maneuver velocity increments errors for 24-hour set are higher than 48-hour. Therefore, although it can be claimed that 24-hour set satisfies orbital element requirements and can be used to for orbit determination operations, the error in maneuver velocity may causes increased error during station-keeping maneuver planning. When the maneuver firing is included during batch orbit determination process, overall orbit errors reduce compared to cases without maneuver since the number of the measurement is doubled.

6.4. Sequential orbit estimation without maneuver

In sequential estimation, Unscented Kalman Filter method is implemented to estimate orbit information effectively. Cases, shown at Table 6.1, are analyzed with sequential estimation method. Similar to batch analysis, sequential estimation is performed with all cases for various noise modes. As seen on Table 6.31 and Table 6.32, when the measurement noise increases, estimation errors also increases. All sequential estimation analysis is performed for 48-hour observation duration.

Table 6.31 Sequential 3D position estimation errors for various noise modes.

Case Name	Mode 1	Mode 2	Mode 3	Mode 4	Unit
Case 1	0.93	1.75	2.20	3.03	km
Case 2	0.84	1.26	2.15	2.71	km
Case 3	0.43	0.85	1.35	2.57	km

Table 6.32. Sequential 3D velocity estimation errors for various noise modes.

Case Name	Mode 1	Mode 2	Mode 3	Mode 4	Unit
Case 1	6.86	12.29	22.94	28.67	cm/s
Case 2	6.28	10.14	18.10	32.87	cm/s
Case 3	3.91	5.72	10.62	20.81	cm/s

Noise mode 1 is selected for presenting estimation results more detailed. Since UKF gives results sequentially, the duration effects on estimation accuracy can easily be seen on error graphs.

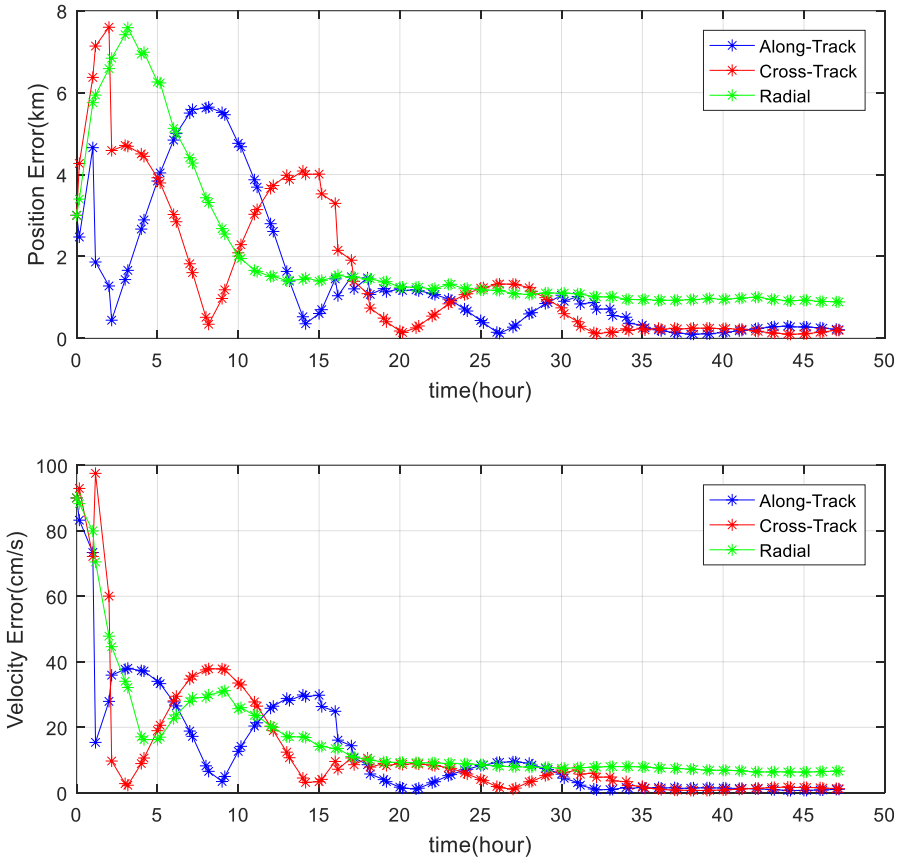

Figure 6.4. Case-1 sequential position and velocity estimation errors

From Figure 6.4, it is clearly seen that increase in measurement number decreases error dramatically. When observation duration is less than 35 hours, errors grow increased rate. 12-hour observation duration is not sufficient to estimate orbit

effectively. Main error contribution comes from radial component of the position and velocity vector.

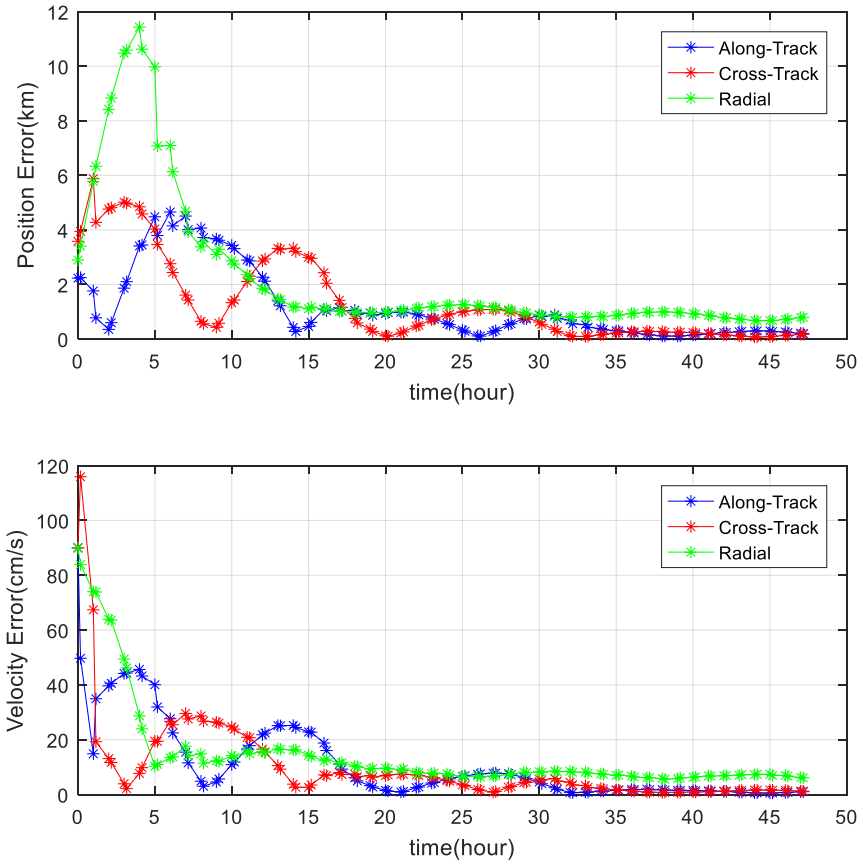

Figure 6.5. Case-2 sequential position and velocity estimation errors

From Figure 6.5, it is clearly seen that use of range measurements instead of angular measurements causes reduction in error. Exact error comparison can be seen on Table 6.31. The effect of the position and velocity error on requirements are investigated in next graphs.

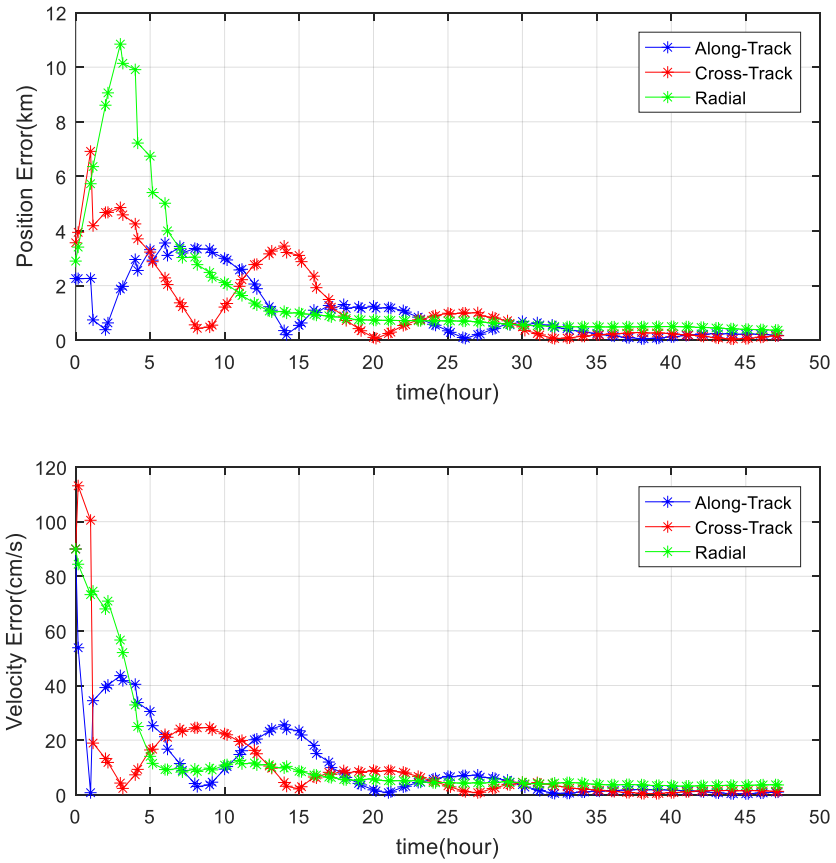

Figure 6.6. Case-3 sequential position and velocity estimation errors

From Figure 6.6, best results are achieved in Case-3 since two separate range measurements are effective than turn-around measurements. For 24-hour observation duration, position and velocity errors are lower than previous cases. In order to claim 24-hour set's effectiveness, orbital element error should be investigated.

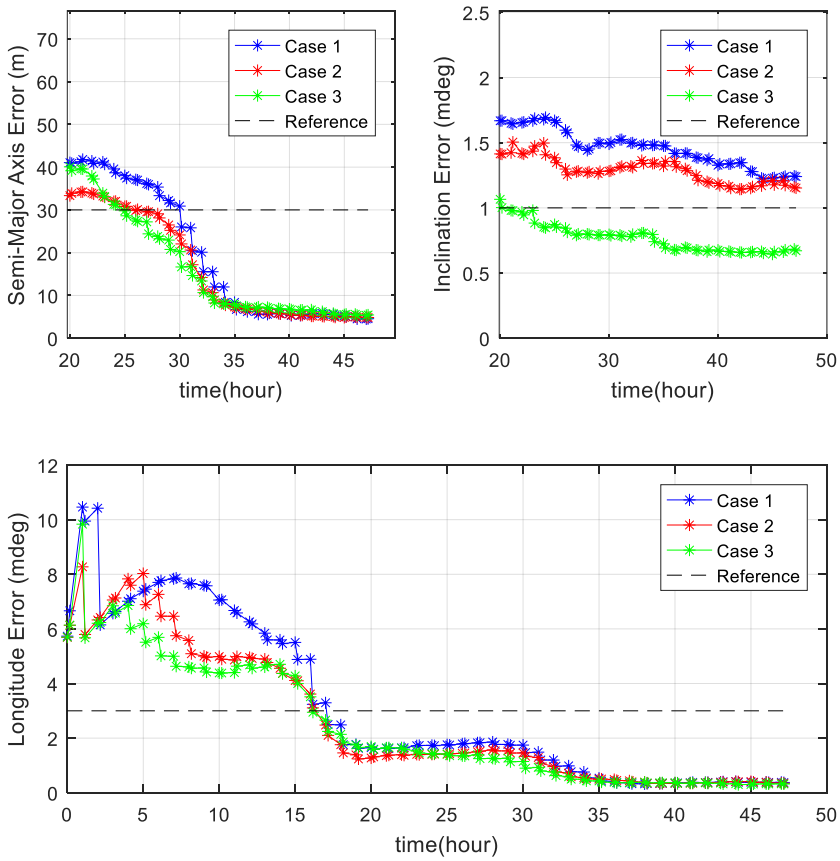

Figure 6.7. Orbital elements estimation errors for Case-1, Case-2 and Case-3

In Figure 6.7, when the observation duration increases, estimation errors decreases as expected. It is clearly seen that when observation duration exceeds 25 hours, all orbital element errors for Case-3 is below the reference values. Therefore, Case-3 can satisfy requirements for sequential method similar to batch method. Case-1 and Case-2 results can only achieve required semi-major axis and longitude accuracy.

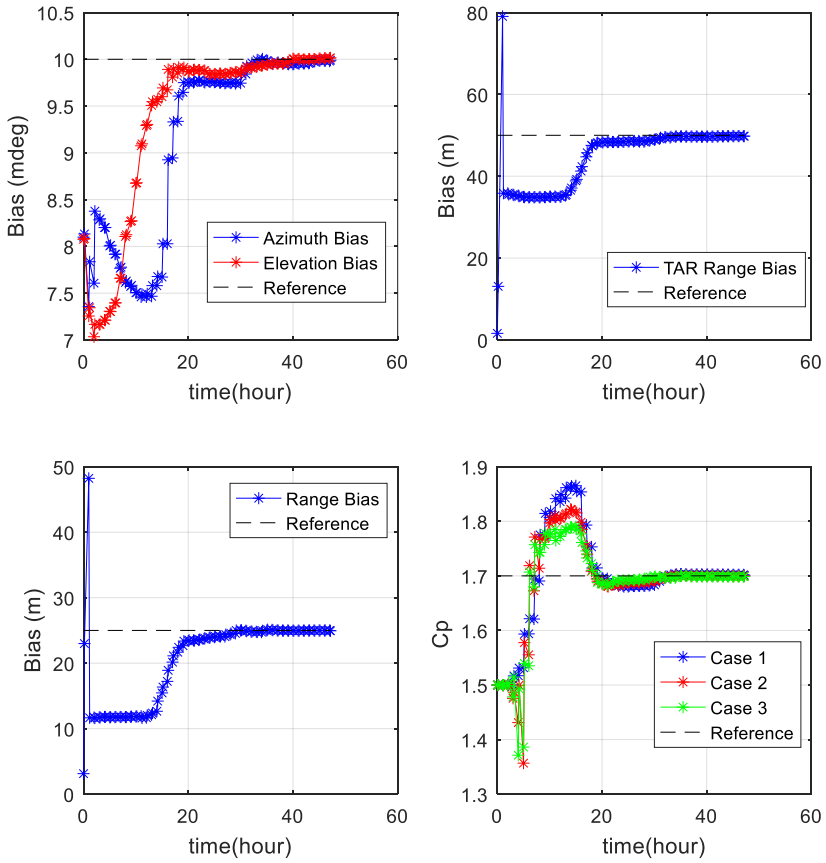

Figure 6.8. Parameter estimation results for Case-1, Case-2 and Case-3

From Figure 6.8, it is clearly seen that all bias estimation results are converged to the reference values when observation duration is higher than 30 hours. Cp parameter are also converging to reference value after 20-hour measurement set is used for estimation.

In following analysis, similar to batch one, sequential estimation is performed for different force model configurations. Since sequential method enables us to compensate mis-modelled dynamic error, Q process noise matrix is re-calculated by tuning parameters in order to reduce estimation error. In Table 6.33 and Table 6.34,

in order to emphasize the effect of dynamic model compensation, the estimation results are presented without tuning proper Q values. It is clearly seen that when Q values are not properly tuned, estimation error may increase dramatically. In Table 6.23, it is mentioned about weakness of the batch algorithm to mismodelled dynamic errors. In sequential method, this weakness can be eliminated considerable amount by tuning Q values.

Table 6.33 Estimation results for different force model configuration without Q tuning.

Force Model Configuration	Case 1	Case 2	Case 3	Units
Two Body + J8x8 + Third Body + SRP	0.93	0.84	0.43	km
Two Body + J4x4 + Third Body + SRP	0.97	0.88	0.50	km
Two Body + J2x2 + Third Body + SRP	5.04	5.46	4.88	km
Two Body + J8x8+ SRP	374.3	539.3	745.9	km

Table 6.34 Estimation results for different force model configuration with Q tuning.

Force Model Configuration	Case 1	Case 2	Case 3	Units
Two Body + J8x8 + Third Body + SRP	0.93	0.84	0.43	km
Two Body + J4x4 + Third Body + SRP	0.96	0.87	0.49	km
Two Body + J2x2 + Third Body + SRP	3.54	1.44	0.76	km
Two Body + J8x8+ SRP	4.88	4.37	4.47	km

6.5. Sequential orbit estimation with maneuver

In this analysis, sequential estimation method is applied to the measurements including N/S maneuver similar to the batch estimation.

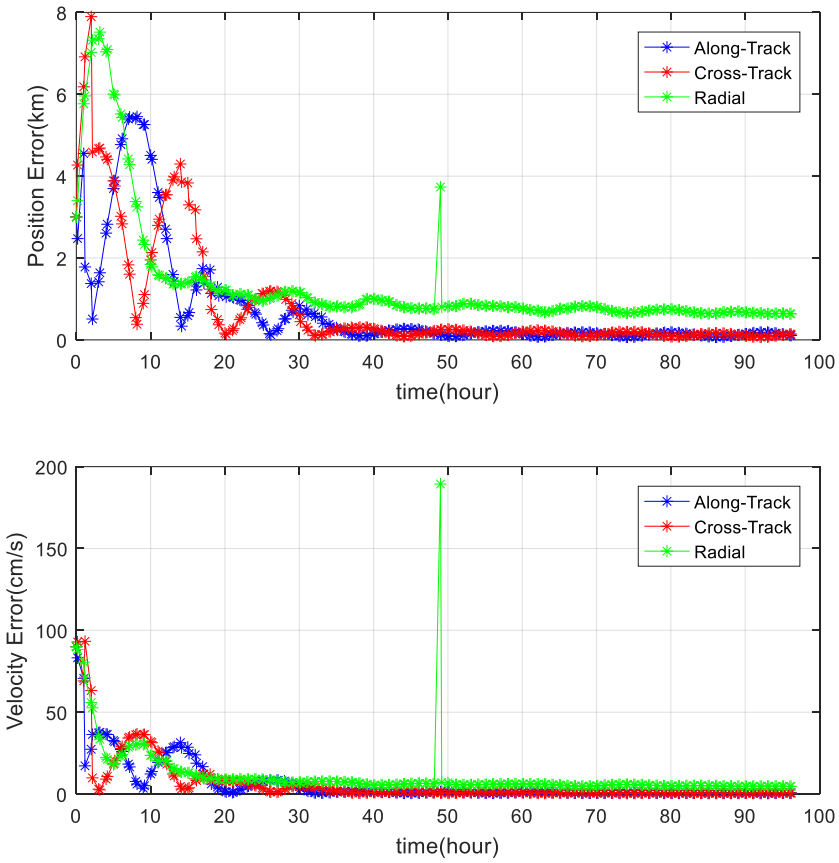

Figure 6.9. Case-1 sequential position and velocity estimation errors for N-S maneuver

From Figure 6.9, the estimation results are similar with previous no-maneuver case. In radial direction, there is an instant jump for both position and velocity estimation due to instant maneuver firing. Sequential estimation quickly converges after the maneuver is performed.

Position and velocity estimation results for Case-2 and Case-3 are similar with previous cases without maneuver. Therefore, these graphs are given in annex B. There is no jump in both position and velocity estimation results since N/S maneuver doesn't cause high instant difference for range measurements.

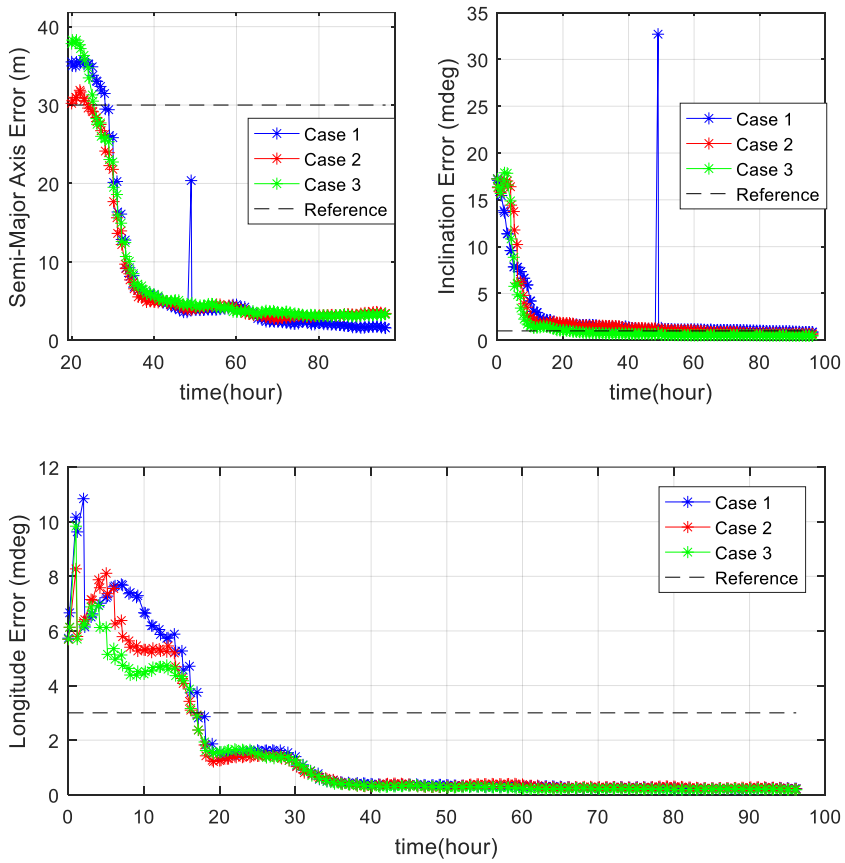

Figure 6.10. Orbital elements estimation errors for Case-1, Case-2 and Case-3 for N-S maneuver

From Figure 6.10, all estimation errors converge with increasing observation duration as expected. Since the maneuver is performed in North-South direction, there is a jump

in semi-major axis and inclination values for only Case-1. The same jump is not seen for Case-2 and Case-3 since range measurements are not affected by instant maneuver as much as the angular measurements. Semi-major axis and longitude requirements are satisfied with all cases when observation duration is higher than 20-hour. In Figure 6.11, inclination error results are shown in more detail.

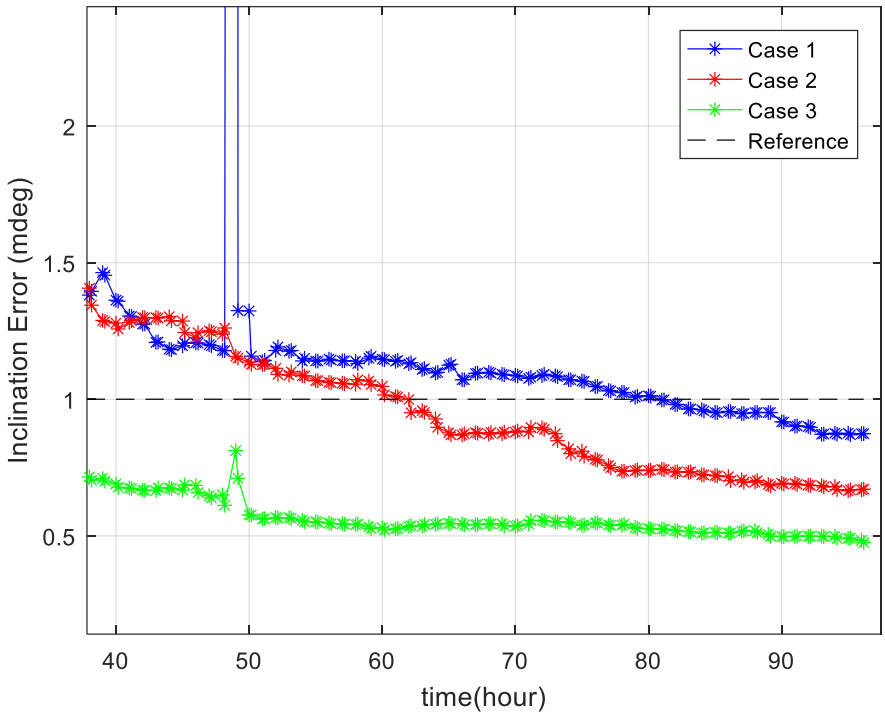

Figure 6.11. Inclination estimation errors for Case-1, Case-2 and Case-3 for N-S maneuver

From Figure 6.11, it is clearly seen that when observation duration exceed 80-hour , all 3 cases satisfy inclination requirements as well as semi-major axis and longitude.

All parameter estimation results are converged as expected since the number of measurements are two times higher than no-maneuver cases. Parameter estimation error graphs are given in annex B.

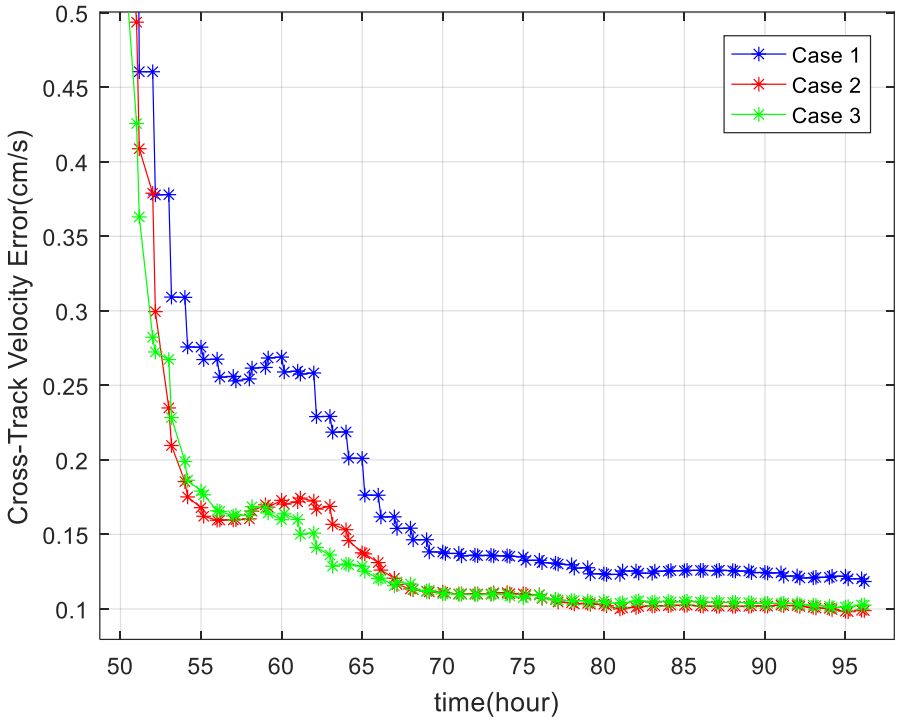

Figure 6.12. Cross-Track (north) maneuver velocity estimation error for Case-1, Case-2 and Case-3 for N-S maneuver

From Figure 6.12, the maneuver velocity increment estimation errors are seen for all cases. When the observation duration increases, estimation error decreases. After some point, errors become stable and filter is converged. Case-3 gives best results as expected. Overall errors are less than 0.15 cm/s for all cases. Generally, the estimation accuracy of the sequential method is quite well compared to batch method for maneuver velocity estimation as seen from comparison between Figure 6.12 and Table 6.30.

CHAPTER 7

VERIFICATION

7.1. Test Setup Parameters

In this section, batch orbit determination algorithm is compared with the reference software used at TURKSAT ground stations and analyzed cases are shown at Table 7.1. Initial Conditions and necessary measurements parameters for all case are taken from TURKSAT reference ground station software for T4B satellites. All measurements used in orbit determination analysis are taken from ground stations antennas used for real-time satellite operations at TURKSAT. There are 24 cases including different maneuver and measurement configurations. In nominal operations, 48 hour measurements with once per hour are used to estimate initial position, velocity, solar radiation coefficients, and measurement bias if maneuver is not applied. When E/W or N/S maneuver is available, 96-hour measurement sets with once per hour are used to estimate same parameters like nominal case with the addition of the maneuver velocity increments. The E/W represents East/West maneuver applied for the longitude correction. The N/S represents North/South maneuver applied for the inclination correction. These 96 hour measurements are taken from the ground station antennas for 2 day duration before and after the maneuver firing time.

Table 7.1. Case Summary for satellite T4B

Number of Total Test Case	Measurement Configuration	Maneuver Configuration	Observation Time
6	Range-Turnaround	No Manev-N/S-E/W	March-July
6	Range-Range	No Manev-N/S-E/W	March-July
6	Az-El-Range	No Manev-N/S-E/W	March-July
6	Az-El-Range-Turnaround-Range	No Manev -N/S-E/W	March-July

In order to clarify analysis cases, all cases are categorized according to the measurement configurations as shown at Table 7.1. Measurement configuration includes four sub-configurations. These sub-configurations are formed with the use of measurement from three ground station antenna. These antennas are defined by following:

- Station A: it is located at Ankara. It only produces azimuth, elevation and range measurements.
- Station B: it is located at Ankara. It only produces range measurement and it is also used for turn-around range measurement generation.
- Station C: it is located at Balıkesir. It only produces turn-around range measurement by using Station B and Station C together.

In first sub-configuration, only range and turn-around range measurements taken from Station B and Station C are used to estimate initial orbit parameters, turn-around range bias and maneuver velocity increments if E/W or N/S maneuver are included. In second sub-configuration, there are two different range measurements taken from Station A and Station B. The estimated parameters are almost similar to previous, except instead of turn-around range bias, range bias from Station B is estimated. In third sub-configuration, angle and range measurements from Station A are included in analysis. In this time, only angular measurement biases are estimated. In final sub-

configuration, all of the three station's measurements are used for orbit estimation. This configuration is redundant and used to verify the robustness of the batch estimation algorithm. Since it includes three different station, the following measurement biases are estimated: Angular and range bias from Station A, range bias from Station B and turn-around range bias from Station C. Since all these biases are also estimated in previous configurations, estimated biases can be compared with other configurations and checked whether there is significant deviation between estimated parameters or not. Each measurement configuration includes two sub-cases determined by maneuver configuration type and observation time. Maneuver configuration includes three case, namely, E/W maneuver, N/S maneuver and no maneuver included. In Figure 7.1, the details of the maneuver configurations are shown. Before N/S maneuver, orbit determination (OD) is performed by using 48-hour measurements in order to estimate orbit information. After that, N/S maneuver is planned by using estimated orbit information. After the maneuver firing is performed, 96 hour measurements (48 hour before and after firing time) are used to estimate initial conditions and maneuver velocity. In this way, maneuver performance can be calculated more effectively and initial orbit estimation is also improved by using more observation data. Same strategy is applied for E/W maneuver. All of the analysis are performed by using measurements taken during March and July 2018.

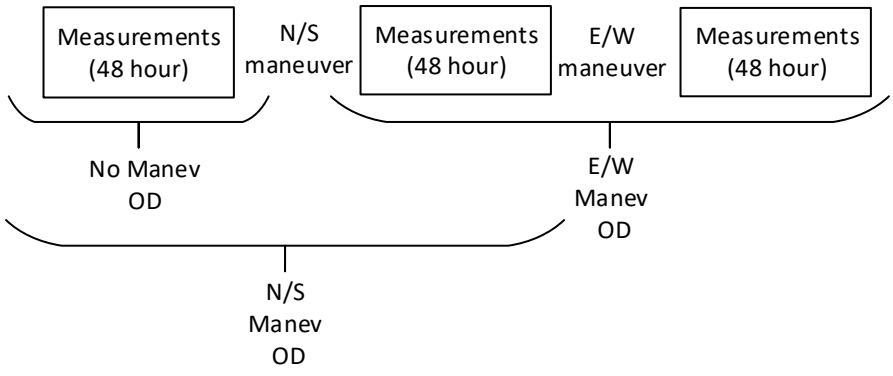

Figure 7.1 Orbit determination procedure during Station-Keeping operation

In order to avoid any confusion, the following names are used to categorize analyzed measurement configurations:

- Measurement configuration including azimuth, elevation and range measurements from Station A is named as “single station case”.
- Measurement configuration including range and turn-around measurements from Station B and Station C is named as “range and turn-around case”.
- Measurement configuration including range measurements from Station A and Station B is named as “range and range case”.
- Measurement configuration including azimuth, elevation and range measurements from Station A and range and turn-around measurements from Station B and Station C is named as “triple station case”.

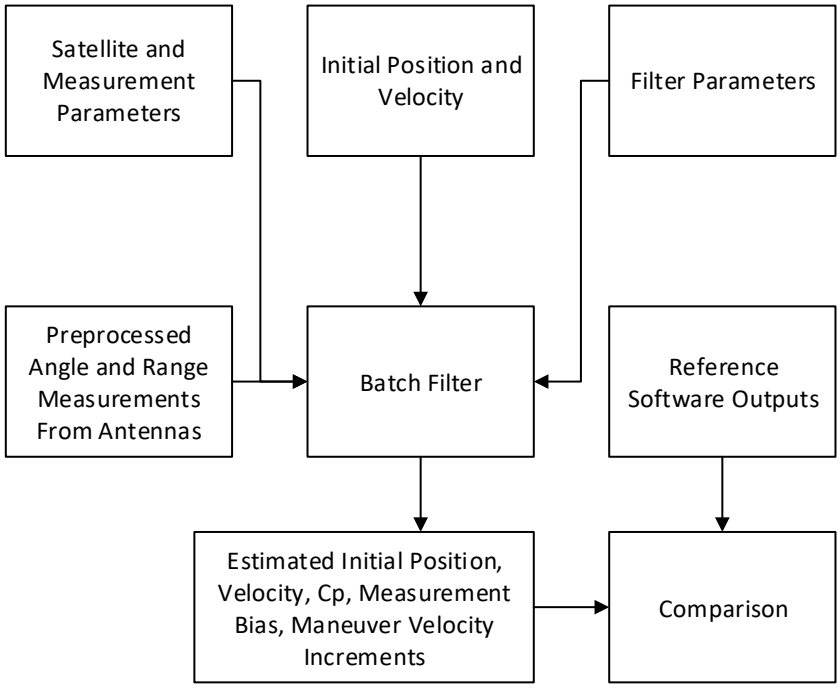

Figure 7.2 Orbit Determination Flow Chart for Verification

Orbit determination process is shown at Figure 7.2. Initial parameters including satellite, measurement parameters, position, and velocity are taken from the reference software. Filter parameters are determined by tuning these parameters. After the batch estimation is performed, the estimated parameters are compared with the reference software outputs. These comparison results are shown and discussed in next sections for each measurement configuration.

In Figure 7.3 and Figure 7.4, there are measurements taken from TURKSAT ground station antenna during real operations for the single station case during March. These measurements are generated by preprocessing raw antenna data. Raw ranging data are generated by measuring time delay of signal from the station to the spacecraft (up-link) and back (down-link) via the on-board transponder. Raw pointing data can be obtained from down-link auto track ground antenna with narrow beam width. Preprocess algorithm rejects undesired data from raw data by comparing standard deviation of total data with each data. Preprocess procedure is not of the scope for this thesis. All real measurements used for verification process are preprocessed measurements. Observation duration is approximately 7.5 day with including two maneuver shown by red line. However, the effective observation duration is around 6 day since there is a time gap between before and after maneuver firing time. First red line refers to N/S maneuver and second red line refers to E/W maneuver. The real measurements taken from antennas for July are given in appendix C.

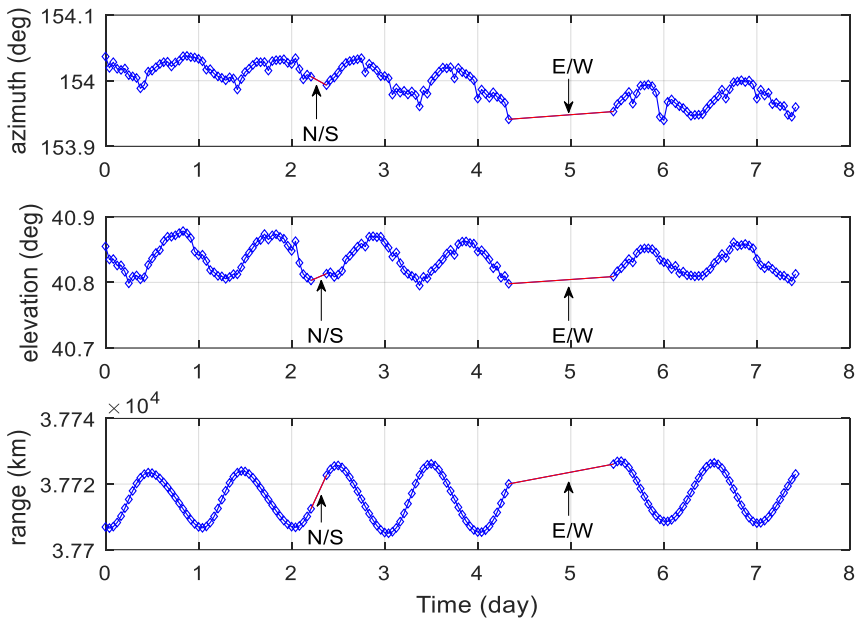

Figure 7.3 Azimuth (top), elevation (mid), range (bottom) measurements taken from TURKSAT ground station antenna during March for single station case

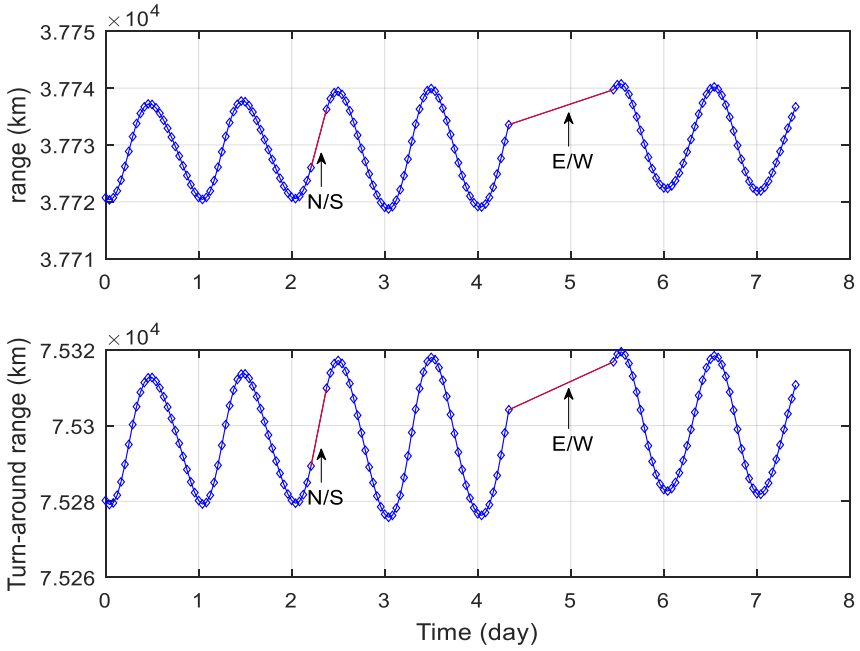

Figure 7.4 Range (top), turn-around range (bottom) measurements taken from TURKSAT ground station antenna during March for two station case

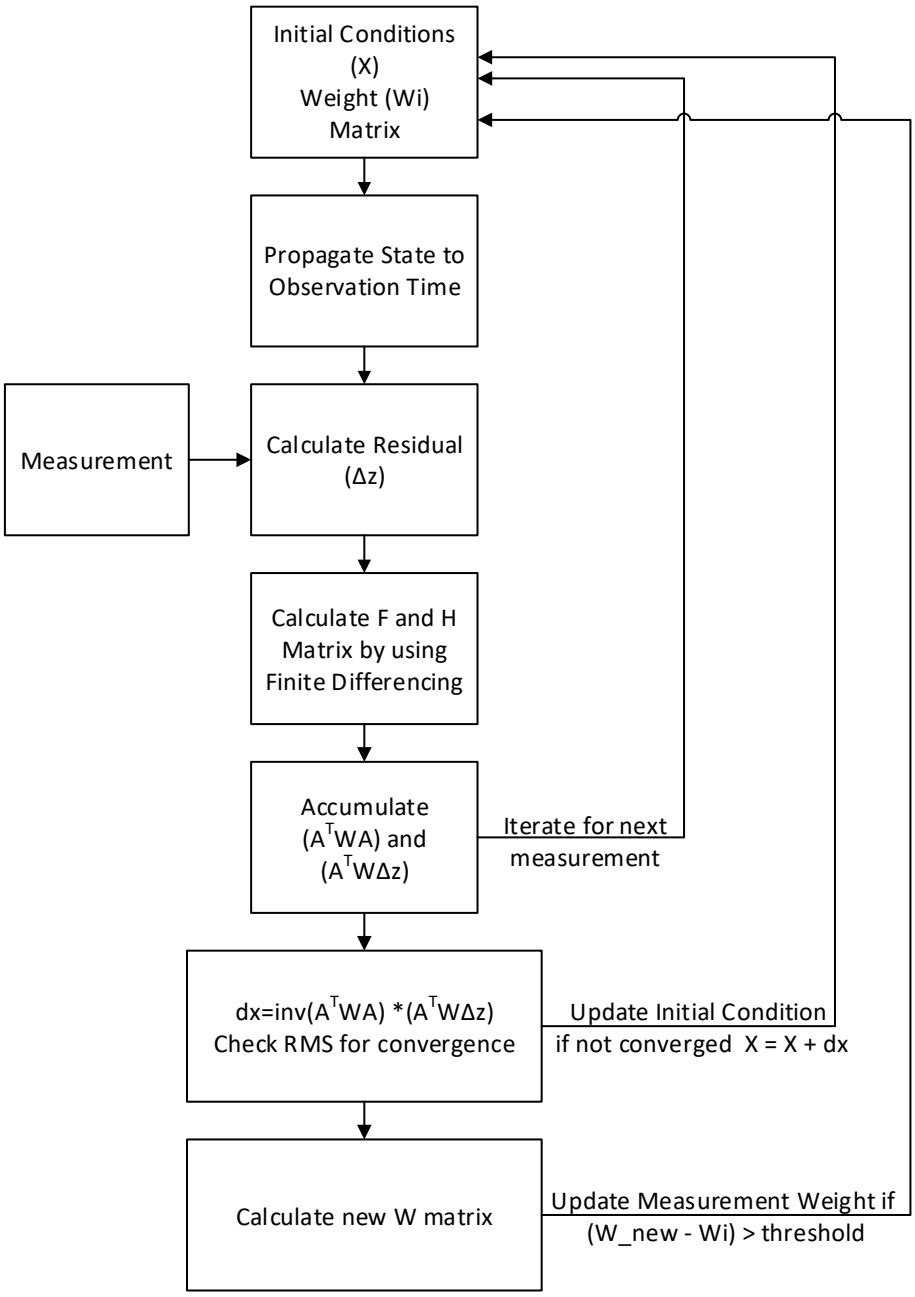

Figure 7.5 Batch Estimation Algorithm Flow Chart for Verification

In Figure 7.5, the standard batch algorithm is modified in order to perform estimation more effectively during verification analysis. In simulated case, measurement weight matrix (W) is determined during initial parameter settings and keeps constant during

iterations. However, in real estimation process, it may be not easy to determine initial weight matrix correctly. Therefore, measurement's weight values are also re-calculated when state information is estimated. After first iteration sets, if calculated and initial weight information difference is higher than pre-defined threshold, calculated W is used for the next iteration sets.

7.2. Single Station Case Verification

In single station case, azimuth, elevation and range measurements taken from single ground stations are used to estimate initial conditions and other parameters.

Table 7.2. Estimated 3-D position and velocity difference between batch estimation and Reference Software for Single Station Case

Case Name	Position (km)	Velocity (cm/s)
No Manev-March	1.27	5.34
N/S Manev-March	2.38	3.66
E/W Manev-March	1.32	6.00
No Manev-July	0.55	3.44
N/S Manev-July	0.72	8.10
E/W Manev-July	0.58	3.79

From Table 7.2, it is clearly seen that position difference between batch estimation and reference software oscillates between 0.5 and 2.5 km. Velocity difference is less than 10 cm/s. Acceptability of this difference becomes more meaningful when orbital element differences are checked.

Table 7.3. Total rms and solar radiation pressure coefficient (Cp) comparison between batch estimation and Reference Software for Single Station Case

Case Name	Batch Total Rms	Reference Total Rms	Batch Cp	Reference Cp
No Manev-March	1.00	1.00	1.173	1.173
N/S Manev-March	1.00	1.00	1.173	1.176
E/W Manev-March	0.99	1.00	1.174	1.177
No Manev-July	1.00	0.98	1.217	1.171
N/S Manev-July	1.00	1.00	1.216	1.169
E/W Manev-July	1.00	1.00	1.215	1.169

Total root mean square (rms) of sum of measurements residual are calculated for each case. In Table 7.3, total rms and estimated Cp values are compared with reference software. If rms is close to unity, it shows that weight parameter of Nonlinear Batch Filter matches with real measurement noise. Batch estimation gives results close to unity for all cases. From Cp estimation results, it is seen that there is constant difference about 0.04 between two results for July measurements. However, for March measurements, results are very close to each other. Each software is consistent with each other since all cases are belong to same satellite. Differences may arise due to setting different filter parameters.

Table 7.4. Estimated orbital element difference between batch estimation and Reference Software for Single Station Case

Case Name	Semi-Major Axis (m)	Inclination (mdeg)	Longitude (mdeg)
No Manev-March	9.55	1.16	0.57
N/S Manev-March	10.58	2.65	0.65
E/W Manev-March	8.07	1.39	0.58
No Manev-July	7.37	0.38	0.91
N/S Manev-July	6.77	0.57	0.62
E/W Manev-July	6.69	0.43	0.96

Three orbital elements, namely semi-major axis, inclination and longitude are compared with the reference software. The required semi-major axis determination accuracy is less than 30 meter (3 sigma) for planning nominal station-keeping operations. The required accuracy for inclination and longitude is less than 0.001 (3 sigma) and 0.003 (3 sigma) degree, respectively. In Table 7.4, it is clearly seen that estimated orbital element differences between two software are less than required values for semi-major axis and longitude. However, first three case doesn't satisfy inclination requirements.

Table 7.5. Azimuth residual rms comparison and estimated azimuth bias difference between batch estimation and Reference Software for Single Station Case

Case Name	Batch Azimuth Residual Rms (mdeg)	Reference Azimuth Residual Rms (mdeg)	Azimuth Bias Difference (mdeg)
No Manev-March	6.02	6.30	1.03
N/S Manev-March	7.00	7.34	1.02
E/W Manev-March	7.54	7.84	1.09
No Manev-July	9.89	9.93	1.26
N/S Manev-July	11.76	11.66	1.27
E/W Manev-July	11.65	11.54	1.23

From Table 7.5, the calculated azimuth residual rms values for batch estimation software are less than the reference value for most cases. The estimated bias difference between two software is less than 0.0012 degree. These differences are within acceptable limits. It is also seen that azimuth bias estimation difference from reference software is around 1 mili degree. Therefore, these differences may cause deviation between batch estimation and reference software.

Table 7.6. Elevation residual rms comparison and elevation estimated elevation bias difference between batch estimation and Reference Software for Single Station Case

Case Name	Batch Elevation Residual Rms (mdeg)	Reference Elevation Residual Rms (mdeg)	Elevation Bias Difference (mdeg)
No Manev-March	4.96	4.04	0.38
N/S Manev-March	5.45	4.13	0.32
E/W Manev-March	5.13	4.82	0.19
No Manev-July	5.04	4.13	1.04
N/S Manev-July	6.43	6.47	0.39
E/W Manev-July	7.39	7.41	0.37

From Table 7.6, the calculated elevation residual rms results are deviated from each other for first four case. This deviation may be responsible for higher inclination difference between both software. Estimated elevation bias differences are within acceptable limits since it is below elevation measurement noise value.

Table 7.7. Range residual rms comparison between batch estimation and Reference Software for Single Station Case

Case Name	Batch Range Residual Rms (m)	Reference Range Residual Rms (m)
No Manev-March	0.16	1.14
N/S Manev-March	0.18	1.07
E/W Manev-March	0.23	0.86
No Manev-July	0.13	0.42
N/S Manev-July	0.13	0.62
E/W Manev-July	0.14	0.73

From Table 7.7, the range residual rms values are less than reference software results for all cases. This indicates that batch estimation software estimation results are better fit with real measurements. In this measurement configuration, range measurements are used as a reference and TAR bias values are estimated. Range rms indicates that range noise is around 0.2 meter which shows better performance. Batch estimation results consistent with each other since range rms is approximately constant during all 6 case, but, reference software results shows more deviation. However, the range rms difference between batch estimation and reference software can be considered within the acceptable limits since overall orbital element estimation results are mostly close to each other.

Table 7.8. Maneuver velocity estimation difference in RSW frame between batch estimation and Reference Software for Single Station Case

Case Name	East (cm/s)	North (cm/s)	Radial (cm/s)
N/S Manev-March	0.008	1.94	0.23
E/W Manev-March	0.007	2.61	0.3
N/S Manev-July	0.002	0.99	0.11
E/W Manev-July	0.0008	0.32	0.02

In Table 7.8, it is clearly seen that the east and radial maneuver velocity estimation difference is below 1 cm/s. The north maneuver velocity contributes main difference between batch estimation and reference. Maximum difference is around 2.5 cm/s.

7.3. Range and Turn-Around Case Verification

In this case, range and TAR range measurements are taken from two ground stations. TAR range include both range information from two separate stations. However, due to this combination, its measurement noise higher than the range only measurement.

From Table 7.9, the position and velocity difference is lower than 0.5 km and 4 cm/s, respectively. These differences are lower than the single station case as expected.

Table 7.9. Estimated 3-D position and velocity difference between batch estimation and Reference Software for Range and Turn-Around Case

Case Name	Position (km)	Velocity (cm/s)
No Manev-March	0.12	0.95
N/S Manev-March	0.14	1.13
E/W Manev-March	0.18	1.54
No Manev-July	0.49	3.56
N/S Manev-July	0.50	3.57
E/W Manev-July	0.48	3.49

Table 7.10. Total rms and solar radiation pressure coefficient (Cp) between batch estimation and Reference Software for Range and Turn-Around Case

Case Name	Batch Total Rms	Reference Total Rms	Batch Cp	Reference Cp
No Manev-March	1.00	0.95	1.174	1.175
N/S Manev-March	1.00	0.95	1.175	1.178
E/W Manev-March	1.00	0.95	1.175	1.176
No Manev-July	1.00	0.94	1.217	1.172
N/S Manev-July	1.00	0.95	1.216	1.170
E/W Manev-July	1.00	0.95	1.215	1.169

In Table 7.10, the total rms of the batch estimation is more close to unity compared to reference value. This indicates that batch estimation is better fit with the real measurements. Cp estimation results are similar with single station case.

Table 7.11. Total rms and solar radiation pressure coefficient (Cp) between batch estimation and Reference Software for Range and Turn-Around Case

Case Name	Semi-Major Axis (m)	Inclination (mdeg)	Longitude (mdeg)
No Manev-March	9.51	0.02	0.78
N/S Manev-March	10.08	0.03	0.77
E/W Manev-March	7.45	0.03	0.84
No Manev-July	7.28	0.04	0.94
N/S Manev-July	6.89	0.01	0.95
E/W Manev-July	6.68	0.04	0.93

In Table 7.11, it is clearly seen that all orbital element differences are lower than requirements. Therefore, these results shows that batch algorithm range-TAR range configuration can achieve the required performance criteria.

Table 7.12. TAR residual rms comparison and estimated Tar bias difference between batch estimation and Reference Software for Range and Turn-Around Case

Case Name	Batch TAR Residual Rms (m)	Reference TAR Residual Rms (m)	TAR Bias Difference (m)
No Manev-March	0.49	2.17	8.32
N/S Manev-March	0.55	2.04	8.26
E/W Manev-March	0.57	1.65	9.04
No Manev-July	0.25	0.77	10.06
N/S Manev-July	0.38	1.26	10.15
E/W Manev-July	0.37	1.61	9.71

In Table 7.12, TAR bias differences changes between 8 to 10 meter. Estimated bias difference along with different estimated Cp parameter may be the main sources of the difference between two software. TAR residual rms for batch estimation is always lower than reference value similar to single station case. Maneuver velocity difference and range residual rms results are similar with single station case. From Table 7.13 and Table 7.14, it is clearly seen that maneuver velocity differences are lower than single station case as shown in Table 7.8. As seen on single station case, main difference in maneuver velocity is observed along north direction.

Table 7.13. Range residual rms comparison between batch estimation and Reference Software for Range and Turn-Around Case

Case Name	Batch Range Residual Rms (m)	Reference Range Residual Rms (m)
No Manev-March	0.23	1.12
N/S Manev-March	0.25	1.03
E/W Manev-March	0.27	0.79
No Manev-July	0.13	0.43
N/S Manev-July	0.15	0.63
E/W Manev-July	0.15	0.79

Table 7.14. Maneuver velocity estimation difference in RSW frame between batch estimation and Reference Software for Range and Turn-Around Case

Case Name	East (cm/s)	North (cm/s)	Radial (cm/s)
N/S Manev-March	0.005	1.11	0.14
E/W Manev-March	0.005	1.82	0.2
N/S Manev-July	0.0014	0.76	0.09
E/W Manev-July	0.0014	0.41	0.03

7.4. Range and Range Case Verification

In this case, the separate range measurements are taken from two ground stations as discussed before. Estimation difference results are given in next tables.

Table 7.15. Estimated 3-D position and velocity difference between batch estimation and Reference Software for Range and Range Case

Case Name	Position (km)	Velocity (cm/s)
No Manev-March	0.17	2.46
N/S Manev-March	0.25	2.66
E/W Manev-March	0.28	2.72
No Manev-July	0.53	3.88
N/S Manev-July	0.53	3.88
E/W Manev-July	0.56	3.92

From Table 7.15, it is clearly seen that position and velocity estimation differences are similar with range-TAR case.

Table 7.16. Total rms and solar radiation pressure coefficient (Cp) between batch estimation and Reference Software for Range and Range Case

Case Name	Batch Total Rms	Reference Total Rms	Batch Cp	Reference Cp
No Manev-March	1.00	1.00	1.174	1.172
N/S Manev-March	1.00	1.00	1.174	1.175
E/W Manev-March	1.00	1.00	1.175	1.175
No Manev-July	1.00	1.00	1.217	1.171
N/S Manev-July	1.00	1.00	1.216	1.170
E/W Manev-July	1.00	1.00	1.216	1.170

From Table 7.16, it is clearly seen that the total rms values are equals to unity for both software. Cp estimation results are similar with the previous cases. From Table 7.17, all the estimated orbital element differences are below the requirements.

Table 7.17. Estimated orbital element difference between batch estimation and Reference Software for Range and Range Case

Case Name	Semi-Major Axis (m)	Inclination (mdeg)	Longitude (mdeg)
No Manev-March	9.38	0.12	0.85
N/S Manev-March	10.25	0.06	0.83
E/W Manev-March	8.02	0.36	0.89
No Manev-July	7.34	0.10	0.98
N/S Manev-July	6.83	0.16	0.98
E/W Manev-July	6.66	0.005	0.97

The estimated range residual rms values are lower than reference for all cases similar to the previous cases. Range bias differences are around 4 centimeter level. The maneuver velocity estimation differences are similar with other configurations. Estimation results related to range rms ,bias and maneuver velocity for range-range case are given in section 7.6.

7.5. Triple Station Case Verification

In this section, the measurements from three station is used for estimation. These measurements include azimuth, elevation and range from one station, range and TAR from two stations. This analysis is performed in order to show the robustness of the batch estimation algorithm.

Table 7.18. Estimated 3-D position and velocity difference between batch estimation and Reference Software for Triple Station Case

Case Name	Position (km)	Velocity (cm/s)
No Manev-March	0.13	0.90
N/S Manev-March	0.13	0.61
E/W Manev-March	0.17	1.35
No Manev-July	0.49	3.50
N/S Manev-July	0.49	3.57
E/W Manev-July	0.49	3.57

From Table 7.18, it is clearly seen that position and velocity differences are similar level with range-TAR and range-range cases.

Table 7.19. Azimuth residual rms comparison and estimated azimuth bias difference between batch estimation and Reference Software for Triple Station Case

Case Name	Batch Azimuth Residual Rms (mdeg)	Reference Azimuth Residual Rms (mdeg)	Azimuth Bias Difference (mdeg)
No Manev-March	6.58	6.56	1.03
N/S Manev-March	7.59	7.58	1.03
E/W Manev-March	7.88	7.88	1.11
No Manev-July	10.06	10.08	1.26
N/S Manev-July	12.05	12.05	1.28
E/W Manev-July	12.09	12.08	1.22

From Table 7.19 and Table 7.20, it is seen that the estimated angular residual rms is almost same with the reference value. In single station case, there is a deviation angular residual rms comparison as previously shown in Table 7.5 and Table 7.6. Extra range and TAR measurements dominates estimation results and residual rms differences reduces as expected. This also shows that batch estimation algorithm results are consistent for cases including more than two station. Other results are given in section 7.6 since the most of the results are similar with previous cases.

Table 7.20. Elevation residual rms comparison and estimated elevation bias difference between batch estimation and Reference Software for Triple Station Case

Case Name	Batch Elevation Residual Rms (mdeg)	Reference Elevation Residual Rms (mdeg)	Elevation Bias Difference (mdeg)
No Manev-March	4.34	4.31	0.35
N/S Manev-March	4.81	4.75	0.35
E/W Manev-March	4.95	4.97	0.37
No Manev-July	4.22	4.22	0.39
N/S Manev-July	6.61	6.59	0.39
E/W Manev-July	7.55	7.54	0.37

7.6. Summary of the Verification Results

Overall estimation results for all cases are shown at Table 7.21. For each measurement configuration, the average value of all six cases results is calculated. The average position differences for all cases except the single station case are around 0.3 km. This shows close agreement between batch and reference results. Differences for the single station are higher than other configurations since the estimation accuracy of the single station results are lower than other configurations including range measurements. The average semi major axis differences are almost same with for all configuration. The average inclination differences are lower than 1 mili degree for all configurations except for the single station case. Finally, the average longitude differences are lower

than 1 mili degree for all configurations. From these results, it is claimed that all orbital element requirements are satisfied for all configuration except for the single station case.

Table 7.21. Average estimation difference and comparison between batch estimation and Reference Software for all cases

	Single Station Case	**Range and Turn-Around Case**	**Range and Range Case**	**Triple Station Case**	**Unit**
Position Diff.	1.139	0.316	0.386	0.314	km
Velocity Diff.	5.056	2.373	3.254	2.250	cm/s
Batch total rms	0.997	1.000	1.000	1.000	-
Ref total rms	0.997	0.948	1.000	0.980	-
Batch Cp	1.195	1.196	1.195	1.196	-
Ref Cp	1.173	1.173	1.172	1.173	-
Semi-major axis Diff.	8.171	7.982	8.079	8.036	m
Inclination Diff.	1.098	0.027	0.134	0.074	mdeg
Longitude Diff.	0.714	0.867	0.917	0.849	mdeg
Batch az rms	8.975	-	-	9.377	mdeg
Ref az rms	9.101	-	-	9.369	mdeg
Batch el rms	5.732	-	-	5.412	mdeg
Ref el rms	5.165	-	-	5.395	mdeg
Batch range rms	0.164	0.198	0.187	0.206	m
Ref range rms	0.808	0.795	0.787	0.795	m
Batch TAR rms	-	0.436	-	0.456	m
Ref TAR rms	-	1.581	-	1.600	m
Az Bias Diff.	1.149	-	-	1.155	mdeg
El Bias Diff.	0.449	-	-	0.368	mdeg
Range Bias Diff.	-	-	0.039	0.039	m
Tar Bias Diff.	-	9.256	-	9.267	m
Manev Vel. Diff.	1.47	1.03	1.3	1.08	cm/s

In order to analyze the effect of the difference between batch estimation and reference software on real station keeping operations, the estimated initial conditions from both software are propagated along two weeks. The difference between propagated orbital elements and position values are shown in Figure 7.6.

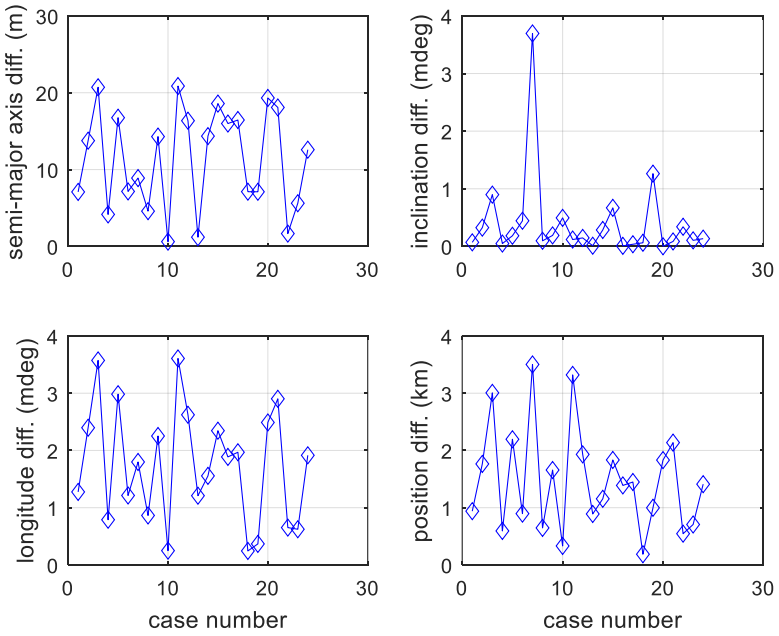

Figure 7.6 Orbital elements and position difference after propagating estimated initial conditions during two week.

Final maximum position difference is around 3.5 km. Maximum longitude difference is below 4 mili degree. This shows that the longitude error requirement , 9 mili degree (Chapter 1.3), due to two-week propagation is satisfied for all cases as shown in Figure 7.6.

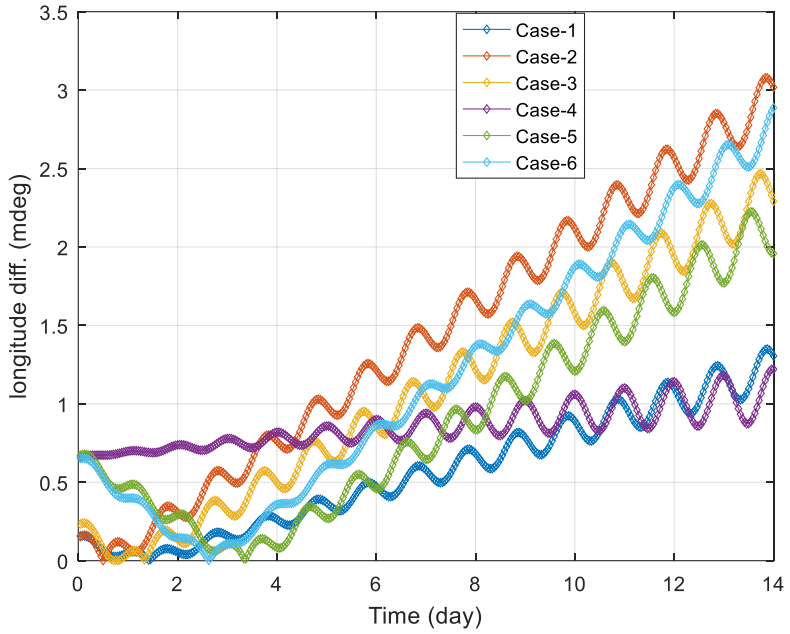

Figure 7.7 Longitude error after propagating estimated initial conditions during two week for range-TAR measurement configuration.

Range and turn-around range configuration is the main configuration used for station-keeping operating in the TURKSAT ground station. Therefore, in order to emphasize the effect of the estimation differences between reference software and batch estimation on two-week orbit propagation requirement, longitude change during propagation is also shown in more detail in Figure 7.7. Although some oscillations exist, the final maximum longitude error is around 3 mili degree which is much lower than 9 mili degree.

In this chapter, only batch estimation verification by using the real measurements is presented. This verification includes only the performance verification of the batch algorithm for nominal conditions. Therefore, this comparison between batch estimation and reference software can only be accepted as a limited verification process. Sequential estimation is only verified by simulation due to the lack of the real measurement data.

CHAPTER 8

CONCLUSION

In this thesis, batch and sequential orbit determination methods are presented and investigated. In order to show the accuracy of orbit determination method, multiple measurement and maneuver configurations are analyzed by conducting nonlinear computer simulations. Estimation results are compared with pre-simulated reference orbit results. The effect of the different noise values and observation duration is also investigated for both batch and sequential estimation method.

In angle-only estimation method, only EKF and UKF methods are applied to simulated measurements. There are two cases including different measurement frequency and observation durations. In measurement frequency case, the observation duration is fixed at 600 minutes and the measurement sampling interval is changed from 60 second to 3600 second. The estimation results obtained using UKF and EKF can reduce the position error to 0.25 km for the maximum observation duration. When the observation number drops a certain point, lower than 60 point, UKF generally gives better results compared to EKF since UKF can handle the nonlinear nature of the problem with unscented transformation (UT) method. In measurement duration case, the measurement sampling frequency is fixed at 1 minutes and total observation duration is changed from 60 to 600 minutes. For 60-minute duration, both UKF and EKF can't converge a final value since the oscillations in estimation results exist. When the observation duration exceeds 120 minutes, both method can converge to a stable value. This shows that 120-minute duration can be a turning point for the angle-only orbit estimation in order to estimate effectively the position of a GEO satellite by using sequential methods. In addition to this, it can be concluded that when the measurement data is sparse and limited, UKF can generally give more accurate estimation results than EKF.

In standard orbit determination process, batch and sequential methods are investigated separately. Three different measurement configurations are analyzed and compared with each other. These are single station, range-TAR and range-range. At first, batch estimation is applied to the simulated measurements including various observation duration and noise values in order to determine which the noise values can achieve desired orbit determination accuracy. When the angular and range noise is around 7.5 mili degree and 4.5 meter, respectively, it is seen that the estimated position error, lower than 1.5 km, can be achievable when the observation duration is 48-hour without including any maneuver. Since mission requirements are given in orbital element notation, the results of three measurement configuration are investigated in more detail. The most successful configuration is range-range configuration which satisfies all the orbital element requirements for both sequential and batch estimation method for 48-hour duration. The range-TAR and single station configurations can satisfy semi-major axis (< 30 m) and longitude requirement (< 3 mdeg). However, the inclination requirement is not satisfied although the estimated inclination results for range-TAR are more close to 1 mili degree compared to the single station. For these analysis, it is also shown that other parameters such as measurement bias and solar radiation pressure coefficient (Cp) can be also successfully estimated along with the position and velocity vector when the observation duration is 48-hour. For 24-hour duration, batch algorithm can still estimate desired parameters with a loss of accuracy. When observation duration is around 12-hour, batch algorithm can't estimate the desired parameter effectively. Since best results are achieved with 48-hour observation duration, it is recommended that 2-day observation with once an hour measurement sampling interval should be used in order to perform the orbit determination process effectively for GEO satellites. Same analysis is also conducted with the simulated measurements including N/S maneuver. The results show that the velocity changes due to maneuver can be estimated and overall orbital element estimation accuracy is similar with no maneuver case. In sequential estimation, the same analysis and measurement configurations are applied to UKF algorithm. The accuracy of the results is very similar with batch method. Only range-range

configuration can satisfy all the orbital element requirements while other two configurations can't achieve the required inclination accuracy. When the N/S maneuver is included, both range-TAR and range-range configuration can satisfy all the requirements since the observation duration is around 96-hour including 48-hour measurement set before and after the maneuver firing is applied. This shows that for range-TAR configuration, UKF method can also be used as an effective orbit determination algorithm along with range-range configuration.

In order to verify batch estimation results, batch algorithm is applied to the real measurements taken from TURKSAT ground station antennas for T4B satellites. The estimation results are compared with reference software used for the real station keeping operations. Orbital element comparison shows that for 24 different cases, differences between batch estimation and reference software are below the orbital element requirements for cases including range measurements. In single station case, there are some cases which doesn't satisfy inclination requirements. However, the measurements from single station are only used when the second ground is not available. In nominal operations at TURKSAT, the range-TAR configuration is actively used for the orbit determination process although the range-range configuration also satisfies the requirements. The reason is that in order to perform an operation by using different ground stations, there must be two separate active ground station systems. This means that there should be an additional operator and ground equipment for second ground station. This may increase the cost of the orbit determination operations. Therefore, it may be claimed that the range-TAR configuration is more cost effective compared to the range-range if the orbital element requirement can be satisfied since the range-TAR configuration only needs one active ground station while other ground station is passively used. Therefore, the performance of the range-TAR configuration is the key point for evaluating whether batch algorithm can be used on real operations or not. In order to ensure about robustness of orbit determination process, same analyses are also repeated with triple

station cases including all the available measurements. Their results are also consistent with other configurations and satisfy the requirements.

In conclusion, this work indicates that batch estimation algorithm shows very close agreement with a software used for real orbit control operation at TURKSAT facilities for about 10 years. This claim is only valid for T4B satellite's March and July measurements. In this thesis, the only limited verification procedure to check the performance of batch algorithm for nominal conditions is carried out. It is obvious that more data is needed to completely trust the performance of the batch estimation algorithm.

In future work, the batch estimation algorithm should be tested with more real measurement data taken during the different month of the year. In order to ensure about robustness, batch algorithm should be applied to the different satellites' measurements such as T3A and T4A. Same procedure should be applied to sequential methods in order to show its effectiveness during real operations. In addition to this, the difference between batch estimation and reference software can be reduced by improving orbit force and measurement model.

REFERENCES

[1] A. Köker, O. Tekinalp, "Angle Only Orbit Determination Using Telescope System", 9th Ankara International Aerospace Conference, Ankara, 2017.

[2] A. Köker, O. Tekinalp, "Orbit Estimation Strategy for Low Earth Orbit And Geostationary Satellites", AAS/AIAA 2018 Astrodynamics Specialist Conference, Snowbird, UT, 2018.

[3] A. H. Jazwinski, Stochastic Processes and Filtering Theory, Academic Press, New York, 1970.

[4] B. D. Tapley, B. E. Schutz and G.H. Born, Statistical Orbit Determination, Elsevier Academic Press, 2004.

[5] Cooley, J. L., "Error Studies for Ground Tracking of Synchronous Satellites," Goddard Space Flight Center (GSFC) Rept. X-551-72-30, Maryland, 1972.

[6] E. Imre, B. Yağlıoğlu, M. Gökce, M. R. Geden, A. Köker, S. Aydın, F. Arberkli, E. Dağ, "Orbital Dynamics System of TUBITAK UZAY for Earth Orbiting Spacecraft", AIAA/IEEE 9th International Conference on Recent Advances in Space Technologies, Istanbul, 2019.

[7] E.-S. Park, S.-Y. Park , K.-M. Roh, K.-H. Choi, "Satellite orbit determination using a batch filter based on the unscented transformation", Aerospace Science and Technology 14 (2010) 387–396.

[8] E. M. Soop, Handbook of Geostationary Orbits, 1st ed., Kluwer Academic, Boston, 1994, pp. 256–285.

[9] E. Wan, R. van der Merwe, in: S. Haykin (Ed.), Kalman Filtering and Neural

Networks, Wiley, New York, 2001.

[10] D.A. Vallado, Fundamentals of Astrodynamics and Applications, 2nd ed., Kluwer Academic Pub., Netherlands, 2001.

[11] D.-J. Lee and K. T. Alfriend, "Sigma Point Filtering for Sequential Orbit Estimation and Prediction," J. Spacecr. Rockets, vol. 44, no. 2, pp. 388–398, 2007.

[12] J. Tombasco, Orbit Estimation of Geosynchronous Objects Via Ground-Based and Space-Based Optical Tracking (Doctoral dissertation), Colorado University, Colorado, USA.

[13] O. Montenbruck and E. Gill, Satellite Orbits Models, Methods and Applications, 2nd ed. , Springer , New York , 2001.

[14] R. Armellin and P. Di Lizia, “Probabilistic initial orbit determination,” Adv. Astronaut. Sci., vol. 158, pp. 3143–3159, 2016.

[15] S. J. Julier and J. K. Uhlmann. A New Extension of the Kalman Filter to Nonlinear Systems. In Proc. of AeroSense: The 11th Int. Symp. on Aerospace/Defence Sensing, Simulation and Controls., 1997.

[16] Y. Hwang , B.-S. Lee, H.-Y. Kim , H. Kim and J. Kim , “Orbit Determination Accuracy Improvement for Geostationary Satellite with Single Station Antenna Tracking Data”, ETRI Journal, Volume 30, Number 6, 2008.

[17] Y. Hwang , B.-S. Lee, B.-Y. Kim, H.-Y. Kim and H. Kim ,”Validation of Geostationary Satellite Orbit Determination Using Single-Station Antenna Tracking Data”, Journal Of Spacecraft And Rockets, Vol. 50, No. 6, 2013.

[18] H. Yoshida, “Construction of higher order symplectic integrators”, Physics Letters A, Vol. 150, Iss. 5-7, 1990.

[19] The Different Frames and the Keplerian Elements ,accessed 12 July 2015, <https://adcsforbeginners.wordpress.com/2015/07/12/adcs-for-beginners-1/>.

[20] J. V. Sickle, GPS and GNSS for Geospatial Professionals, Lesson 5 : Geodetic Datums. Retrieved from <https://www.e-education.psu.edu/geog862/node/1405>.

[21] Wikipedia contributors, "Orbital elements," Wikipedia, The Free Encyclopedia, https://en.wikipedia.org/w/index.php?title=Orbital_elements&oldid=916427044 (accessed October 2, 2019).

APPENDICES

A. Batch Estimation Results

Table A.1. Case-1 semi-major axis estimation errors for various observation duration and noise modes

Duration (hour)	Mode 1	Mode 2	Mode 3	Mode 4	Unit
12	789.587	1528.906	2403.172	4809.062	m
24	41.797	68.817	117.927	264.725	m
48	3.850	7.061	12.445	29.663	m

Table A.2. Case-1 inclination estimation errors for various observation duration and noise modes

Duration (hour)	Mode 1	Mode 2	Mode 3	Mode 4	Unit
12	6.755	12.900	22.930	31.692	mdeg
24	2.376	5.015	9.313	15.985	mdeg
48	1.926	3.226	7.714	9.392	mdeg

Table A.3. Case-1 longitude estimation errors for various observation duration and noise modes

Duration (hour)	Mode 1	Mode 2	Mode 3	Mode 4	Unit
12	33.087	64.130	101.064	199.491	mdeg
24	1.414	2.372	3.687	9.180	mdeg
48	0.327	0.471	1.325	1.843	mdeg

B. Sequential Estimation Results

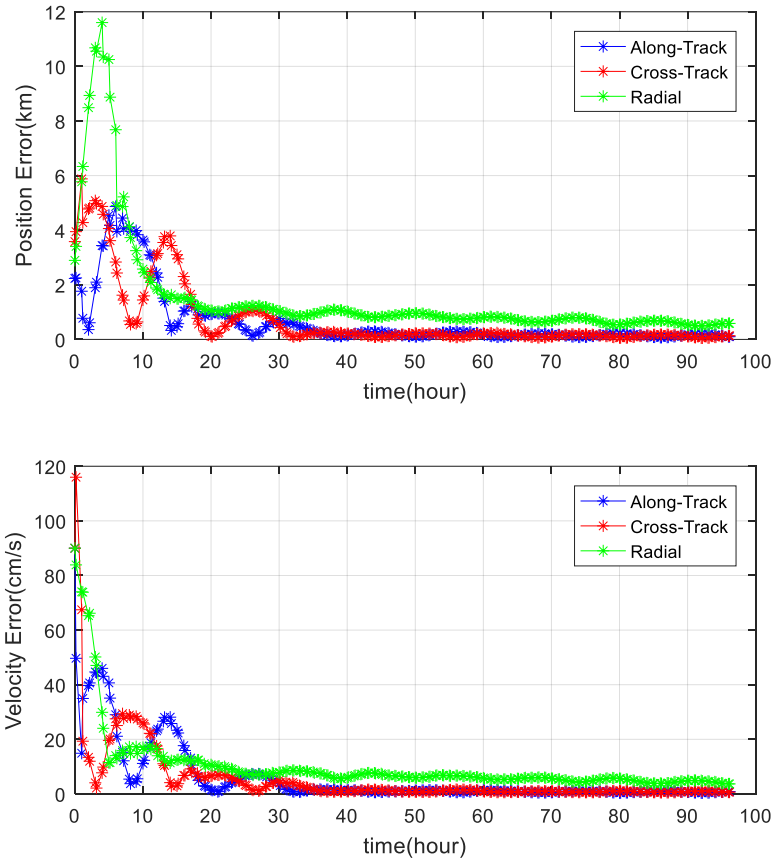

Figure B.1. Case-2 sequential position and velocity estimation errors for N-S maneuver

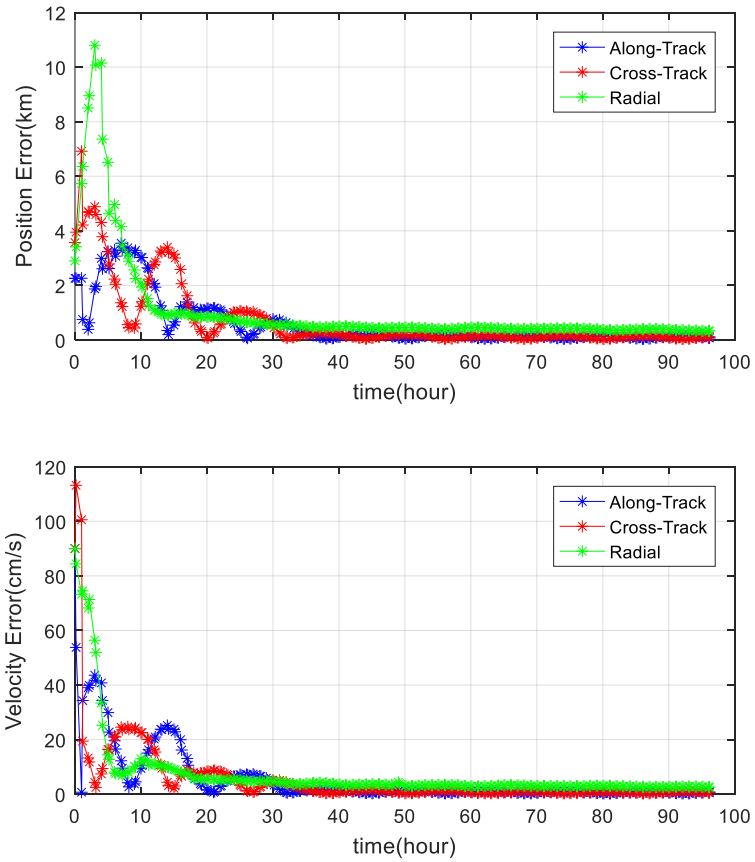

Figure B.2. Case-3 sequential position and velocity estimation errors for N-S maneuver

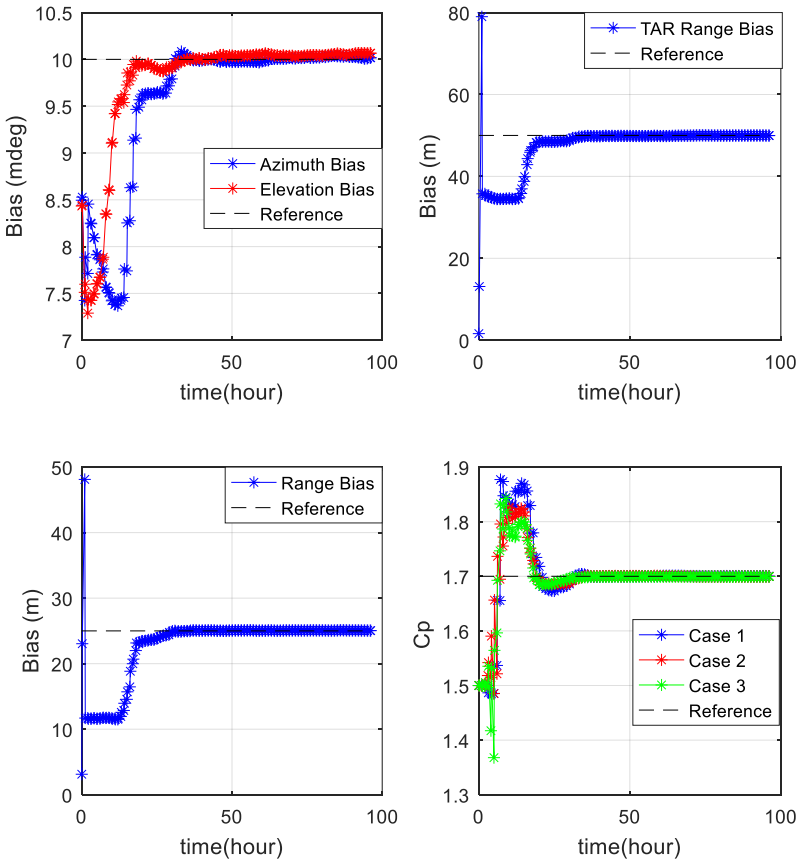

Figure B.3. Parameter estimation results for Case-1, Case-2 and Case-3 for N-S maneuver

C. Real Measurement Data During July

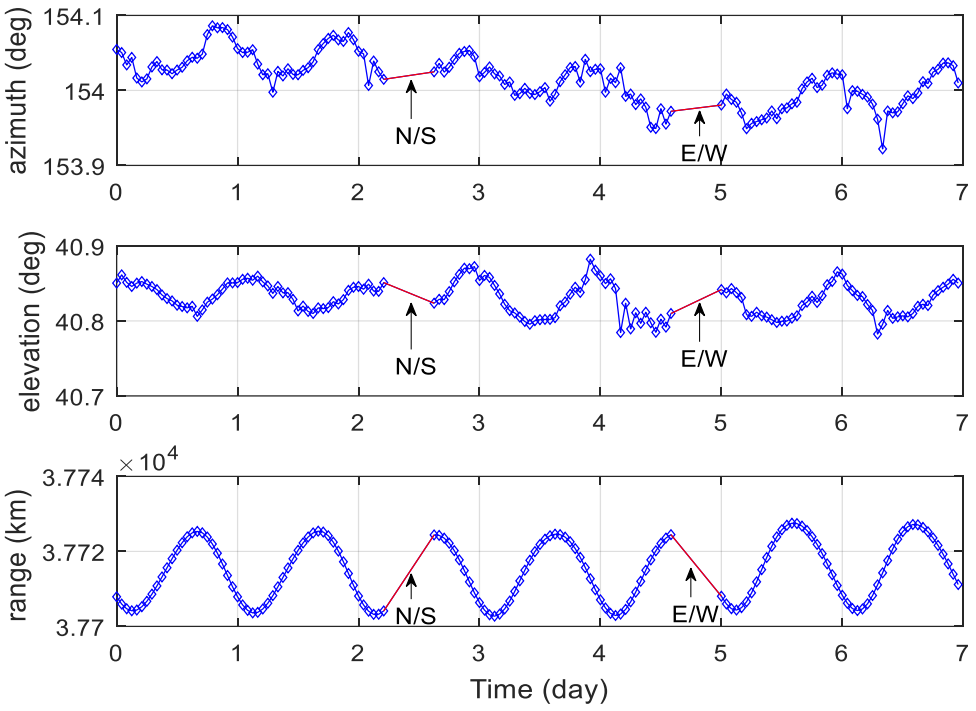

Figure D.1 Azimuth (top), elevation (mid), range (bottom) measurements taken from TURKSAT ground station antenna during July for single station

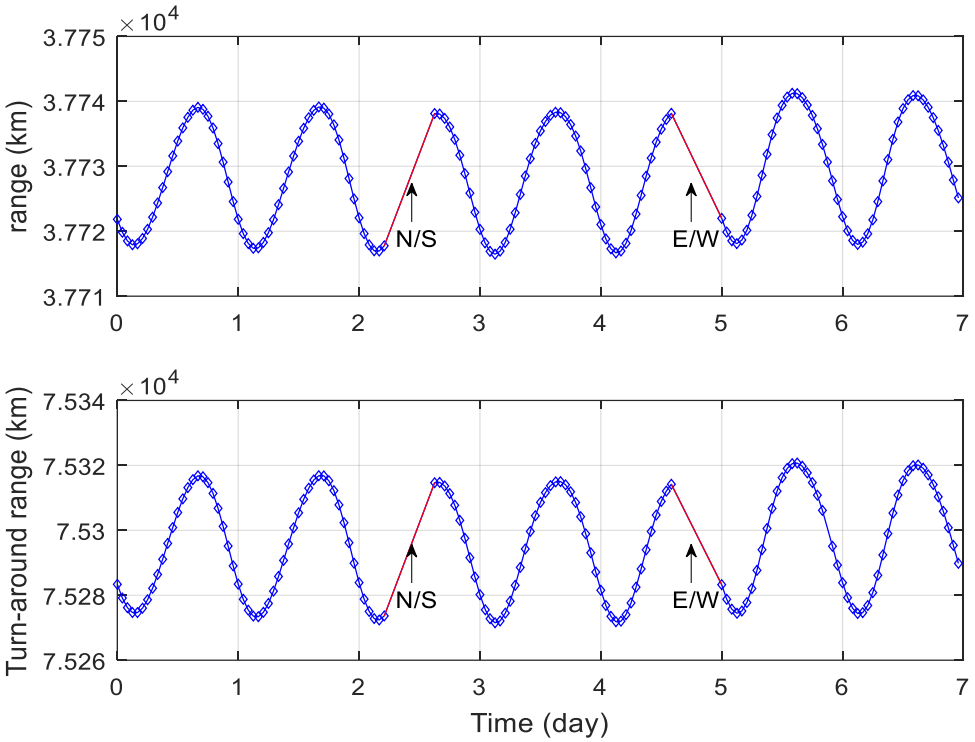

Figure D.2 Range (top), turn-around range (bottom) measurements taken from TURKSAT ground station antenna during July for two station case